UNIVERSITY OF NAVARRA

SCHOOL OF ENGINEERING

DONOSTIA-SAN SEBASTIÁN

LIVER RADIOEMBOLIZATION: COMPUTATIONAL PARTICLE–HEMODYNAMICS STUDIES IN A PATIENT-SPECIFIC HEPATIC ARTERY UNDER LITERATURE-BASED CANCER SCENARIOS

DISSERTATION

submitted for the Degree of Doctor of Philosophy

of the University of Navarra by

JORGE ARAMBURU MONTENEGRO

under the supervision of

RAÚL ANTÓN REMÍREZ

Donostia-San Sebastián, December 2016

Acknowledgments

Journeys always begin at a certain point and usually finish somewhere else. This unique journey started off several years ago with a conversation with Raúl Antón during a summer course on electronics cooling. Determining when this journey ends is going to be difficult. Anyway, doing research within the biomedical field has been truly fascinating. The following lines acknowledge the institutions and people that I have been supported by and worked with during these fruitful years of doctorate.

This work is the result of four years of activity, which have been very enriching and have taken place at TECNUN (Escuela de Ingenieros de la Universidad de Navarra) and Clínica Universidad de Navarra. I am grateful to everyone included in these lines not only for their kindness, but also for their dedication and help. They have been key to succeeding in the purposes of the present thesis.

Yielding fruitful results and making significant contributions was the principal objective of this work. Even though it was sometimes frustrating not to reach the useful methods and tools to advance, the final outcome has been worth it.

Due to the fact that taking all the credit for the contributions resulting from this entire thesis would be unfair, I consider it particularly important to thank—concisely, as it could take too long—the people that have helped me and have been by my side rousing me whenever I needed throughout these four years.

First, I would like to thank FEUN (Fundación Empresa-Universidad de Navarra) and Universidad de Navarra for the fellowship, Ministerio de Economía Competitividad for funding this piece of research through Proyecto DPI2012-35277, and Cátedra Fundación Antonio Aranzábal–Universidad de Navarra.

I would also like to thank my fellow students I have shared office with: Asier, Yunesky, Alaine, Esti, Iñigo, Fran, Naveiro, Junkal, Julio, Dima, Patricia, Mireia, etc. Moreover, special thanks go to Nebai and Aitor, who helped me with computational-domain discretizations, and Sergio, with whom I have shared frontenis and futbito matches, thesis supervisor, and all the difficulties that making our way from the thesis conception to actual realization have involved.

I gratefully acknowledge the invaluable support of Alejandro, Juan Carlos, and Gorka, the investigators of the Thermal and Fluids Engineering division, and *Nagusi*, the laboratory technician of the division. Their insatiable thirst for knowledge and their willingness to always help have made everything easier.

I am also very grateful to Bruno and Nacho, doctors of Clínica Universidad de Navarra, for their extremely useful pieces of advice on project-related concerns and for voicing their opinion from a medical standpoint.

I am most grateful to Raúl, my doctorate supervisor, who introduced me to the biomedical engineering-related CFD world and inspired me to get involved in this project. His fruitful discussions on every 'interesting' topic that springs to his mind and the passion and enthusiasm he shows in everything he does have been central in completing this work. Furthermore, from the bottom of my heart, I will always thank him for my free Thursday mornings to go out and take care of my mom.

If the above mentioned have been essential in paving the way for my professional development, I must thank my family for being vital in my personal growth.

I owe a word of thanks to my sisters Nerea and Marta for helping me whenever I need it. And last but not least, I owe a word of gratitude to my parents Jorge and Carmen, who brought me up by setting example, for giving me the opportunity to be part of this wonderful world. I am really proud of having the four of them always by my side. I adore them.

Eskerrik asko!

Jorge Aramburu Montenegro,
Zarautz, December 2016

Abstract

Liver radioembolization is a promising treatment for combating primary and metastatic liver tumors. It consists of administering radioactive microspheres via an intraarterially placed microcatheter with the aim of lodging these microspheres, which are driven by the arterial bloodstream, in the tumoral bed. The position of the microcatheter and the microsphere injection velocity are decided during a pretreatment assessment, by which the treatment is mimicked via the infusion of macroaggregated albumin microparticles.

It is assumed that the pretreatment microcatheter placement and microsphere injection velocity are reproduced during the treatment. Even though it is a safe and effective treatment, some complications (e.g., radiation-induced hepatitis or pneumonitis, gastrointestinal ulcers, etc.) may arise due to nontarget radiation, which can occur due to differences between pretreatment and treatment injection conditions related to microcatheter placement, the injection itself, and the patient's bloodstream.

In terms of microcatheter placement, there are a number of parameters that can vary from pretreatment to treatment. Of those, the ones that are of special interest in this thesis are the longitudinal and radial position of the microcatheter tip, the microcatheter's distal direction, the expandable-tip presence (for antireflux catheters only), and the tip orientation (for angled-tip microcatheters only). As for the injection itself, of the parameters that can be modified, this thesis is most concerned with two of them: the quantity and size of the microagent, and the particle injection velocity. With regard to the bloodstream, the arterial blood flow conditions might vary, e.g., due to microsphere-caused embolization of arterioles, leading to a reflux of microspheres. Any alteration in these parameters may be responsible for nontarget radiation and therefore radiation-induced complications.

In order to reduce these radiation-induced complications, it has been suggested that the pretreatment injection conditions be matched as closely as possible during treatment. An alternative solution is to modify the design of microcatheters. For instance, it has been reported that using an antireflux catheter has eliminated particle reflux.

The aim of this thesis is to analyze the influence of the abovementioned parameters on microsphere distribution via computational fluid–particle dynamics simulations. The thesis is divided into four major studies, each of which follows the same numerical strategy (i.e., the liver radioembolization is simulated in a patient-specific hepatic artery model under literature-based liver cancer scenarios). The first study analyzes the pretreatment as an actual treatment surrogate, the second analyzes the influence of an antireflux catheter, the third investigates the influence of the microcatheter distal direction and the injection point and velocity, and the last one explores the influence of an angled-tip microcatheter. Furthermore, prior to conducting these four studies, a methodology was developed to define realistic boundary conditions for numerical simulations in hepatic arteries.

For the study on the pretreatment, results suggest that microcatheter placement is of paramount importance, both in terms of its location in the artery (near a bifurcation or not) and in the longitudinal shifting in microcatheter tip locations between pretreatment and actual treatment. Moreover, the higher the cancer burden, the better the tumor targeting because of the enhanced particle transport power. For the study on antireflux catheter influence, the main conclusion that can be drawn is that injecting from a sufficiently long and tortuous artery branch may ensure a downstream particle distribution that matches flow split, almost regardless of catheter type due to the likely adequate conditions for microsphere redistribution in the bloodstream. With regard to the third study, despite the importance of microcatheter tip position, microcatheter direction and injection velocity seem also to play an important role in particle distribution; results show that unintentional modifications to microcatheter tip and direction and injection velocity during tumor targeting may influence procedure outcome. The final study involving the angled-tip microcatheter shows that the higher the injection velocity the more spread out the particle distribution across cross-sectional areas of artery lumen. Moreover, when only focusing on tip orientation, it is not possible to accurately predict which branch of the bifurcation will take the particles because the complex geometry of hepatic arteries makes the bloodstream take the form of helical and chaotic streamlines. This means that the particle pathlines are not initially intuitive, even though the particle distribution will be similar to flow split.

Laburpena

Gibeleko erradioenbolizazioa tratamendu bat da tumore hepatiko primarioei eta metastasi hepatikoei aurre egiteko. Arterian kokatutako mikrokateter baten bitartez mikroesfera erradioaktiboak odol-fluxuan injektatzen dira, eta mikroesfera horiek itsatsiak geratzen dira tumoreak odoleztatzen dituzten arterioletan. Tratamendua bera bailitzan egiten den aurretratamenduan erabakitzen dira mikrokateterraren kokapena eta partikulen injekzio-abiadura.

Suposatzen da aurretratamenduan erabakitako mikrokateterraren kokapena eta mikroesferen injekzio-abiadura erabiltzen direla tratamendua egitean. Nahiz eta tratamendu segurua eta eraginkorra izan, tratatu behar ez diren guneen irradiazioaren ondorioz hainbat konplikazio eman daitezke (hepatitis-a, pneumonitis-a, ultzera gastrointestinalak, eta abar). Irradiazio kaltegarri hau gerta daiteke injekzioaren ezaugarriak aurretratamendutik tratamendura alda daitezkeelako. Hauek dira ezaugarri horiek: mikrokateterraren kokapena, injekzioa bera eta odol-fluxua.

Mikrokateterraren kokapenari dagokionez, besteak beste parametro hauek alda daitezke aurretratamendutik tratamendura: mikrokateterraren muturraren posizio longitudinala eta radiala, mikrokateterraren direkzio distala, muturraren irekiera-angelua (errefluxua ekiditen duen kateterretan) eta muturraren orientazioa (muturra 45º-ko angeluan duen mikrokateterretan). Injekzioaren inguruan, parametro hauek alda daitezke: injektatutako partikulen tamaina eta kopurua, eta partikulen injekzio-abiadura, besteak beste. Odol-fluxuari dagokionez, aldaketak egon daitezke arrazoi ezberdinengatik; adibidez, partikulen errefluxua eman daiteke arteriolen enbolizazioa dela eta. Parametro hauen aldaketen

ondorioz emandako irradiazio kaltegarria izan daiteke lehenago aipatutako konplikazioen iturri.

Konplikazio hauen agerraldia ekiditeko, gomendatzen da aurretratamendua eta tratamendua injekzio-ezaugarri berdinekin egitea. Ikerlari askok mikrokateterraren diseinua ere garrantzitsutzat jo dute. Adibidez, esan izan da errefluxua ekiditen duen kateterrari esker partikulen errefluxua desagerrarazi dela.

Tesi honen helburua aipatutako parametroek mikroesferen distribuzioan duten garrantzia ikertzea da. Horretarako, odol-fluxuaren eta partikulen garraioaren simulazio numerikoak egin dira. Lau lan bereiz badaitezke ere, laurek estrategia numeriko berdina dute oinarri: gibeleko erradioenbolizazioaren simulazioa paziente baten arteria hepatikoaren ereduan eta literaturan oinarritutako minbizi-egoerak erabiliz. Lehen lanak aurretratamenduaren eta tratamenduaren arteko desberdintasunak ikertzen ditu. Bigarrenak, errefluxua ekiditen duen kateterraren eragina aztertzen du. Hirugarrenak, mikrokateterraren direkzio distala eta partikulen injekzio-puntua eta injekzio-abiadura ikertzen ditu; eta laugarrenak, muturra 45º-ko angeluan duen mikrokateterraren eragina aztertzen du. Gainera, lan hauek burutu baino lehenago, metodologia bat garatu zen muga-baldintzak definitzeko. Muga-baldintza horiek beharrezkoak dira arteria hepatikoaren odol-fluxuaren simulazio numerikoak egiteko.

Aurretratamenduari buruzko lanari dagokionez, emaitzen arabera oso garrantzitsua da mikrokateterraren kokapena; eragina dute bai arterian zehar mikrokateterrak duen kokapenak (bifurkazio batetik gertu ala ez) eta baita mikrokateterraren muturrak aurretratamenduaren eta tratamenduaren beraren artean jasan ditzakeen mugimendu longitudinal txikiek ere. Gainera, zenbat eta minbizi bolumen handiagoa, hainbat eta hobea izango da tumoreen tratamendua, partikulak garraiatzeko gaitasuna handiagoa baita. Errefluxua ekiditen duen kateterraren eraginaren inguruko lanari buruz atera daitekeen ondorio garrantzitsuena hau da: partikulak nahikoa luzea eta tortuosoa den arteria batetik injektatuz gero, partikulen distribuzioak odol-fluxuaren banaketaren berdina izatera joko du, erabiltzen den kateterra erabiltzen dela, partikulak fluxuarekin lerroka baitaiztezke. Hirugarren lanari dagokionez, aipatzekoa da mikrokateterraren direkzioak eta injekzio-abiadurak garrantzia izan dezaketela partikulen distribuzioan, nahiz eta parametro garrantzitsuena injekzio-puntua izan. Horrela, hiru parametroen aldaketek eragin dezakete tratamendu guztiz ezberdina. Azken lanari buruz, bi puntu azpimarratu beharko lirateke: alde batetik, zenbat eta injekzio-abiadura handiagoa, hainbat eta sakabanatuago bidaiatuko dutela partikulek arterian zehar; bestetik, muturraren orientazioa ere garrantzitsua dela, aldaketak sortzen baititu muturraren inguruko hemodinamikan, zeina, berez, kaotikoa den hepatikoa bezalako arteria konplexuetan.

Resumen

La radioembolización hepática es un tratamiento para combatir tumores hepáticos primarios y metástasis hepáticas. Consiste en administrar microesferas radiactivas mediante un microcatéter situado en la arteria hepática, de modo que esas microesferas, que son llevadas por la corriente sanguínea, se depositan en la malla tumoral. La posición del microcatéter y la velocidad de inyección de las partículas se deciden durante el pretratamiento, mediante el cual se emula el tratamiento por medio de la infusión de micropartículas de macroagregados de albúmina.

Se supone que tanto la posición del microcatéter como la velocidad de inyección se repiten durante el tratamiento. Aunque sea un tratamiento seguro y efectivo, pueden aparecer complicaciones (hepatitis, neumonitis, úlceras gastrointestinales, etc.) por la irradiación de zonas que no debían irradiarse. Esta irradiación no deseada puede deberse a diferencias entre las condiciones de la inyección del pretratamiento y las del tratamiento. Esas condiciones son: el posicionamiento del microcatéter, la inyección y el flujo sanguíneo.

En lo que respecta al posicionamiento del microcatéter, los parámetros que pueden variar del pretratamiento al tratamiento, entre otros, son: las posiciones longitudinal y radial de la punta del microcatéter, el direccionamiento distal del microcatéter, la presencia de una punta expandible (para el caso del catéter antirreflujo) y la orientación de la punta del microcatéter (sólo para los microcatéteres con la punta a 45º). En cuanto a la inyección, los parámetros que pueden ser alterados son: el tamaño y la cantidad del microagente inyectado, y la velocidad de inyección de las partículas, entre otros. En cuanto al flujo sanguíneo, éste puede variar, por ejemplo, debido a la embolización de las arteriolas, lo que

puede conllevar el reflujo de partículas. La variación de los citados parámetros puede ocasionar irradiación no deseada, lo que conlleva complicaciones debidas a dicha irradiación.

Para reducir estas complicaciones, por un lado se ha recomendado ajustar, durante el tratamiento, la posición del microcatéter y la velocidad de inyección definidas durante el pretratamiento. Por otro lado, se han propuesto diferentes diseños de microcatéteres. Por ejemplo, el reflujo de partículas se ha eliminado gracias al catéter antirreflujo.

El objetivo de esta tesis es analizar la influencia de los parámetros citados en la distribución de microesferas mediante simulaciones numéricas del flujo de sangre con transporte de partículas. La tesis se divide en cuatro estudios que siguen la misma estrategia de simulación; es decir, la radioembolización es simulada en un modelo de arteria hepática específica de paciente bajo unos escenarios de cáncer basados en la literatura. El primer estudio analiza las diferencias que pueden darse entre el pretratamiento y el tratamiento. El segundo, estudia la influencia del catéter antirreflujo. El tercero, la influencia de la dirección distal del microcatéter, del punto de inyección y de la velocidad de inyección; y el cuarto, la influencia del microcatéter acabado con la punta a 45º. Además, antes de llevar a cabo estos cuatro estudios se tuvo que desarrollar una metodología para definir condiciones de contorno realistas aplicables a simulaciones numéricas en arterias hepáticas.

En lo que respecta al estudio sobre el pretratamiento, los resultados muestran que la posición del microcatéter es muy importante, tanto en su posición en la arteria (cerca o lejos de una bifurcación) como en pequeños movimientos longitudinales de la punta del microcatéter entre el pretratamiento y el tratamiento. Además, cuanto mayor es el volumen de cáncer, tanto mayor es la capacidad de llegar a los tumores porque aumenta la capacidad de transportar las partículas. En cuanto al estudio sobre el catéter antirreflujo, la conclusión principal es que inyectar en una arteria lo suficientemente larga y tortuosa posibilita el alineamiento de las partículas con el flujo; de modo que, sea cual sea el catéter empleado para la inyección, la distribución de partículas tiende a parecerse a la distribución del flujo de sangre. Con respecto al tercer estudio, se concluye que a pesar de la importancia de la posición de la punta del microcatéter, también son importantes tanto la dirección distal del microcatéter como la velocidad de inyección de las partículas. Así, variaciones involuntarias de cualquiera de los tres parámetros puede conllevar resultados no deseados en el tratamiento. Por último, el cuarto estudio muestra que cuanto mayor es la velocidad de inyección de las partículas, más esparcidas viajan las partículas en el lumen de la arteria. Además, fijándose únicamente en la orientación de la punta del microcatéter no es posible predecir la rama de la bifurcación que van a tomar las partículas porque la complejidad de la geometría de las arterias hepáticas hace que el flujo sanguíneo tome estructuras hemodinámicas helicoidales y caóticas, por lo que la trayectoria de las partículas no es intuitiva, aunque la distribución de las partículas será similar a la del flujo de sangre.

Table of Contents

List of Figures

List of Tables

Nomenclature

List of Symbols

Variable	Unit	Description
A	(GBq)	Activity
A_{resin}	(Bq)	Activity per resin microsphere
A_{Sc1}, A_{Sc2}, A_{Sc3},	(GBq)	Activity for the treatment of each scenario
BSA	(m^2)	Body surface area for activity calculation
C_{D}	(–)	Drag coefficient
C_{V}	(–)	'Virtual mass' coefficient
d	(m)	Internal diameter of the vessel for Womersley number calculation
d_{MAA}	(m)	MAA microparticle diameter
d_{p}	(m)	Particle diameter
d_{resin}	(m)	Resin microsphere diameter
f	(Hz)	Cardiac cycle frequency for Womersley number calculation

$\vec{f}$	(N/kg)	Body force vector per unit fluid mass acting on fluid
$\vec{f}_{\mathrm{D}}$	(N/kg)	Drag force vector per unit particle mass acting on particles
$\vec{f}_{\mathrm{G}}$	(N/kg)	Gravity force vector per unit particle mass acting on particles
$\vec{f}_{\mathrm{P}}$	(N/kg)	Pressure force vector per unit particle mass acting on particles
$\vec{f}_{\mathrm{V}}$	(N/kg)	'Virtual mass' force vector per unit particle mass acting on particles
$\vec{g}$	(m/s^2)	Gravity vector
H	(m)	Patient's height
m	(–)	Outlet counter from 1 to M (in this case, M=29)
M	(–)	Number of outlets (in this case, M=29)
n	(–)	Depth level: the number of bifurcations that blood has passed through before passing through this artery branch, beginning from the inlet of the domain, in which the depth level equals one, until N, the deepest depth level. (In this case, N=10.)
N	(–)	The depth level of the most distal outlet (in this case, N=10)
N_{Sc1}, N_{Sc2}, N_{Sc3},	(–)	Number of resin microspheres for the treatment of each scenario
p	(Pa)	Fluid pressure
q_{inlet}	(mL/min)	Blood flow rate at the inlet
q_m	(mL/min)	Blood flow rate at outlet m
Re_{p}	(–)	Particle Reynolds number
T	(s)	Cardiac pulse period
t	(s)	Time
Δt	(s)	Time-step value

$\vec{u}$	(m/s)	Velocity vector of fluid
$\vec{u}_{\mathrm{p}}$	(m/s)	Particle velocity vector
V	(m^3)	Normal-liver volume
V_{c}	(m^3)	Tumor volume
W	(kg)	Patient's weight
$\dot{\gamma}$	(1/s)	Shear rate of fluid
λ	(1/s)	Shear stress modifier in simplified Quemada model
μ	(Pa·s)	Dynamic viscosity of fluid
μ_0	(Pa·s)	Minimum viscosity in simplified Quemada model
μ_∞	(Pa·s)	Asymptotic viscosity in simplified Quemada model
ρ	(kg/m^3)	Density of fluid
ρ_{MAA}	(kg/m^3)	Density of MAA microparticles
ρ_{p}	(kg/m^3)	Density of particles
ρ_{resin}	(kg/m^3)	Density of resin microspheres
$\bar{\bar{\tau}}$	(Pa)	Stress tensor
τ_0	(Pa)	Apparent yield stress in simplified Quemada model
ϕ_{MAA}	(–)	Shape factor for MAA microparticles
ϕ_{resin}	(–)	Shape factor for resin microspheres

Subscripts

0	For minimum viscosity of apparent yield stress in simplified Quemada model
∞	Asymptotic value (in simplified Quemada viscosity model)
c	Related to cancer
D	Related to drag force on particles
G	Related to gravity force on particles

inlet	The variable at the inlet
m	Outlet counter from 1 to 29
MAA	Related to macroaggregated albumin microparticles
p	Related to particles
P	Related to pressure force on particles
resin	Related to resin microspheres
Sc1–Sc3	Related to treatments for cancer scenarios 1 to 3
V	Related to 'virtual mass' force

Abbreviations

AASLD	American Association for the Study of Liver Diseases
ARC	Antireflux catheter
ATM	Angled-tip microcatheter
BC	Boundary condition
Bif.	Bifurcation
CFD	Computational fluid dynamics
CFPD	Computational fluid–particle dynamics
CHA	Common hepatic artery
CMMP	Computational medical management program
DL	Depth level (of an artery branch)
EASL	European Association for the Study of the Liver
eqn.	Equation
FSI	Fluid–structure interaction
GDA	Gastroduodenal artery
HA	Hepatic artery
HABR	Hepatic arterial buffer response

Inl.	Inlet
LHA	Left hepatic artery
MAA	Macroaggregated albumin
M01 to M17	Computational domain meshes from mesh 1 to mesh 17
MSA	Microsphere supply apparatus
OP	Operating system
PHA	Proper hepatic artery
PRM	Particle release map
RE	Radioembolization
RHA	Right hepatic artery
S1 to S8	Liver segments from segment 1 to segment 8
Sc0 to Sc3	Scenarios from scenario 0 to scenario 3
SM	Smart microcatheter
SMA	Superior mesenteric artery
SMC	Standard end-hole microcatheter

Chapter 1

Introduction

"*Dreams without goals are just dreams and they ultimately fuel disappointment. So have dreams, but have goals; life goals, yearly goals, monthly goals, daily goals. I try to give myself a goal every day*" Denzel Washington during the commencement address at Dillard University in 2015

This introductory chapter provides the research motivation and objectives, together with a brief and concise description of the state of the art, in which only the aspects of liver radioembolization (RE) that have to do with the present thesis are explicitly specified. Furthermore, the connection between numerical simulations and RE is described and the structure of this dissertation is presented.

1.1 Research motivation

Multidisciplinarity is becoming prevalent when trying to rise to big challenges, and so is happening in the medical field. For instance, liver RE, which consists of the catheter-based intraarterial injection of radiation-emitting microspheres to locally

attack tumors, is a complex treatment that involves specialists from many medical fields, such as interventional radiology, radiation oncology, nuclear medicine, medical physics, hepatology, surgical oncology, medical oncology, and radiation safety. Because of this complexity, new sources of major discussion arise among practitioners [1].

The underlying hypothesis for this work is that engineers might shed some light on the discussed matters, by using computational fluid–particle dynamics (CFPD) tools.

Hence, being able to provide CFPD-based insights into matters that concern physicians is what motivates this piece of research.

1.2 Research objectives

The general aim of the research is to numerically address the RE-related questions that can be tackled from the particle–hemodynamics standpoint via a coupled Euler–Lagrange CFPD framework applied to a patient-specific hepatic artery under literature-based cancer scenarios. In particular, the following specific goals are set:

- Objective I: To analyze whether the RE pretreatment is a sufficient surrogate of the actual RE in terms of microagent distribution over the segments of the segments.
- Objective II: To analyze the influence of the catheter type (standard end-hole microcatheter, SMC, vs. antireflux catheter, ARC) and location on segment-to-segment microsphere distribution during RE.
- Objective III: To analyze the influence of the microcatheter distal direction and microsphere injection point and velocity on segment-to-segment microsphere distribution during RE.
- Objective IV: To analyze the influence of the orientation of an angled-tip microcatheter (ATM) and microsphere injection velocity on segment-to-segment microsphere distribution during RE.

Note that the first stage of the particle travel in the arterial bloodstream is considered, i.e., from the injection point to the segmental and subsegmental level. Analyzing the intrasegmental capillary-level blood-flow–particle-transport, particle distribution and lodging, and the effect of radiation on tumor tissue, all of which involve blood flow through complex tumor-related vasculature [2] and particle transport phenomena [3], among other phenomena, is beyond the scope of the present work.

1.3 State of the art

In this section, in-a-nutshell versions of the liver, liver cancer, and liver RE are presented. These subsections aim to provide the general understanding of RE that is necessary to comprehend the studies that have been carried out in the present thesis. Additionally, some good reads are recommended for further information on these topics. Moreover, the RE-related numerical studies that have been published in the literature are set forth.

1.3.1 The liver: general remarks

The liver is one of the most important organs in the human body. Indeed, the significance of the liver has been recognized since ancient times. According to Greek mythology, Zeus punished Prometheus to be eternally chained to a rock and have his liver eaten by an eagle every day for having stolen fire from Mount Olympus and giving it to humans (https://en.wikipedia.org/wiki/Prometheus).

The main functions of the liver include production and secretion of proteins, breakdown of hormones and toxins, and storing of high-energy substances such as glucose, etc. The liver also works as a blood volume reservoir [4].

The liver is unique due to its dual blood supply. From the macroscale standpoint, the hepatic artery system provides well-oxygenated blood, accounting for 20–40% of the total liver blood supply, whereas the portal venous system, accounting for the rest 60–80%, delivers nutrient-rich and partially deoxygenated blood from the digestive organs. Drainage is done via the hepatic vein system [4]. The anatomy of the liver had been historically classified based on the external appearance, while in the last decade different functional anatomies have been defined based on the aforementioned vessels that supply and drain the liver [5]. In line with this, Couinaud divided the liver into eight segments (S1–S8), based on the third order portal vein distribution [6]. Figure 1.1 illustrates Couinaud's hepatic segmental distribution and the vessels involved in the blood supply and drainage.

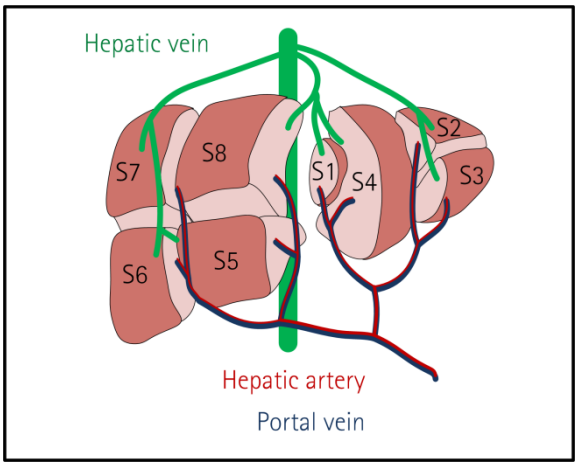

Figure 1.1: Liver segments 1 to 8 as defined by Couinaud [6], the hepatic artery and the portal vein for blood supply, and the hepatic vein for drainage.

From the microscale point of view, the liver is mainly made of hepatocytes, which are arranged in hexagonal functional segments, namely liver lobules. In the classic liver lobule definition, the central vein is in the center and a portal triad is located in each corner. These portal triads consist of a bile duct, a hepatic arteriole, and a portal venule. The bile duct gathers and drains bile. On its path from the portal triads to the central vein, blood is guided through columns of hepatocytes, that is, the liver-specific capillaries called sinusoids. Figure 1.2 illustrates a hepatic lobule and the vessels involved in the blood supply and drainage.

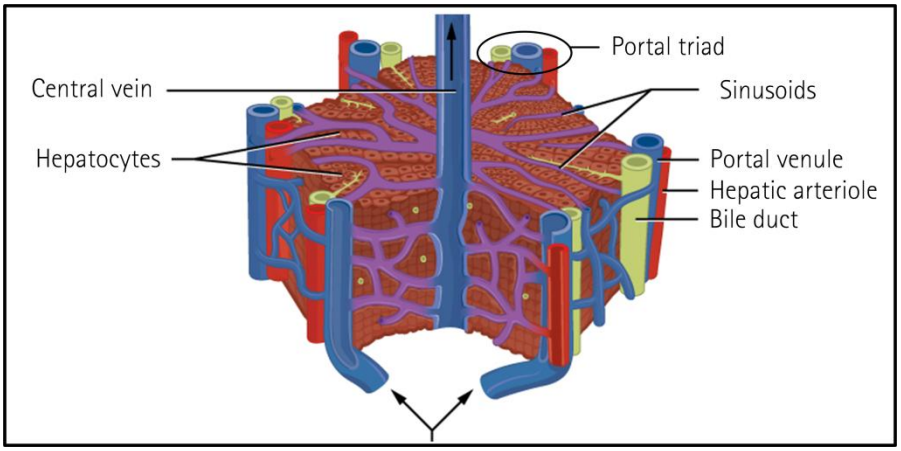

Figure 1.2: Classic liver lobule definition: The central vein in the center and a portal triad in each corner. (The original image of the lobule was obtained from Wikipedia.)

Another characteristic specific to the liver is the so-called hepatic arterial buffer response (HABR) [7], which is also related to its dual blood supply. This HABR is a mechanism that controls and allows constancy of hepatic blood flow and essentially consists of the hepatic artery ability to produce compensatory flow changes in response to changes in portal venous flow [8].

1.3.2 Liver cancer

Liver cancer is the second leading cause of cancer-related deaths worldwide, with an estimated 745,500 deaths in 2012 [9]. Hepatocellular carcinoma (HCC) represents approximately 90% of all cases of primary cancer in the liver [10], which is a predominant location for metastatic cancer. Indeed, 60–80% of patients with colorectal carcinoma, pancreatic carcinoma, breast carcinoma, and other types will develop liver metastases [11].

Depending on the stage, size, and location of the tumors, the objective of the treatment can be to cure, to downstage for subsequent surgery, or to obtain palliation. Table 1.1 tabulates the treatment options that are listed in Llovet et al. [10] for the treatment of HCC. Most of them are also applicable to other primary and metastatic liver cancer. For more specific details on these treatments refer to Llovet et al. [10].

Note: for more information on liver cancer characteristics that are not essential for the purpose of the present thesis and are therefore not specified here, i.e., incidence and mortality rates worldwide, risk factors for developing liver cancer, molecular pathogenesis and classification, surveillance and detection programs, disease management, etc. several text published in the literature can be consulted. For example, Torre et al. [9], Llovet et al. [10], and El-Serag [12].

Table 1.1: Arrangement of the treatments for HCC based on category, whether or not they are accepted in the guidelines of European Association for the Study of the Liver (EASL) and American Association for the Study of Liver Diseases (AASLD), and whether or not they are areas of ongoing research. (Information taken from Llovet et al. [10])

Category	Treatment	Accepted[†]	Investigated[††]
Surgical treatment	Resection	X	X
	Liver transplantation	X	X
Locoregional treatment	Local ablation	X	
	Other ablative therapies (microwave, cryoablation, laser, irreversible electroporation, high-intensity focused ultrasound)		X
	Chemoembolization	X	X
	Radioembolization		X
	External 3D conformal radiotherapy		X
Systemic treatment	Sorafenib	X	
	Chemotherapy and hormonal compounds		X
	Other molecular targeted therapies		X
Palliative care	Palliative support	X	
	Radiotherapy to alleviate pain		X

[†] Treatments accepted in EASL and AASLD guidelines. [††] Treatments under investigation or that require further evidence before being included into guidelines.

1.3.3 Liver radioembolization

Since the 1990s, liver RE has emerged as a safe and effective treatment for unresectable and chemorefractory primary [13] and metastatic [14] liver malignancies [1,15]. However, RE is still in its infancy. Even though it was reported for the first time in the 1960s [16], a standardization of terminology and reporting criteria has been established recently due to the growing use of this therapy [17], and it has been catalogued by Llovet et al. [10] as a treatment under investigation (see Table 1.1). Furthermore, there is an increasing body of evidence supporting that RE is a promising treatment option for combating not only tumors in advanced stage as palliative care, but also tumors at early and intermediate stages with curative intent or with downstaging intention for subsequent transplantation. The

outcomes of performing RE to a wide range of tumors are being investigated via clinical trials. These tumors include HCC, metastatic colorectal cancer, and neuroendrocrine tumors, among others [18].

By taking advantage of the dual blood supply to the liver (60–80% via portal vein and 20–40% via hepatic artery) and the preferential arterial blood supply of tumors [19], RE consists of intraarterially administering via catheter ^{90}Y-labeled resin or glass microspheres (^{90}Y is a pure beta emitter with a 2.6-day half-life and a average tissue penetration of 2.5 mm), which are infused into the bloodstream at the hepatic artery and work as radiation emitters, selectively delivering high doses of radiation to tumors and avoiding excessive radiation of the normal liver parenchyma [20,21].

This therapeutic strategy is a complex and multidisciplinary approach that involves specialists from many different medical fields, such as interventional radiology, radiation oncology, nuclear medicine, medical physics, hepatology, surgical oncology, medical oncology, and radiation safety. Because of this complexity and multidisciplinarity, in order to deem a patient as being suitable for undergoing RE, a meticulous pretreatment assessment is routinely carried out. This pretreatment consists of three parts. First, the arterial configuration is analyzed and the hepatic lesions are assessed via a computed tomography and magnetic resonance imaging arteriography. Second, various arteries are occluded in order to reduce extrahepatic diffusion of microspheres. Third, RE is simulated by means of infusing ^{99m}Tc-labeled maccroaggregated albumin (MAA) in order to assess hepatopulmonary shunt and detect gastrointestinal deposition [22]. These pretreatment results can also be used to estimate the dose that is going to be absorbed in both normal and tumor tissues during RE [23].

Even though it is a safe and effective treatment, some patients may develop complications due to nontarget radiation (radiation-induced hepatitis or pneumonitis, gastrointestinal ulcers, etc.) [18,21,24]. In reducing these complications, several investigations have been carried out.

One of the research lines involves the analysis of to what extent the pretreatment mimics the actual RE treatment. Jiang et al. [25] analyzed 81 paired ^{99m}Tc-MAA hepatic perfusion imaging and post-RE ^{90}Y imaging cases in order to determine possible incidences that may play a role in segmental perfusion differences. They defined a pair as showing segmental perfusion differences if the mismatch involved a least one hepatic segment (according to Couinaud's [6] hepatic distribution). The

variables analyzed were difference in microcatheter tip position along the artery, the presence of an arterial bifurcation close to the microcatheter tip, and the presence of a small arterial branch near the microcatheter tip. The combination of a difference in microcatheter tip position and the presence of either a bifurcation or an arterial branch near the microcatheter tip was statistically significant in the group of pairs that showed segmental perfusion differences (21 out of 31) between RE pretreatment and actual treatment.

Wondergem et al. [26] analyzed 39 paired ^{99m}Tc-MAA hepatic perfusion imaging and post-RE ^{90}Y imaging cases in order to study differences in intrahepatic distribution. In total, 225 liver segments (according to Couinaud's [6] hepatic distribution) were analyzed. Differences in mean activity per milliliter greater than 10%, 20%, and 30% were found in 153 (68%), 97 (43%), and 72 (32%) segments, respectively. The effect of tumor load, microcatheter position, and the proximity of a bifurcation near the microcatheter tip were analyzed. Tumor load was found to play and important role, as the greater the tumor involvement, the smaller the disagreement. Microcatheter tip position difference and the presence of a bifurcation near the microcatheter tip during pretreatment and actual treatment were likewise found to be important. They concluded that the limited agreement (between pretreatment and actual treatment images) should be taken into account when calculating the dose to be administered in clinical practice. However, after this study was published, Kao [27] and Lam et al. [28] stated that the results are not as discouraging as Wondergem et al. [26] reported.

Ulrich et al. [29] studied whether the intratumoral ^{99m}Tc-MAA uptake in colorectal liver metastases was predictive for the RE response. Lesion-based and patient-based responses were evaluated using the Response Evaluation Criteria in Solid Tumors 1.1 guidelines [30]. They found that there is no statistical significance in the relationship between tumor response to RE and ^{99m}Tc-MAA uptake, tumor response and microcatheter tip position, and tumor response and the interaction of ^{99m}Tc-MAA uptake and microcatheter position. A similar study was previously carried out by Dhabuwala et al. [31], where they concluded that ^{99m}Tc-MAA uptake is not a predictor of tumor response after RE. Based on Ulrich et al.'s [29] study, Lam and Smits [32] and Ulrich et al. [33] discussed the methodology for relating the ^{99m}Tc-MAA uptake and tumor response. Lam and Smits suggested a step-wise methodology: first, analyze the ^{99m}Tc-MAA uptake and post-RE ^{90}Y distribution, both of which depend on technical aspects of RE; second, analyze the ^{90}Y distribution and tumor response, which depends on clinical and biological aspects. Also, based on

Ulrich et al.'s [29] study, a more in-depth discussion arose between Chiesa et al. [34] and Amthauer et al. [35], where the quantification method, the lack of dosimetric evaluation, the radiologic evaluation of response, and the microcatheter position were discussed, as well as the possible extrapolation of their conclusions to the possible results of other cancer types, the type of RE microspheres, and the possibility of there being an embolic effect instead of an induced-by-radiation effect for the response of lesions with a low degree of ^{99m}Tc-MAA uptake.

Another research line focuses on the design of the microcatheters, which has been claimed as important in solving the issues regarding a patient's suitability to undergo RE and in avoiding nontarget gastrointestinal irradiation. In this regard, one particular antireflux catheter (ARC) (Surefire® Infusion System; Surefire Medical, Inc., Westminster, CO, USA) has emerged as an innovative and potentially cost-effective approach [36]. This ARC has a funnel-shaped expandable tip, which prevents retrograde flow when fully expanded [37]. Several in vivo, ex vivo, in vitro, and in silico studies have analyzed the qualities of the ARC.

Rose et al. [37] analyzed (in vivo) the downstream arterial pressure changes due to the ARC tip deployment in 18 patients (a total of 29 liver chemoembolization or RE procedures). Due to the tip-deployment-caused pressure decrease they measured, they came to the conclusion that the use of ARC not only prevents the particle upstream reflux, but also creates a low-pressure-based hepatopetal flow, which prevents the extrahepatic deposition of microagents.

Arepally et al. [38] evaluated (ex vivo) in a porcine model (three swine) the possibility of quantifying the reflux and the nontarget embolization by injecting radiopaque tantalum microspheres in the renal arteries. In the right renal artery they employed the ARC, while in the left renal artery they used a standard end-hole microcatheter (SMC). Based on their results, they reached the conclusions that the ARC permits both the near-complete reflux elimination and a deeper penetration of microspheres.

In an in vivo study, van den Hoven et al. [39] evaluated for three patients the outcomes of RE without coil embolizing. They pointed out successful therapies. In addition, it is worth mentioning that one of the patients would have been deemed unsuitable for conventional RE since cannot be coil embolized. In conclusion, although they call for further research regarding safety issues, they reported that the use of ARC seems a highly promising option, especially for patients that cannot

be treated with SMCs, because they did not observe extrahepatic microsphere deposition despite the absence of coil embolization.

Pasciak et al. [40] analyzed (in vivo), for nine patients, the differences in particle distribution when SMC or ARC was employed during the pretreatment with ^{99m}Tc-MAA (ARC was used during the treatment). They observed, on average, a 58% reduction in nontarget area deposition and a 68% increase in tumor deposition when using ARC compared to SMC. Furthermore, they noted that infusing the ^{90}Y resin microspheres with ARC during actual RE led to excellent agreement between the pretreatment and treatment particle deposition.

In an in vitro study, van den Hoven et al. [41] analyzed the differences between injecting via a SMC or an ARC. They experimentally simulated the particle injection and tracked the particle travel. Regarding the SMC, they observed a random position of the microcatheter tip, with the particles entering the bloodstream in a laminar-like fashion, and being distributed over the branches nonhomogeneously. As for the ARC, the experiments showed centered catheter tip position, with the particles entering the bloodstream in a turbulent-like manner, and being distributed in a more homogeneous way.

Xu et al. [42] modeled and analyzed (in silico) for a realistic hepatic artery system the relationship between the pressure drop across the ARC expandable tip and the embolization level of the downstream vasculature.

The last research line among those that are focused on reducing nontarget irradiation is the innovative strategy that has been defined by Kleinstreuer and colleagues as 'direct drug-targeting strategy' [43]. This strategy addresses tumor targeting and the healthy-tissue sparing, and involves a computer-controlled procedure, contrary to the everyday practice by which the microspheres are manually injected. In developing this procedure, not only was the injection position in the cross-sectional area of the artery lumen studied for a representative hepatic artery system [44–50], but so was the microsphere injection velocity [46–48]. Moreover, the best temporal interval in the cardiac cycle for injecting particles was analyzed [45,46,48–50]. Furthermore, a controllable catheter was developed and the influence of that catheter's presence on particle distribution was investigated [46,47].

Note: for detailed aspects of RE-related topics the book by Bilbao and Reiser [18] should be consulted. This book is written by up to 35 experts in the field and collects in-depth explanations of RE-related topics in well-structured 18 chapters.

1.3.4 Numerical studies on 'direct drug-targeting strategy'

The direct drug-targeting strategy developed by Kleinstreuer and colleagues has been proposed as part of a bigger program called the Computational Medical Management Program (CMMP), which seeks the inclusion of the direct drug-targeting strategy into clinical practice. This CMMP consists of three stages: patient evaluation, computer modeling, and clinical implementation [43]. Within the second stage, computer simulations are performed. The aim of these computer simulations is to determine the optimal delivery characteristics (e.g., microcatheter position, particle injection velocity, etc.) in terms of targeting tumor-bearing liver segments and avoiding normal liver and other organ bombarding. In order to develop the methodology, one-way coupled blood flow and particle transport phenomena were numerically simulated in representative and patient-inspired truncated hepatic arteries. If incorporated into clinical practice, the computational domain would be patient specific. The following paragraphs detail the series of numerical studies published in the literature about this innovative strategy because computer simulations of similar characteristics were run for the present thesis.

Kennedy et al. [44] analyzed the dependence of boundary conditions (BCs) at the outlets on flow split and exiting-particle distribution when injected with the same velocity as blood and with two different particle concentration profiles (uniform and parabolic) through a cross-sectional area at the common hepatic artery (CHA). This study consisted of numerical steady-state simulations of particle–hemodynamics in a representative hepatic artery (HA) system. This HA system includes the CHA, which splits into the gastroduodenal artery (GDA) and the proper hepatic artery (PHA), which bifurcates into the right and left hepatic arteries (RHA and LHA), both of which further bifurcate into two daughter segmental vessels. Each injected particle was tracked and the exiting branches of particles were recorded. The authors concluded that BCs are important in terms of flow split and particle distribution. The particle concentration profile in the cross-sectional area is also important in particle distribution. Moreover, the particle distribution tends to match the flow split when the particle concentration profile is parabolic. Later on, Richards et al. [51] validated experimentally this modeling approach.

Basciano et al. [45] studied the transient computational particle–hemodynamics in the same representative HA system as Kennedy et al. [44] did. In this study, resin SIR-Spheres® (Sirtex Medical Limited, Australia) and glass TheraSpheres® (MDS Nordion Inc., Canada) were modeled according to their actual physical characteristics. In addition to the characteristics of the microspheres, the injection characteristics (temporal and spatial points) were analyzed, as well as the influence of the restitution coefficients of particle–wall collisions on particle distribution. Particle release maps (PRMs) were defined for the first time. These PRMs correlate each injection point of the injection cross-sectional area and the exiting branch of the HA system. According to the authors, injecting during the systolic peak reduces the influence of the particle characteristics in its trajectory and particles travel less dispersed. However, when injecting during the diastole the particle characteristics become more important and particles travel more dispersed. Furthermore, determining PRMs for different temporal points allows the selection of the most appropriate injection point (both spatial and temporal) to target the desired branch.

At that time Kleinstreuer patented a computer-controlled microcatheter, i.e., the smart microcatheter (SM), whose tip can be positioned in the desired location within the cross-sectional area of the artery lumen [52]. Once the SM had been patented, Kleinstreuer et al. [47] analyzed in the aforementioned representative HA the influence of the SM in the pulsatile particle–hemodynamics. The injection velocity of particles was also addressed via steady particle–hemodynamics. Results showed that the presence of the SM only affects locally and modifies the PRMs with respect to the case where there is no SM. This influence is dispersed due to the viscous dissipation and the BCs at the outlets. On the other hand, the injection velocity can alter the endpoint dictated by the PRM, because particle inertia increases as injection velocity increases and they can cross blood streamlines.

Therefore, up to this point, how the microcatheter positioning and the injection velocity, duration, and specific point in the cardiac cycle alter the particle–hemodynamics had been analyzed.

Childress et al. [46] defined what CMMP is and used another geometric model for the first time. This model is a patient-inspired HA that includes the superior mesenteric artery (SMA), which gives rise to the CHA, from which the RHA and LHA arise. In the previous study (Kleinstreuer et al. [47]) the best temporal point for injecting particles had been determined. However, the treatment could take a long time to be completed. In order to reduce the treatment time to reasonable duration, the composite particle release map (CPRM) was defined. This CPRM is defined by

combining the PRM results for ten injection intervals of the cardiac cycle. The concept of CPRMs is applied to both the representative and patient-inspired HAs. Another device that was patented by Kleinstreuer was the microsphere supply apparatus (MSA), by which particles are injected with a certain velocity profile (i.e., the injection velocity as a function of time). This work also studied different injection velocity profiles such as 'step', 'ramp-up, ramp-down', 'ramp-up', and 'S-curve' profiles. They highlighted the possibility of determining CPRMs, together with the spatial and temporal points for injection. They also indicated that injection with 'S-curve' profile is the safest one because particles do not disperse when leaving the microcatheter, and that injection with 'step' profile is the least safe because particles tend to disperse when leaving the microcatheter.

Meanwhile, Basciano et al. [48] published the most relevant results and conclusions of the previous works, stressing the importance of the resistive behavior of the downstream vasculature, the anatomy and morphology of vessels, the injection velocity, and the spatial and temporal points.

In order to overcome the limitation of rigid walls of the arteries, Childress and Kleinstreuer [50] studied the fluid–structure interaction (FSI) of blood flow (with particle transport) and artery wall. They performed a FSI simulation and compared it to two computational particle–hemodynamics simulations, where artery walls were assumed rigid. These rigid geometries were the geometry of the representative HA system during the diastole and the time-averaged geometry resulting from the FSI simulation. They concluded that the optimum interval for injection might be during the diastole because the changes in artery diameters were smaller than in other intervals. Furthermore, they pointed out that the best rigid geometry is the one that better reproduces the flexible geometry during the injection interval and they recommended not simulating via FSI due to high computational cost in favor of CFPD simulations.

In reducing the computational cost of computer simulations, Childress and Kleinstreuer [49] analyzed whether it is possible to simulate steady-state FSI simulations (instead of pulsatile FSI simulations) when studying PRMs. They simulated one transient simulation and 27 steady simulations. Some of the conclusions that they reached include the following ones: injecting during the diastole enables the longest injection interval due to the semi-steady behavior for almost half of the cardiac cycle; the steady state of the average flow and pressure could be a valuable case between the systole and the diastole, and so could be the steady state of averaged values during the diastole if the injection was done during

the diastole; the methodology is very efficient and sufficiently precise for the transient phenomena of particle–hemodynamics.

1.4 Connection between CFPD and RE

The aim of this section is to explain the connection between CFPD simulations and RE treatment. The former is the mathematical tool that is used to simulate the particle–hemodynamics that takes place during the latter in the hepatic arteries. As explained in '1.1 Research motivation', the motivation behind this investigation is to provide CFPD-based insights in RE-related matters.

The results of numerical simulations depend mainly on the following elements:

- Fluid–particle dynamics modeling (explained in '2.3 Fluid–particle dynamics theory')
- Geometric domain (explained in '2.4 Computational domains')
- Boundary conditions (explained in '2.5 Boundary conditions')

The outcome of RE in terms of segment-to-segment particle distribution depends on three main injection conditions, each of which includes more specific parameters. The injection conditions and specific parameters for each condition that affect the RE outcome are listed below:

- Injection
    - Microparticle size and quantity
    - Injection velocity
    - Particle concentration profile
    - Injection temporal point
- Bloodstream
    - Liver state
- Microcatheter placement
    - Microcatheter position along the artery
    - Longitudinal shift of the microcatheter tip
    - Radial shift of the microcatheter tip
    - Microcatheter distal direction
    - Expandable-tip presence (for ARC)
    - Angled-tip orientation (for ATM)

There are two additional parameters that affect the particle–hemodynamics but they are not related to the main three injection conditions:

- Microcatheter presence (although every injection implies a microcatheter, this parameter was studied because previous numerical studies on RE did not model the microcatheter when injecting microspheres [46,47])
- HA geometry

The 13 parameters listed above influence the particle–hemodynamics from a fluid–particle dynamics standpoint. Note that analyzing possible real-life events (e.g., patient motion, respiration, and arterial response to the presence of particles, among others) are neglected (see '4.3 Study limitations'). The first 11 parameters have been related to the three main injection conditions, and all 13 can be related to the three elements that influence numerical simulations. For example, 'microparticle size and quantity' has to do with 'fluid–particle dynamics modeling'. The parameters related to 'boundary conditions' are 'injection velocity', 'particle concentration profile', 'injection temporal point', and 'liver state'. The rest are related to 'geometry'.

Given that it is the interventional radiologist who actively controls the microcatheter positioning and particle injection force, another parameter, 'reproducibility', can be defined. This parameter is the ability of the interventional radiologist to match each of the 13 parameters during both pretreatment and actual treatment. The criterion for setting high reproducibility, H, or low reproducibility, L, is personal and is based on the idea that the interventional radiologist manually controls the microcatheter positioning and the particle injection force. Therefore, in general the reproducibility of most parameters is low, except for 'microparticle size and quantity' (which is supplied by the manufacturer), 'injection velocity' (practitioners usually inject at a constant velocity), and 'microcatheter position along the artery' (for example, interventional radiologists can visually determine whether or not they are near a bifurcation).

Furthermore, some of the 13 parameters have been already studied via clinical and numerical studies (see '1.3.3 Liver radioembolization' and '1.3.4 Numerical studies on 'direct drug-targeting strategy''). In clarifying the ideas pointed out so far, Table 1.2 summarizes the 13 parameters that influence the outcome of RE, the relationship of the parameters with numerical simulation elements, the relationship of the parameters with RE injection conditions, the reproducibility of the parameters, and the studies that have analyzed each parameter. Moreover, the parameters that are studied in this thesis are in italics, and those that are being analyzed for the first time are in bold. Furthermore, Figure 1.3 illustrates the parameters related to 'injection', 'bloodstream', and 'microcatheter placement' conditions for RE injection.

Table 1.2: Parameters that can affect the outcome of RE in terms of segment-to-segment particle distribution. The parameters' relationship to numerical simulation elements and RE injection conditions are included, as well as the reproducibility of each parameter and the reference to clinical and numerical studies. The parameters that are studied in this thesis are in italics, and those that are being studied for the first time are in bold.

CFPD simulation elements	Parameters that can affect the outcome of RE	Repro-ducibility	References	RE injection conditions
Fluid–particle dynamics	*Microparticle size and quantity*	H	[45]	Injection
Boundary conditions	*Injection velocity*	H	[46–48]	
	Particle concentration profile	L	[44]	
	Injection temporal point	L	[45,46,48–50]	
	Liver state	L	[44,48]	Bloodstream
Geometry	***Catheter position along the artery***	H	–	Microcatheter placement
	Longitudinal shift of the tip	L	–	
	Radial shift of the tip	L	[44–51]	
	Microcatheter distal direction	L	–	
	Expandable-tip presence (for ARC)	L	[37–42]	
	Angled-tip orientation (for ATM)	L	–	
	Microcatheter presence	–	[46,47]	
	HA geometry	–	[46,48]	

To sum up, in order to fulfill the objectives listed in '1.2 Research objectives', this thesis is divided into four major studies that investigate the nine parameters that are in italics in Table 1.2, that is, 'microparticle size and quantity', 'injection velocity', 'liver state', 'catheter positioning along the artery', 'longitudinal shift of the tip', 'radial shift of the tip', 'microcatheter distal direction', 'expandable tip presence (for ARC)', and 'angled-tip orientation (for ATM)'.

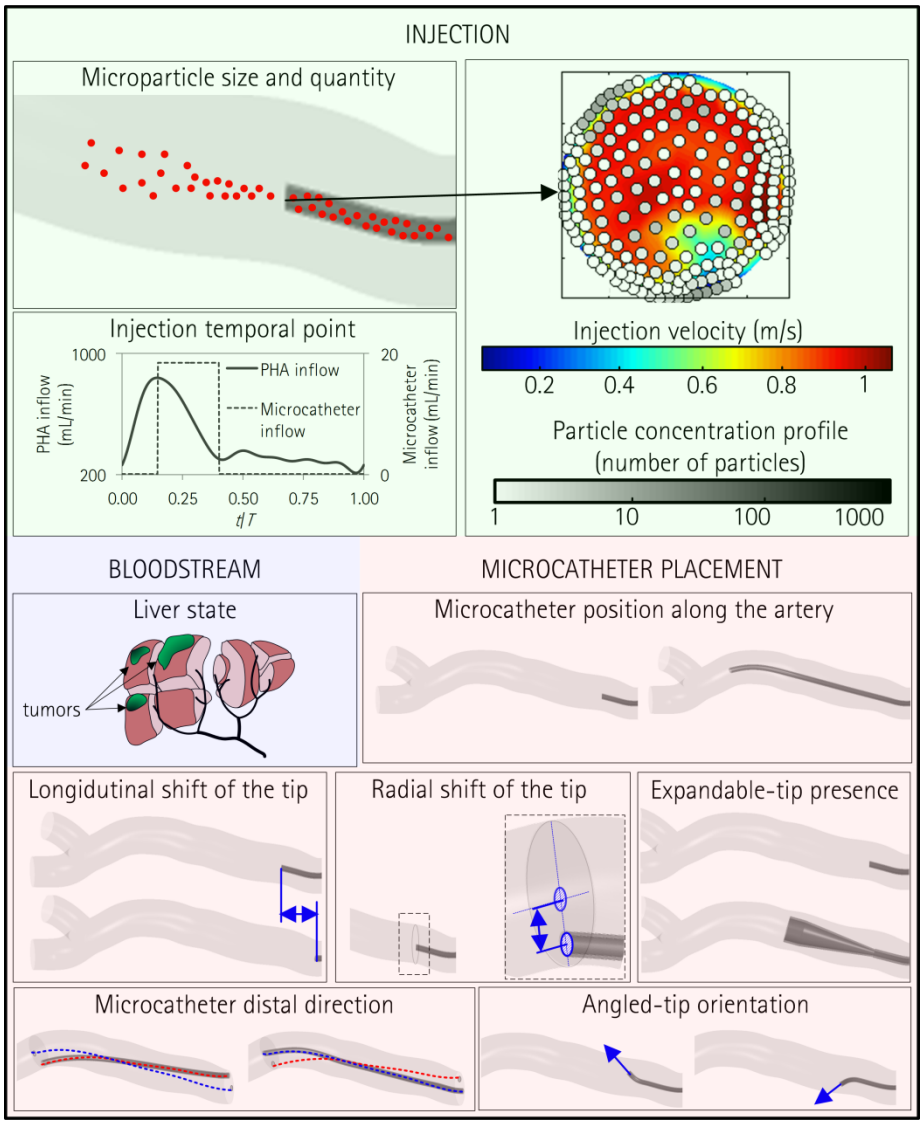

Figure 1.3: Parameters related to RE injection conditions 'injection', 'bloodstream', and 'microcatheter placement'.

1.5 Chapter overview

This dissertation provides a home for publications by the author and aims to connect them in a well-organized manner. In order to do so, the present thesis consists of five chapters and three appendices. This introductory chapter presents the research motivation and objectives, together with a brief and concise description of the state of the art, in which only the aspects of RE that has to do with the present thesis are explicitly specified, along with the bare bones of the connection between CFPD and RE. The second chapter, 'Methods', includes the basics of the modeling approaches that have been adopted, and defines the studies that have been carried out. The third chapter, 'Results and Discussion' provides the results and discussion of the four studies defined in Chapter 2. The fourth chapter, 'Concluding Remarks', sums up the contributions made by this thesis, the conclusions of the four studies carried out, the study limitations, and the closing thoughts. The last chapter, 'Bibliography', provides the references to the works cited throughout the thesis.

Regarding the appendices, Appendix A, 'Approach Justification', discusses six important modeling approaches that are not discussed in the chapters. Appendix B, 'Copyright Permissions', includes the permissions to reuse the published papers. Finally, Appendix C, 'Papers', includes the papers that have been published.

Chapter 2

Methods

"*All models are wrong, but some models are useful*" George E. P. Box

---

This chapter includes the basics of the modeling approaches that have been adopted, and defines the studies that have been carried out. As regards the modeling, a fictional patient, Matthew, has been postulated, the fluid–particle dynamics theory is explained, and the numerical settings are specified, i.e., computational domains, BCs, and solution method.

2.1 Patient description and radioembolization planning

2.1.1 Patient history and hepatic artery

It is my honor to introduce Matthew to you. Matthew is our fictional, yet unfortunate patient. He is a 1.76-m and 74-kg male. In 2008, at the age of 49, he was diagnosed with colorectal cancer. As a standard medical practice, he had his liver explored to see whether the cancer had metastasized. No metastasis was observed then. This stage is named scenario 0 (Sc0). By 2010, the cancer had metastasized into the liver, specifically the right lobe, with a 10% liver involvement.

This is the scenario 1 (Sc1). Having a liver-dominant disease, first- and second-line therapies failed and the treatment with ^{90}Y was considered. Matthew undergone liver RE, but his misfortune did not end. In 2013, it was observed that 30% of the liver was occupied by colorectal metastases. Another RE was planned for this new stage: scenario 2 (Sc2). Matthew's liver seemed to heal at first, but in 2015, at the age of 56, even if some metastases had reduced its size, others appeared. As a result, another RE was planned for this scenario 3 (Sc3).

Table 2.1 tabulates and Figure 2.1 illustrates the liver volumes per liver segment at each scenario. Couinaud's hepatic segment classification was adopted [6], i.e., from S1to S8. The total volume for healthy/normal tissue (1510 mL) and the total cancer volume for the 30% liver involvement (647 mL) were taken from the average volumes of the control and patient groups reported by Oktar et al. [53]. The 10% liver involvement scenario (Sc1) was not taken directly from literature, but it was a realistic case. The distribution of normal volume over segments was done using the percentage values reported by Mise et al. [54], whereas the distribution of tumor volume over the segments was done in such a way that different studies can be conducted. It should be clarified that 'normal tissue' corresponds to the healthy tissue of a tumor-bearing liver, that is, 'healthy tissue' is used when referring to Sc0, whereas 'normal tissue' is used when referring to the healthy tissue in Sc1–Sc3.

Table 2.1: Healthy, normal, and tumor tissue volume per segment for each scenario.

Segment	Sc0[†] (mL)	Sc1[††] (mL)	Sc2[††] (mL)	Sc3[††] (mL)
S1	70.30	–	–	15.87
S2	157.76	–	–	106.40
S3	157.37	–	–	106.39
S4	239.09	–	–	54.00
S5	151.70	–	100	107.85
S6	193.10	56	147	97.88
S7	155.30	–	100	106.98
S8	385.39	112	300	51.55
Total	1510.0	168	647	647

[†] Healthy or normal tissue volume. [††] Tumor tissue volume

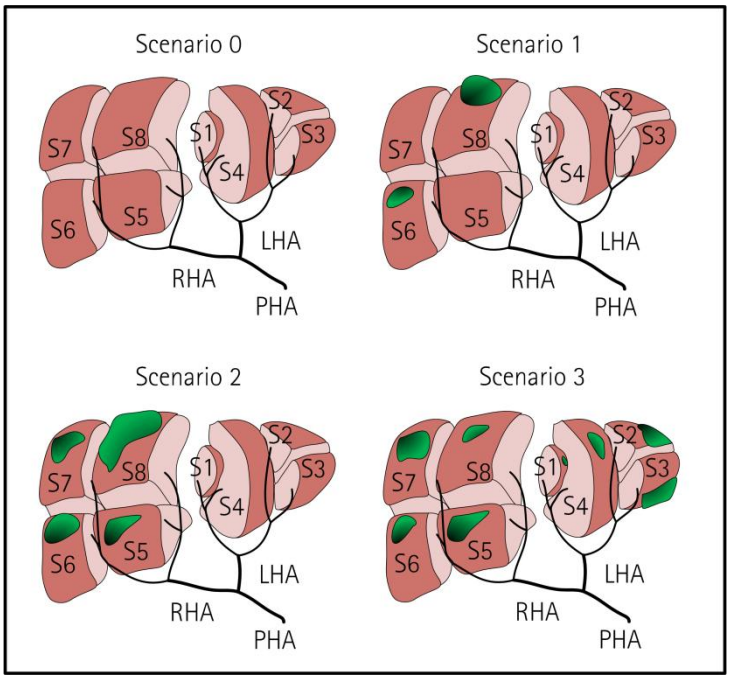

Figure 2.1: Matthew's liver state for each scenario with tumor masses in green. PHA: proper hepatic artery; RHA: right hepatic artery; LHA: left hepatic artery.

The HA defined for Matthew is the unique patient-specific item in this work. This HA was obtained from the MeVis (MeVis Medical Solutions AG, Bremen, Germany) image (see Figure 2.2) of an anonymous patient provided by Clínica Universidad de Navarra, the University Hospital of the University of Navarra. This image is an interactive image of the HA which can be rotated, zoomed in, zoomed out, etc. and shows the liver geometry and HA distribution: the PHA, RHA, LHA, and also the segmental and subsegmental arteries. This configuration corresponds to the most common vascular anatomy; it was observed in 55% (out of 200 subjects) and 75% (out of 1000 subjects) of the cases reported by Michels [55] and Hiatt et al. [56], respectively. This specific truncated HA consists of one inlet and twenty-nine outlets, where two outlets feed S2, seven outlets feed S3, three outlets feed S1 and S4, one outlet feeds S5, four outlets feed S6, three outlets feed S7, and nine outlets feed S8.

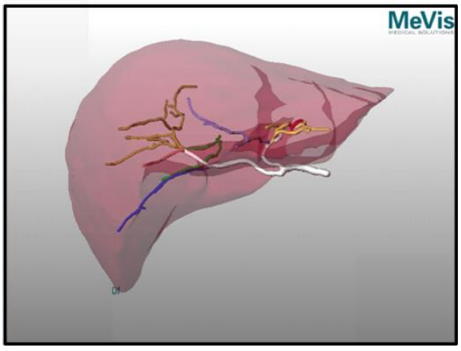

Figure 2.2: MeVis image of the patient-specific hepatic artery

2.1.2 Radioembolization planning

During RE planning, the standard practice is to conduct a treatment-mimicking pretreatment, by which ^{99m}Tc-MAA microparticles are infused in order to (i) analyze the hepatic arterial configuration, (ii) assess hepatopulmonary shunting (i.e., the percentage of MAA shunted into the lungs), and (iii) detect any gastrointestinal deposition [23]. Furthermore, the particle injection force and the injection device are decided.

In this project, the choices for ^{99m}Tc-MAA and ^{90}Y radioactive microagents made were TechneScan™ LyoMAA microparticles (Mallinckrodt Medical B.V., Petten, the Netherlands) and resin SIR-Spheres® (Sirtex Medical Limited, Australia), respectively. Table 2.2 shows the physical properties of resin microspheres and MAA microparticles.

Table 2.2: Resin microsphere and MAA microparticle characteristics

Parameter	Resin microspheres[†]	MAA microparticles[††]
Manufacturer	Sirtex Medical Inc.	Mallinckrodt Medical B.V.
Mean diameter (μm)	d_{resin}=32	d_{MAA}=15
Density (kg/m^3)	ρ_{resin}=1600	ρ_{MAA}=1100
Activity per microagent (Bq)	A_{resin}=50	N/A
Shape factor[†††]	ϕ_{resin}=1	ϕ_{MAA}=0.6 [57]

[†] Kennedy et al. [1]. [††] Wondergem et al. [26]. [†††] The shape factor is the ratio between the surface of a sphere having the same volume as the non-spherical particle and the actual surface area of the particle. N/A: not applicable.

In estimating the activity to be delivered during RE, the body surface area method was employed. It rests on calculating the activity (A in GBq) based on the body surface area (BSA in m^2), liver normal (V in mL) and tumor (V_c in mL) volumes, and patient's weight (W in kg) and height (H in m). Thus, $A = (BSA - 0.2) + V_c/(V + V_c)$, where $BSA = 0.20247 \cdot H^{0.725} \cdot W^{0.425}$. Assuming that the lung shunt observed during the pretreatment is below 10%, then the full amount of resin microspheres can be infused [23].

Particularizing for Matthew, the following table (Table 2.3) shows the RE treatment and pretreatment characteristics.

Table 2.3: Treatment and pretreatment dosage.

Parameter	Treatment	Pretreatment[†]
Activity (GBq)	A_{Sc1}=1.8 A_{Sc2}=A_{Sc3}=2.0	A_{Sc1}=A_{Sc2}=A_{Sc3}=0.15
Number of microspheres	$N_{resin,Sc1}$=36×10^6 $N_{resin,Sc2}$=$N_{resin,Sc3}$=40×10^6	$N_{MAA,Sc1}$=$N_{MAA,Sc2}$=$N_{MAA,Sc3}$=0.411×10^6

[†] The pretreatment is the same for Sc1–Sc3; that is, the one used by Wondergem et al. [26]

Regarding the particle injection force, injection flow rates were 18.5 mL/min and 5 mL/min. The former was calculated from a real-life treatment observation. On average, it took 16–17 s for the interventional radiologist to infuse a 5-mL syringe (e.g., TERUMO®, Code: SS+05L2325 [Terumo Medical Corporation, Tokyo, Japan]). The latter rate was chosen so that the average velocities of the PHA flow and microcatheter flow were similar for Sc2 and Sc3.

Three different injection devices were modeled in this study.

- Standard end-hole microcatheter (SMC): TERUMO®, REF: MC-PP27131 (Terumo medical corporation, Tokyo, Japan).
- Antireflux catheter (ARC): Surefire® Infusion System (Surefire Medical, Inc., Westminster, CO, USA).
- Angled-tip microcatheter (ATM): DIREXION™ Torqueable Microcatheter (Boston Scientific, Marlborough, MA, USA).

The geometric characteristic of the aforementioned devices are illustrated in Figure 2.3. The SMC, in Figure 2.3(a), consists of an outer diameter of 0.9 mm (2.7 F) and an

inner diameter of 0.65 mm (0.025 in) (see Figure 2.3(a), which also includes de PHA diameter, 5 mm). The ARC, in Figure 2.3(b), consists of outer and inner diameters of 1.27 mm (3.8 F) and 0.69 mm (0.027 in), and an expandable tip. For the ARC expandable tip, the distal outer diameter (4 mm), the thickness (0.21 mm), the funnel-shaped length (10.5 mm) and the cylinder-shaped length (2.2 mm) were defined (see 'A.1 Expanding state of the ARC expandable tip' for justification). Figure 2.3(c) shows the ATM, angled 45º in the tip and with outer and inner diameters of 0.74 mm (≈2.4 F) and 0.54 mm (≈0.021 in).

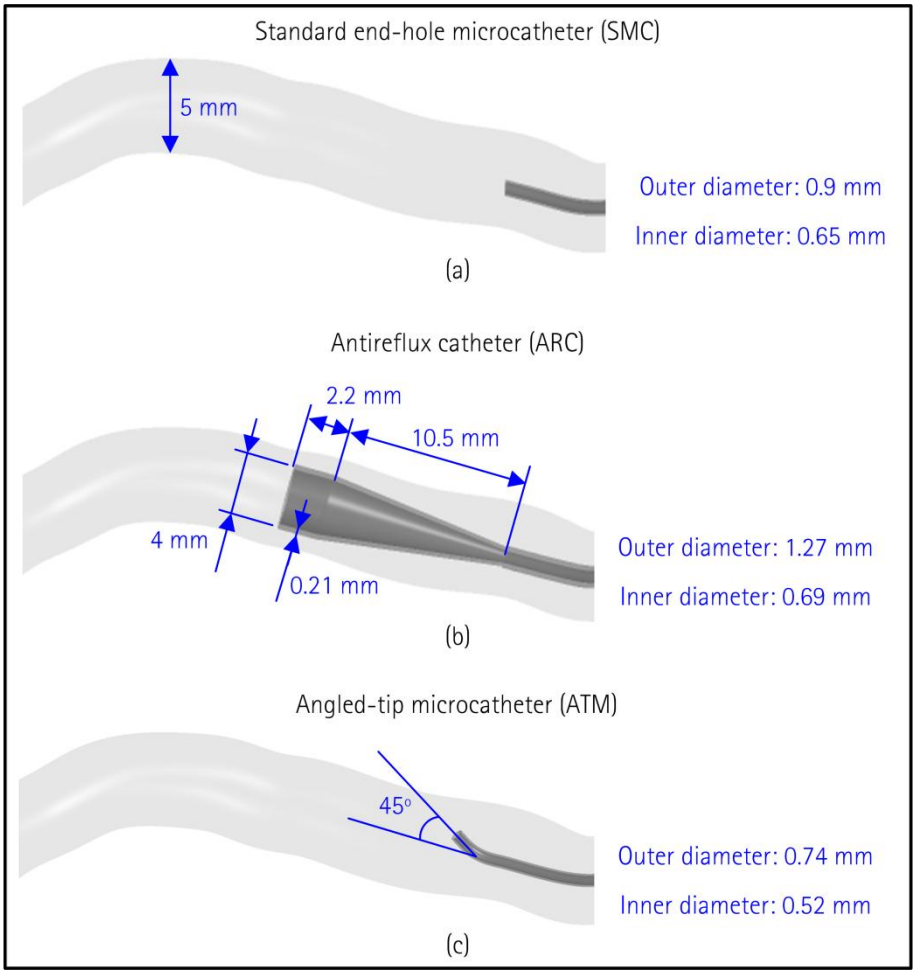

Figure 2.3: Geometric characteristics of (a) SMC, (b) ARC, and (c) ATM.

2.2 Introduction to computational fluid–particle dynamics

Computational fluid–particle dynamics (CFPD) is the combination of computational fluid dynamics (CFD) and particle transport. In essence, CFD is the art of replacing the partial differential equations of the fluid dynamics (in this case, eqns. (2.1) and (2.2)) with discretized algebraic forms, which in turn are solved by numerical methods to obtain numbers for the flow field values (i.e., pressure and components of velocity vector) at discrete points in time and space. CFPD stands for the coupled fluid–particle dynamics numerically solved.

The ingredients for a successful CFPD simulation are the correct modeling of the fluid–particle dynamics, three-dimensional geometric domain, and BCs. It is of utmost importance to state that in the absence of knowledge concerning numerical simulations, one could mistakenly underestimate the significance of BCs.

The following sections describe each of the ingredients mentioned in the above paragraph: the fluid and particle dynamics mathematical modeling, the computational domains utilized in this work, and the BCs. Additionally, the numerical solution method is defined and the specific studies carried out are detailed.

2.3 Fluid–particle dynamics theory

The physical phenomena studied consist of the blood flow and particle transport.

2.3.1 Blood flow: The continuous phase

In hepatic artery hemodynamics, blood exhibits a non-Newtonian, incompressible, isothermal, and laminar behavior. The governing equations are the standard Navier–Stokes equations [58] in a Eulerian reference frame. These equations include the continuity equation (eqn. (2.1)) and the equation for the conservation of linear momentum (eqn. (2.2)):

$$\nabla \cdot \vec{u} = 0 \tag{2.1}$$

$$\frac{\partial \vec{u}}{\partial t} + \nabla \cdot (\vec{u}\vec{u}) = \frac{1}{\rho}(-\nabla p + \nabla \cdot \bar{\bar{\tau}}) + \vec{f} \tag{2.2}$$

where the scalars ρ and p are the blood density (1050 kg/m^3 [59]) and pressure, the vectors $\vec{u}$ and $\vec{f}$ are the fluid velocity vector and the body force (per unit mass)

vector, which accounts for gravitation and discrete-phase-related forces, and $\bar{\bar{\tau}}$ is the stress tensor, defined as

$$\bar{\bar{\tau}} = \mu(\dot{\gamma})[\nabla\vec{u} + (\nabla\vec{u})^{\mathrm{T}}] \tag{2.3}$$

where $\mu(\dot{\gamma})$ is the blood apparent viscosity, which is a function of the shear rate ($\dot{\gamma}$) as modeled by Buchanan et al. [60]:

$$\mu(\dot{\gamma}) = \max\left\{\mu_0, \left(\sqrt{\mu_\infty} + \frac{\sqrt{\tau_0}}{\sqrt{\lambda} + \sqrt{\dot{\gamma}}}\right)^2\right\} \tag{2.4}$$

$$\dot{\gamma} = \sqrt{\nabla\vec{u}[\nabla\vec{u} + (\nabla\vec{u})^{\mathrm{T}}]} \tag{2.5}$$

where μ_0=0.00309 Pa·s is the minimum viscosity, μ_∞=0.002654 Pa·s is the asymptotic viscosity, τ_0=0.004360 Pa is the apparent yield stress, and λ=0.02181 s^{-1} is the shear stress modifier. Even though small arteries were analyzed, it was not necessary to include the Fahraeus–Lindqvist effect (i.e., the drop in the apparent viscosity of blood due to a relatively high plasma-skimming layer near the arterial wall) in the model [61]. Indeed, the smallest outlet is 1.5 mm in diameter.

2.3.2 Particles: The discrete phase

The discrete phase, which interacts with the continuous phase in a two-way fashion, is tracked in a Lagrangian reference frame. The governing equation for particles is the conservation of momentum expressed as Newton's Second Law of Motion (eqn. (2.6)). The forces that were considered were based on some recommendations (e.g., depending on the particle size) by ANSYS Fluent® Theory Guide (2013) and previous works that apply this model to the same physics [45–47,49,50,62]. Thus, the conservation of momentum equation per unit particle mass results in

$$\frac{\mathrm{d}\vec{u}_{\mathrm{p}}}{\mathrm{d}t} = \vec{f}_{\mathrm{V}} + \vec{f}_{\mathrm{P}} + \vec{f}_{\mathrm{G}} + \vec{f}_{\mathrm{D}} \tag{2.6}$$

where $\vec{u}_{\mathrm{p}}$ is the particle velocity vector and $\vec{f}_{\mathrm{V}}$, $\vec{f}_{\mathrm{P}}$, $\vec{f}_{\mathrm{G}}$, and $\vec{f}_{\mathrm{D}}$ are the 'virtual mass' force (per unit particle mass) vector (that is, the force required to accelerate the fluid surrounding the particle), the force vector due to the pressure gradient in the fluid, the gravitation force vector, and the drag force vector (ANSYS Fluent® 15.0. ANSYS Fluent Theory Guide, November 2013) (see 'A.2 Particle tracking model' for justification). Specifically,

$$\vec{f}_{\mathrm{V}} = C_{\mathrm{V}} \frac{\rho}{\rho_{\mathrm{p}}} \left[(\vec{u}_{\mathrm{p}} \cdot \nabla)\vec{u} - \frac{\mathrm{d}\vec{u}_{\mathrm{p}}}{\mathrm{d}t} \right] \tag{2.7}$$

where C_{V} is the 'virtual mass' coefficient (C_{V}=0.5) and ρ_{p} is the particle density. Moreover,

$$\vec{f}_{\mathrm{P}} = \frac{\rho}{\rho_{\mathrm{p}}} (\vec{u}_{\mathrm{p}} \cdot \nabla)\vec{u} \tag{2.8}$$

and

$$\vec{f}_{\mathrm{G}} = \frac{\rho_{\mathrm{p}} - \rho}{\rho_{\mathrm{p}}} \vec{g} \tag{2.9}$$

where $\vec{g}$ is the vector –9.81 m/s^2 in the direction of the z-axis, which takes into consideration the patient's recumbent position during particle injection,

$$\vec{f}_{\mathrm{D}} = \frac{18\mu}{\rho_{\mathrm{p}} d_{\mathrm{p}}^2} \frac{C_{\mathrm{D}} Re_{\mathrm{p}}}{24} (\vec{u} - \vec{u}_{\mathrm{p}}) \tag{2.10}$$

where d_{p} is the particle diameter, C_{D} is the drag coefficient (Morsi and Alexander's [63] for spherical particles and Haider and Levenspiel's [64] for non-spherical particles), and Re_{p} is the particle Reynolds number, defined as:

$$Re_{\mathrm{p}} = \frac{\rho |\vec{u}_{\mathrm{p}} - \vec{u}| d_{\mathrm{p}}}{\mu} \tag{2.11}$$

2.4 Computational domains

2.4.1 From the medical image to the discretized domain

From the MeVis image of the patient-specific HA the front, top, and right-side views were recorded. Then, Rhinoceros 5 (Robert McNeel & Associates, Seattle, WE, USA) was used to define points in the three aforementioned planes in order to reconstruct the HA geometry. By joining these points the artery centerlines were obtained. Finally, by means of PTC Creo Parametric 2.0 (PTC®, Needham, MA, USA) the three-dimensional HA geometry was reconstructed, by extruding tapering cylinders. The resulting geometry was a non-dimensional geometry where the relationship between diameters and artery lengths were conserved. So, defining the

diameter of the inlet, which was at the PHA, the rest of the diameters and lengths were set. According to medical staff recommendation for this patient-specific model, 5-mm diameter was set to the inlet and the patient-specific HA was eventually defined. Figure 2.4 shows the HA views.

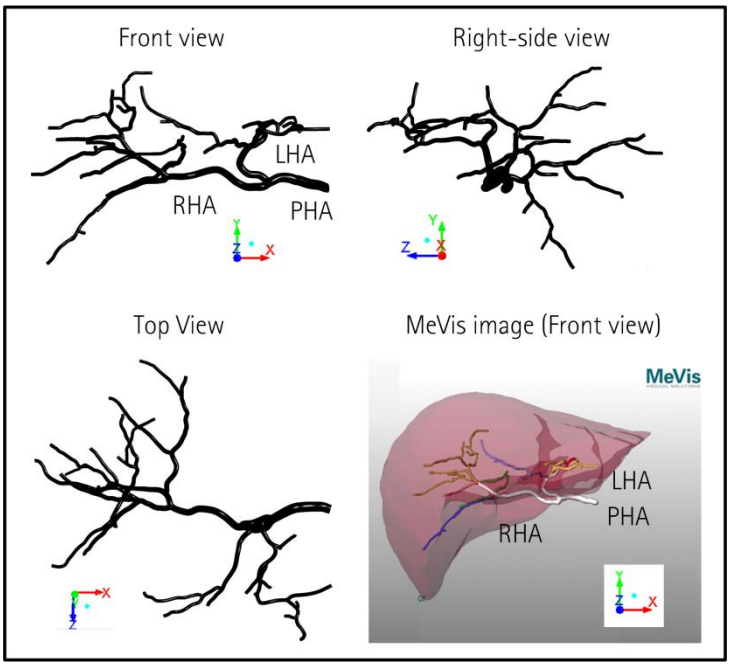

Figure 2.4: Front, right-side, and top views of the reconstructed HA. The MeVis image the HA is based on is on the right bottom.

The boundaries of the computational domain were defined as 'inlet', at PHA level, and the twenty-nine outlets as 'O*m*(*n*)'. The outlet number is *m*, (with *m*=1, … , *M*, where *M*=29) and *n* accounts for the depth level (with *n*=1, … , *N*, where *N*=10). The depth level (DL) of an artery branch was defined by the number of bifurcations that the blood passed through before passing through that artery branch, beginning from the inlet of the domain, in which DL equals 1. For example, O01(4) means outlet *m*=1 with DL=4. Figure 2.5 illustrates a sketch of the hepatic artery; the boundaries are specified and the segment that each outlet feeds is depicted.

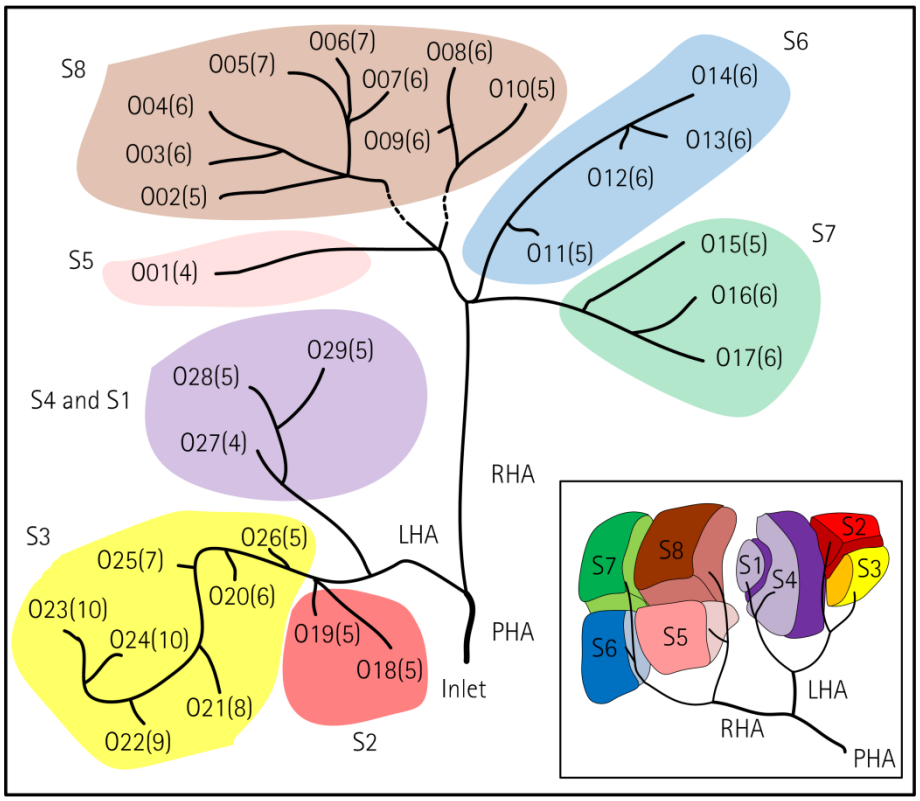

Figure 2.5: Simplified HA representation. The PHA, RHA and LHA are shown, as well as the segments that each outlet feeds. O*m*(*n*) means outlet *m*, which is at DL=*n*. The segments are shown in the bottom right box.

The rigid geometry was discretized generating a mesh by the Gambit 2.4 grid generation package (ANSYS Inc., Canonsburg, PA, USA) (see 'A.3 Rigid geometry and 'outflow'-type BC' for justification). The geometry was divided into two types of volumes: longitudinal volumes (i.e., one inlet and one outlet) and bifurcation volumes (i.e., one inlet and multiple outlets). Longitudinal volumes were meshed with hexahedral elements, while bifurcation volumes were meshed with tetrahedral elements. Firstly, longitudinal volumes were meshed by means of the 'size function' tool of Gambit attached to the each volume, being the source of the mesh the arterial wall with initial value 0.166 mm, a growth rate 1.25 and final value 0.416 mm. Then, bifurcation volumes were meshed using the same size-function parameters.

Regarding the microcatheters, which were created with Gambit 2.4, the mesh of the first longitudinal volume—where the microcatheter is placed—were re-meshed with a finer mesh. In that microcatheter-containing part of the computational domain

four zones could be distinguished. Zone I goes from the beginning of the RHA and LHA through the segmental and subsegmentals. Zone II takes the PHA bifurcation and the PHA, except for the part of the PHA where the microcatheter was inserted. Zone III corresponds to the PHA lumen in which the microcatheter was inserted. Zone IV is the microcatheter lumen. Table 2.4 tabulates the characteristics of the size function employed for the four zones of the computational domain and Figure 2.6 illustrates the four zones for the case of an ATM and the details of the mesh at a RHA section and at a PHA section. If a sufficient mesh quality was not reached with the given values, then the size-function parameters were refined (e.g., for the case of the computational domain where an ARC was inserted).

Table 2.4: Size-function characteristic for creating the mesh for zones I to V. The maximum value was not always reached in the meshes created for each zone.

Zone	Initial value	Growth rate	Maximum value
Zone I	0.166 mm	1.25	0.416 mm
Zone II	0.133 mm	1.25	0.166 mm
Zone III	0.083 mm	1.25	0.133 mm
Zone IV	0.05 mm	1.2	0.166 mm

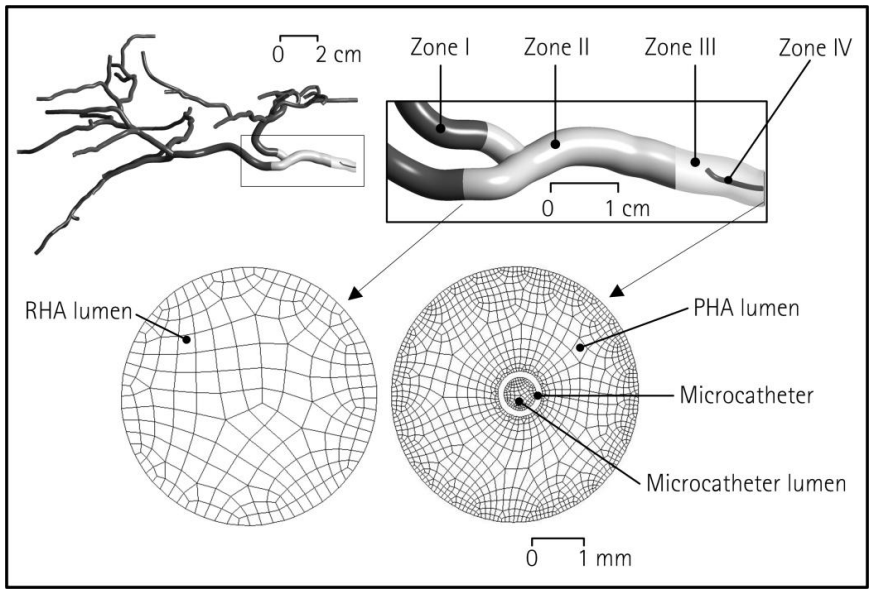

Figure 2.6: The four zones (zones I to IV) of the mesh and details of the mesh at two sections of the computational domain.

2.4.2 Meshes

Based on the discretized domain of the patient-specific HA, a specific microcatheter was rigidly inserted with a specific configuration for each case. Up to 16 microcatheter-containing scenarios were defined. Two microcatheter tip longitudinal positions were defined: 'inlet' position, near the inlet of the computational domain (5.7 mm from the inlet of the computational domain) and 'bifurcation' position, near the PHA bifurcation (29 mm from the inlet of the computational domain), illustrated in Figure 2.7. These two positions were defined for SMC (M02 and M04) and ARC (M06 and M07), with the microcatheter defined through the artery lumen centerline. In addition, a 5-mm shift was defined for the case of the SMC (M03 and M05).

For the SMC, different distal directions were defined as well. To define the direction of the SMC, two sections of the PHA were considered. Section X was close to the inlet of the truncated artery system, while section Y was close to the bifurcation into RHA and LHA and represents the point where the tip of the SMC was located. Sections X and Y are 28 mm apart (in x-axis, see Figure 2.7). In each section, the SMC had four possible positions: N, S, E, and W, which are 1.75 mm away from the lumen center (see Figure 2.7). The SMC direction was consequently defined by using the positions in the two sections. For instance, N-S means that the SMC went from point N in section X to point S in section Y, and point S in section Y is the point from which particles were released into the bloodstream. N-S (M08), E-S (M09), E-W (M10), W-W (M11), E-E (M12), and W-E (M13) were arbitrarily chosen as SMC directions, as illustrated in Figure 2.7. For each SMC direction, realistic trajectories of the SMC were manually defined.

As for the ATM, four scenarios were created for the tip orientation. Orientations are U (upward, M14), R (rightward, M15), D (downward, M16), and L (leftward, M17). These orientations are based on yz-plane, looking towards $-x$-axis (see Figure 2.7).

Figure 2.7 shows the geometries of the catheters and the characteristics of each mesh are tabulated in Table 2.5.

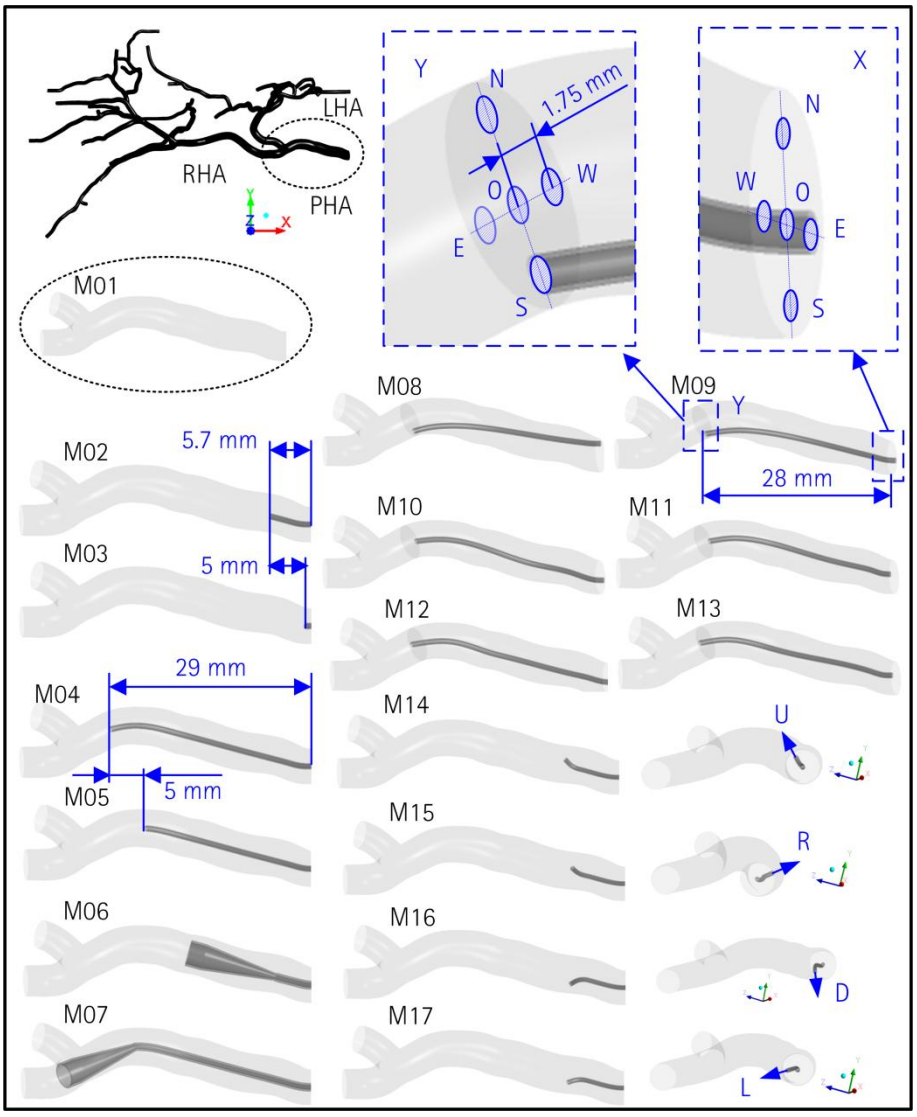

Figure 2.7: Computational domains. Domains with SMC (M02-M05, M08-M13), ARC (M06 and M07), and ATM (M14-M17).

Table 2.5: Summary of meshes. Mesh name; microcatheter type, direction, and position; number of elements; and references are included.

Mesh	Microcatheter	Direction	Tip Position	Elements	Work
M01	N/A	N/A	N/A	1,956,942	[65,66]
M02	End-hole	O-O	Inl.	4,145,135	[67,68]
M03	End-hole	O-O	Inl.–5 mm	4,145,135	[67]
M04	End-hole	O-O	Bif.	4,145,135	[67,68]
M05	End-hole	O-O	Bif.–5 mm	4,145,135	[67]
M06	Antireflux	O-O	Inl.	7,804,054	[68]
M07	Antireflux	O-O	Bif.	10,800,169	[68]
M08	End-hole	N-S	Bif.	4,428,088	[69]
M09	End-hole	E-S	Bif.	4,667,057	[69]
M10	End-hole	E-W	Bif.	4,686,129	[69]
M11	End-hole	W-W	Bif.	4,108,383	[69]
M12	End-hole	E-E	Bif.	4,066,831	[69]
M13	End-hole	W-E	Bif.	4,732,366	[69]
M14	Angled-tip	O-O	Inl. (U)	4,300,384	[70]
M15	Angled-tip	O-O	Inl. (R)	4,294,748	[70]
M16	Angled-tip	O-O	Inl. (D)	4,294,475	[70]
M17	Angled-tip	O-O	Inl. (L)	4,295,932	[70]

N/A: not applicable; Inl.: inlet; Bif.: bifurcation; U: tip pointing upward; R: tip pointing rightward; D: tip pointing downward; L: tip pointing leftward;

All the meshes except M01—which does not contain any microcatheter—were extended by ten times the inlet diameter in the inlet section so that setting a uniform velocity profile in the new inlet results in a physiology-like profile at the patient-specific artery inlet. A parabolic profile was set in simulations with the mesh M01 (for the simulations in Papers I and II in 'C Papers' that are not reported in this dissertation).

With the aim of deeming a mesh sufficiently fine, a mesh sensitivity study based on Richardson's extrapolation [71] was carried out for M01 [66] and M04 [67]. For the

rest, the same meshing strategy employed for M04 was used (i.e., zones I to IV) since the parameters were quite conservative.

2.5 Boundary conditions

2.5.1 Boundary conditions for the continuous phase

It is worth mentioning that much attention has been paid to formulating the BCs. In fact, two publications have resulted from this effort [65,66].

In Aramburu et al. [65] (see Paper I in 'C Papers') the outflow BCs are derived for arterial trees with multiple outlets. The following conditions are necessary to use this methodology:

1. The arterial tree must be made of small arteries (i.e., the resistive behavior is much more important than the compliant effect).
2. The tree must exhibit a symmetry-like structure.
3. The tissue to perfuse must be of homogeneous perfusion characteristics.
4. The artery branching has to be dichotomous.

In short, the BCs are derived by taking into account exclusively the branching structure of the arterial tree. These conditions (1–4) apply to a healthy liver scenario, so this methodology could be used to define the BCs for Sc0, but not for Sc1, Sc2, and Sc3 because the condition (3) would not be fulfilled. In fact, the presence of a tumor makes the perfusion characteristic nonhomogeneous.

Hence, another methodology was created, which do not only takes into account the hepatic arterial tree structure, but also the liver state, that is, normal and tumor volumes over liver segments and their perfusion characteristics (see Paper II in 'C Papers') [66]. This methodology, which focuses on hepatic arteries, is a general methodology that also applies to the healthy liver scenario. That is why this second methodology was employed when defining both inflow and outflow BCs for Sc0, Sc1, Sc2, and Sc3.

In addition to the normal and tumor volumes in the liver (Table 2.1) and the hepatic arterial tree structure (Figure 2.5) that have already been defined, the perfusion characteristics of normal and tumor tissues had to be posited to define the BCs. An average value was chosen for the healthy tissue perfusion: 0.10 $mL \cdot min^{-1} \cdot mL^{-1}$ (it can be derived from Oktar et al. [53] by dividing the flow rate by the liver volume). The same value was chosen for normal tissue: 0.10 $mL \cdot min^{-1} \cdot mL^{-1}$. According to Tsushima et al. [72], a study which analyzed the normal tissue of a colorectal cancer

metastatic liver, this value is in the range of the mean ± standard deviation (0.17 ± 0.16 mL·min^{-1}·mL^{-1}). The tumor-tissue perfusion that has been set is 0.415 mL·min^{-1}·mL^{-1}. To compute this value, the studies from Kim et al. [73] and Tsushima et al. [72] were employed, which analyzed colorectal cancer metastatic livers. An average value of those tumor-tissue perfusion values was computed.

Figure 2.8 illustrates the inflow volumetric flow rate for Sc0–Sc3 that results from applying the methodology developed in Aramburu et al. [66]. The period of the cardiac cycle is T=1 s.

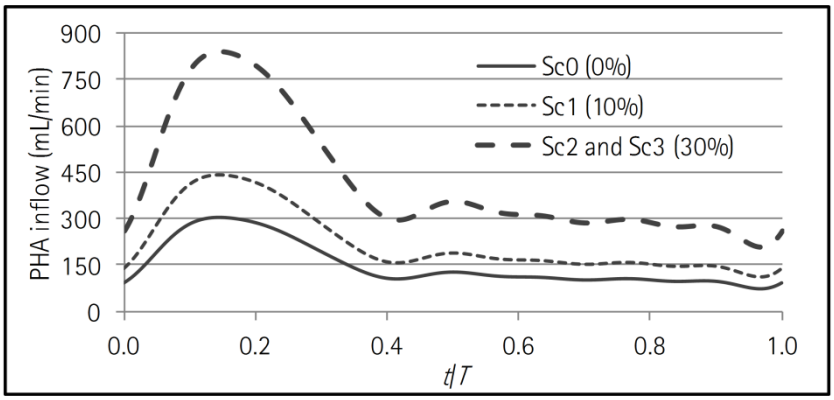

Figure 2.8: Volumetric flow rate at the PHA for Sc0–Sc3.

Table 2.6 shows, for each outlet (*m*), the segment that feeds, the average flow rate (mL/min), and the 'outflow'-type BC for each scenario. 'Outflow'-type BC in ANSYS Fluent® means that a fractional flow rate is set at that outlet (see 'A.3 Rigid geometry and 'outflow'-type BC' for justification).

With regard to the injection characteristics, the fluid flow rate must be specified. Even if the injection fluid is an aqueous solution, it was assumed to be of the same characteristics of blood in terms of viscosity and density. At the inlet, injection flow rates of 18.5 mL/min and 5 mL/min were set (see '2.1.2 Radioembolization planning').

At the walls, the no-slip condition was adopted, which means that the relative velocity between blood and artery wall was zero (see 'A.4 The no-slip condition').

Table 2.6: Average (q_m) and fractional (q_m/q_{inlet}) blood flow rates through each outlet. The segment that is fed by each outlet is also indicated.

Outlet	Segment	Sc0: q_m [mL/min] and (q_m/q_{inlet}(%))	Sc1: q_m [mL/min] and (q_m/q_{inlet}(%))	Sc2: q_m [mL/min] and (q_m/q_{inlet}(%))	Sc3: q_m [mL/min] and (q_m/q_{inlet}(%))
001(4)[†]	S5	15.17 (10.04%)	15.17 (6.87%)	56.67 (13.51%)	59.93 (14.29%)
002(5)	S8	7.71 (5.10%)	17.01 (7.70%)	32.61 (7.77%)	11.99 (2.86%)
003(6)	S8	3.85 (2.55%)	8.50 (3.85%)	16.30 (3.88%)	5.99 (1.43%)
004(6)	S8	3.85 (2.55%)	8.50 (3.85%)	16.30 (3.88%)	5.99 (1.43%)
005(7)	S8	1.93 (1.27%)	4.25 (1.93%)	8.15 (1.94%)	3.00 (0.71%)
006(7)	S8	1.93 (1.27%)	4.25 (1.93%)	8.15 (1.94%)	3.00 (0.71%)
007(6)	S8	3.85 (2.55%)	8.50 (3.85%)	16.30 (3.88%)	5.99 (1.43%)
008(6)	S8	3.85 (2.55%)	8.50 (3.85%)	16.30 (3.88%)	5.99 (1.43%)
009(6)	S8	3.85 (2.55%)	8.50 (3.85%)	16.30 (3.88%)	5.99 (1.43%)
010(5)	S8	7.71 (5.10%)	17.01 (7.70%)	32.61 (7.77%)	11.99 (2.86%)
011(5)	S6	7.72 (5.11%)	17.02 (7.71%)	32.13 (7.65%)	23.97 (5.71%)
012(6)	S6	3.86 (2.55%)	8.51 (3.86%)	16.06 (3.82%)	11.99 (2.86%)
013(6)	S6	3.86 (2.55%)	8.51 (3.86%)	16.06 (3.82%)	11.99 (2.86%)
014(6)	S6	3.86 (2.55%)	8.51 (3.86%)	16.06 (3.82%)	11.99 (2.86%)
015(5)	S7	7.76 (5.22%)	7.76 (3.52%)	28.51 (6.79%)	29.96 (7.14%)
016(6)	S7	3.88 (2.57%)	3.88 (1.76%)	14.26 (3.39%)	14.98 (3.57%)
017(6)	S7	3.88 (2.57%)	3.88 (1.76%)	14.26 (3.39%)	14.98 (3.57%)
018(5)	S2	7.89 (5.22%)	7.89 (3.57%)	7.89 (1.88%)	29.97 (7.14%)
019(5)	S2	7.89(5.22%)	7.89 (3.57%)	7.89 (1.88%)	29.97 (7.14%)
020(6)	S3	3.93 (2.60%)	3.93 (1.78%)	3.93 (0.94%)	14.98 (3.57%)
021(8)	S3	0.98 (0.65%)	0.98 (0.45%)	0.98 (0.23%)	3.75 (0.89%)
022(9)	S3	0.49 (0.32%)	0.49 (0.22%)	0.49 (0.11%)	1.87 (0.45%)
023(10)	S3	0.25 (0.16%)	0.25 (0.11%)	0.25 (0.06%)	0.94 (0.22%)
024(10)	S3	0.25 (0.16%)	0.25 (0.11%)	0.25 (0.06%)	0.94 (0.22%)
025(7)	S3	1.97 (1.30%)	1.97 (0.89%)	1.97 (0.47%)	7.49 (1.79%)
026(5)	S3	7.87 (5.21%)	7.87 (3.56%)	7.87 (1.87%)	29.96 (7.14%)
027(4)	S1&S4	15.47 (10.24%)	15.47 (7.01%)	15.47 (3.68%)	29.96 (7.14%)
028(5)	S1&S4	7.73 (5.12%)	7.73 (3.50%)	7.73 (1.84%)	14.98 (3.57%)
029(5)	S1&S4	7.73 (5.12%)	7.73 (3.50%)	7.73 (1.84%)	14.98 (3.57%)

[†] 001(4): outlet number 1, at DL=4

2.5.2 Boundary conditions for the discrete phase

In order to define the injection, the particle mass flow rate must be specified. Regarding the pretreatment, an injection of 0.8 mg of MAA diluted in 3 mL was assumed, as described by Wondergem et al. [26]. As for the treatment, a 5-mL particle deposit was assumed, so the initial particle concentration was 7.2×10^6 particles/mL for Sc1 and 8×10^6 particles/mL for Sc2 and Sc3 (i.e., number of particles prescribed, tabulated in Table 2.3, divided by the deposit volume). Given that particle

density (ρ_p=1600 kg/m^3) and diameter (d_p=32 μm) were known (see Table 2.2), the particle mass flow rates that are tabulated in Table 2.7 were obtained (i.e., injection-fluid-flow-rate times particle-concentration times particle-density times particle-volume).

Table 2.7: Injection fluid flow rate and particle mass flow rate for the RE treatment of each cancer scenario and for RE pretreatment

Scenario	Sc1	Sc2	Sc2	Sc3	Pretreatment
Microcatheter inflow (mL/min)	18.5	5[†]	18.5	18.5	18.5
Particle mass flow rate (kg/s)	6.11×10^{-5}	1.83×10^{-5}	6.8×10^{-5}	6.8×10^{-5}	8.22×10^{-8}

[†] This inflow was only chosen for the treatment of Sc2 when defining the studies

Additionally, particles were assumed not to collide with each other and not to dissipate any energy when colliding with walls (i.e., elastic collisions with walls).

2.6 Numerical solution method

2.6.1 Simulation strategy and postprocessing

The simulation strategy is illustrated in Figure 2.9. Each simulation reported in this dissertation consisted of six cardiac pulses, where the cardiac pulse period, T, is one second. Therefore, each simulation went from t=−2 s to t=4 s. The first two pulses (t=−2 s to t=0) were intended for the elimination of the initial value of the simulation, and it was the 'presimulation.' The following four pulses (t=0 to t=4 s) were the actual simulation results. Particles were injected during the first pulse (t=0 to t=1 s), and three more pulses were simulated so that the majority of the injected particles exited the computational domain (see 'A.5 Simulation strategy').

For postprocessing purposes, the number of particles that crossed the twenty-nine outlets of the computational domain was recorded. Furthermore, the results for blood flow and particle location at several temporal points were recorded. Those temporal points are systolic acceleration (t/T=0.05), systolic peak (t/T=0.15), systolic deceleration (t/T=0.28), early diastole (t/T=0.40), late diastole (t/T=0.75) and cycle end (t/T=1.00). Figure 2.10 depicts the aforementioned temporal points over the PHA inflow waveform.

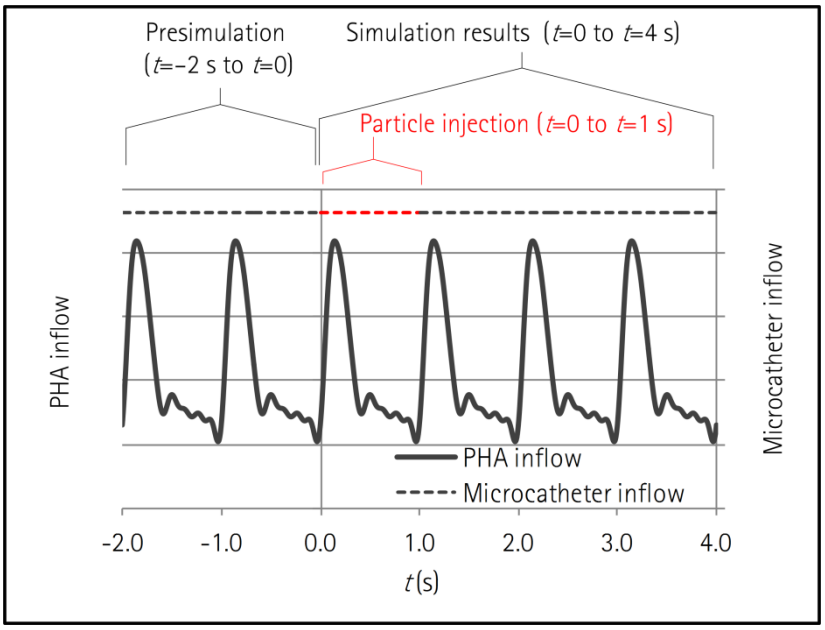

Figure 2.9: Schematics of the simulation strategy. The first part is the presimulation (t=−2s to t=0), intended for the elimination of the initial value of the simulation. Simulation results are recorded from t=0 to t=4 s, where particles are injected from t=0 to t=1 s. PHA lumen and microcatheter lumen representative inflows are depicted inside the panel.

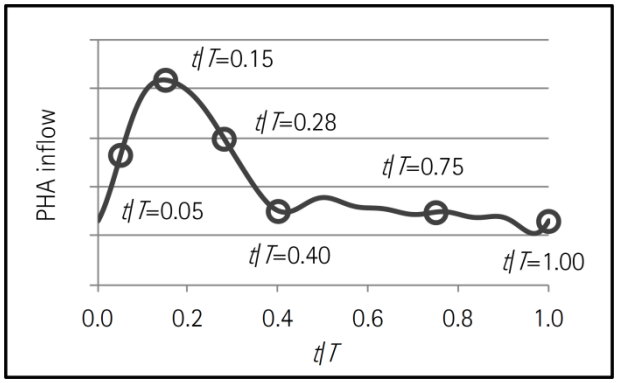

Figure 2.10: Temporal points at which simulation results are recorded: systolic acceleration (t/T=0.05), systolic peak (t/T=0.15), systolic deceleration (t/T=0.28), early diastole (t/T=0.40), late diastole (t/T=0.75) and cycle end (t/T=1.00).

2.6.2 Numerical settings

The two-way coupled blood flow (continuous phase) and particle transport (discrete phase) models were solved by using the solver Fluent 15.0® (ANSYS® Inc., Canonsburg, PA, USA).

With regard to the Navier–Stokes equations (eqns. (2.1) and (2.2)), the SIMPLE algorithm was used to solve the velocity and pressure in a segregated way. Spatial discretization was done by using the least squares cell-based algorithm for gradient computations and the second-order upwind scheme for the convection term of the momentum equations. For pressure interpolation, the second-order algorithm was employed. The transient solver settings were a second-order implicit transient formulation with a time step (Δt) of 2×10^{-3} s (see 'A.6 Time-step value').

As for integrating the particle trajectory equation (eqn. (2.6)), it was done using the same time-step value as the continuous phase via the trapezoidal scheme. However, if stability could not be guaranteed, then the scheme was automatically switched (by the solver) to the implicit scheme.

The coupling source terms were updated every five iterations of the continuous phase, when the discrete-phase iteration was computed. Absolute globally scaled residuals under 10^{-5} for the continuous phase were attained in all the simulations reported in this dissertation.

2.6.3 Servers

Table 2.8 shows the characteristics of the servers that were used to carry out the simulations.

Table 2.8: Server characteristics

Server	Commercial name	OS	Cores	RAM	Clock speed
Server 1	ProLiant DL585 G7	CentOS 5.5	32	64 GB	2.6 GHz
Server 2	ProLiant DL585 G6	CentOS 5.5	24	64 GB	2.8 GHz
Server 3	ProLiant DL585 G7	RedHat Enterprise Linux 6.4	48	96 GB	2.2 GHz
Server 4	ProLiant DL560 G8	Windows 2008 Server R2 Enterprise	32	128 GB	2.2 GHz
Server 5	ProLiant DL560 G8	RedHat Enterprise Linux 6.4	64	128 GB	2.2 GHz

OS: operating system

2.7 Study definition

Four studies were designed based on the specific goals defined in '1.2 Research objectives'. The four studies have in common that the same patient-specific hepatic artery was used for simulations. Moreover, for the studies that did not consider the cancer scenario as a varying parameter, Sc2 was used as cancer scenario.

It is important to note that the varying parameters for each study were chosen by following the recommendations of the physicians involved in this project.

2.7.1 Study I: The pretreatment as an actual treatment surrogate

This study aimed to analyze whether the ^{99m}Tc-MAA pretreatment is a sufficient surrogate of the ^{90}Y RE in terms of microagent distribution over the segments of the liver. The parameters that were varied were the microcatheter position, the cancer scenario, and the particle type (see Paper III in 'C Papers') [67].

Figure 2.11 illustrates the microcatheter positions, the cancer scenarios, and the particle types employed. The microcatheter positions include 'Inlet' position (i.e., near the inlet of the computational domain, 'Inlet–5 mm' position (i.e., 'Inlet' position with a 5-mm shift), 'Bifurcation' position (i.e., near the PHA bifurcation), and 'Bifurcation–5 mm' position (i.e., 'Bifurcation' position with a 5-mm shift). Two cancer scenarios were used: Sc1 and Sc2. As for the particles, pretreatment MAA microparticles and treatment resin microspheres were used.

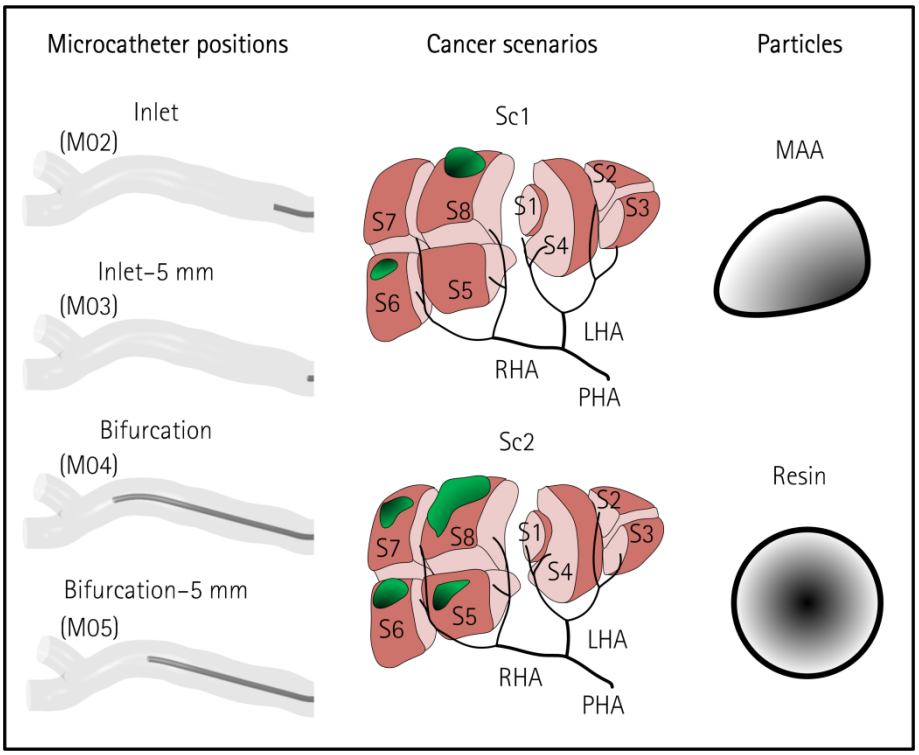

Figure 2.11: Microcatheter positions, cancer scenarios, and particle types for the study on the pretreatment as an actual treatment surrogate.

A set of twelve simulations was designed. Table 2.9 tabulates the simulation characteristics.

Table 2.9: Simulation planning with varying microcatheter position, cancer scenario, and particle type. Sim.: simulation number.

Sim.	Microcatheter position (Mesh)	Cancer scenario	Particle type
1	Inlet (M02)	Sc1	MAA
2	Inlet (M02)	Sc1	Resin
3	Inlet–5 mm (M03)	Sc1	Resin
4	Inlet (M02)	Sc2	MAA
5	Inlet (M02)	Sc2	Resin
6	Inlet–5 mm (M03)	Sc2	Resin
7	Bifurcation (M04)	Sc1	MAA
8	Bifurcation (M04)	Sc1	Resin
9	Bifurcation–5 mm (M05)	Sc1	Resin
10	Bifurcation (M04)	Sc2	MAA
11	Bifurcation (M04)	Sc2	Resin
12	Bifurcation–5 mm (M05)	Sc2	Resin

2.7.2 Study II: The role of the catheter type and location

This study aimed to analyze the influence of the catheter type (SMC vs. ARC) and location during particle injection over segment-to-segment microsphere distribution (see Paper IV in 'C Papers') [68].

The parameters that were varied were the catheter type, the catheter tip position along the artery, and the cancer scenario.

Figure 2.12 illustrates the catheter types and positions, and cancer scenarios employed. The catheter types include the SMC and the ARC, the catheter positions include 'Inlet' position (i.e., near the inlet of the computational domain) and 'Bifurcation' position (i.e., near the PHA bifurcation), and the cancer scenarios include Sc2 and Sc3.

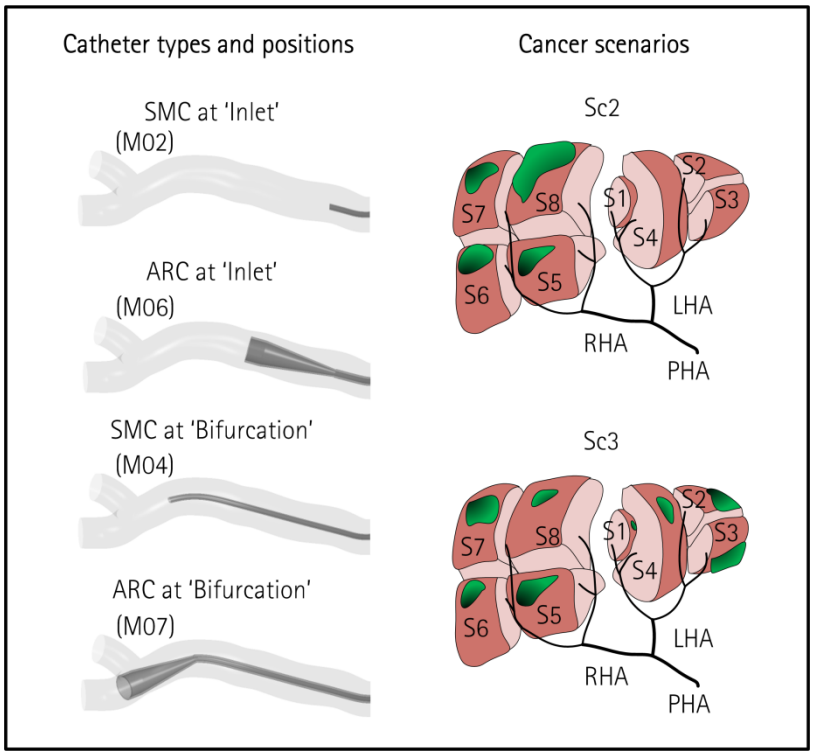

Figure 2.12: Catheter types and positions, and cancer scenarios for the study on the influence of catheter type on particle distribution.

A set of six simulations was designed. Table 2.10 tabulates the simulation characteristics.

Table 2.10: Simulation planning with varying catheter type and tip position, and cancer scenario. A column with the mesh code is included. Sim.: simulation number.

Sim.	Catheter type	Tip position	Cancer scenario	Mesh
1	SMC	Inlet	Sc2	M02
2	ARC	Inlet	Sc2	M06
3	SMC	Bifurcation	Sc2	M04
4	ARC	Bifurcation	Sc2	M07
5	SMC	Inlet	Sc3	M02
6	ARC	Inlet	Sc3	M06

2.7.3 Study III: The role of the microcatheter distal direction and injection point and velocity

This study aimed to analyze the influence of the microcatheter distal direction and injection point and velocity on microsphere segment-to-segment distribution during RE (see Paper V in 'C Papers') [69].

The parameters that were varied were the microcatheter distal direction and the injection flow rate.

Figure 2.13 illustrates the microcatheter directions.

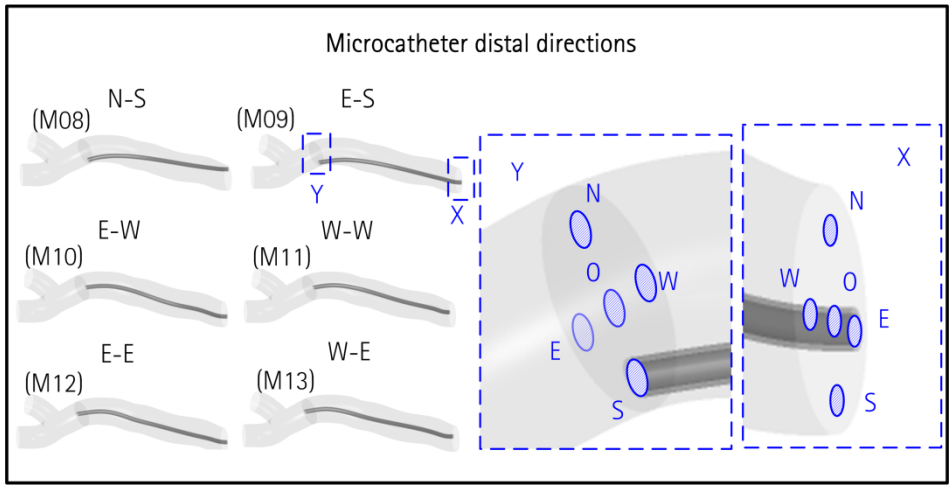

Figure 2.13: Microcatheter distal directions N-S, E-S, E-W, W-W, E-E and W-E.

A set of twelve simulations was designed. Table 2.11 tabulates the simulation characteristics.

Table 2.11: Simulation planning with varying microcatheter direction and injection flow rate. A column with the simulation code is included. Sim.: simulation number.

Sim.	Direction (Mesh)	Injection flow rate (mL/min)	Simulation code
1	N-S (M08)	18.5	N-S:1
2	E-S (M09)	18.5	E-S:1
3	E-W (M10)	18.5	E-W:1
4	W-W (M11)	18.5	W-W:1
5	E-E (M12)	18.5	E-E:1
6	W-E (M13)	18.5	W-E:1
7	N-S (M08)	5.0	N-S:2
8	E-S (M09)	5.0	E-S:2
9	E-W (M10)	5.0	E-W:2
10	W-W (M11)	5.0	W-W:2
11	E-E (M12)	5.0	E-E:2
12	W-E (M13)	5.0	W-E:2

2.7.4 Study IV: The role of the orientation of an angled-tip microcatheter and injection velocity

This study aimed to analyze the influence of the orientation of an ATM and injection velocity on microsphere segment-to-segment distribution (see Paper VI in 'C Papers') [70].

The parameters that were varied were the orientation of the tip and injection velocity. Figure 2.14 illustrates the orientations of the ATM, i.e., upward, rightward, downward, and leftward orientations.

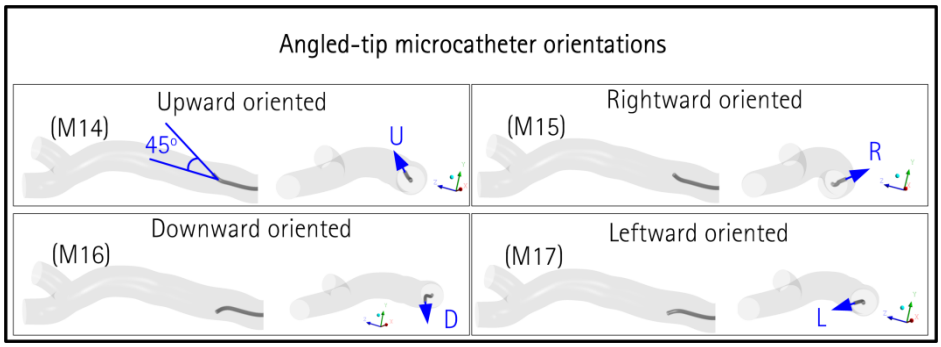

Figure 2.14: Orientations of the ATM tip: upward (U), rightward (R), downward (D), and leftward (L).

A set of eight simulations was designed, tabulated in Table 2.12.

Table 2.12: Simulation planning with varying tip orientation and injection flow rate. A column with the simulation code is included. Sim.: simulation number.

Sim.	Tip orientation (Mesh)	Injection flow rate (mL/min)	Simulation code
1	Upward (M14)	18.5	U:1
2	Upward (M14)	5.0	U:2
3	Rightward (M15)	18.5	R:1
4	Rightward (M15)	5.0	R:2
5	Downward (M16)	18.5	D:1
6	Downward (M16)	5.0	D:2
7	Leftward (M17)	18.5	L:1
8	Leftward (M17)	5.0	L:2

Chapter 3

Results and Discussion

"*No one believes the CFD results except the one who performed the calculation, and everyone believes the experimental results except the one who performed the experiment*" Patrick J. Roache

---

This chapter briefly shows the results and the discussion of the four studies defined in Chapter 2. For a more in-depth analysis refer to the papers that are included in Appendix 'C Papers': Paper III for Study I, Paper IV for Study II, Paper V for Study III, and Paper VI for Study IV.

3.1 Introduction

In this chapter, the results of the simulations are given via tables and figures. The results of each study include at least a table with computational times, a table with the particle distribution and flow split, and a figure with particle distribution over the liver segments.

Moreover, prior to the analysis and discussion of the results, several parameters must be clarified.

When it comes to analyzing the particle distribution, the percentages that are tabulated for a liver segment correspond to the number of particles exiting through that specific segment divided by the total number of particles exiting through the eight segments. That is, the sum of the percentages exiting S1 to S8 is 100%. The non-exiting percentage, instead, is defined as the percentage of injected particles that remained inside the computational domain after simulation completion. When illustrating the results, 'error-bars' are included. Those error bars do not account for errors; instead, they represent the non-exiting particle percentage, weighted with the percentage that actually exited in each segment. For instance, if the non-exiting particles accounted for 4% of the total injected particles and 40% of the particles that exited any of the eight segments exited through S8, then the value for S8 is $40 \pm 1.66\%$.

3.2 Study I: The pretreatment as an actual treatment surrogate

3.2.1 Computational times

Table 3.1 tabulates the information regarding the computational cost of Study I simulations. Specifically, the time per iteration, the number of iterations, and the server utilized are specified for presimulations (t=−2 s to t=0) and simulations (t=0 to t=4 s). The total wall-clock hours that took each complete simulation is indicated.

Table 3.1: Computational cost of Study I simulations in terms of seconds per iteration (s/it), number of iterations (Iterations), and server number (Server #) for presimulation (t=−2 s to t=0) and simulation (t=0 to t=4 s). The total wall-clock hours that took each complete simulation is also indicated (Time (h)).

Sim.	t=−2 s to t=0			t=0 to t=4 s			Time (h)
	s/it	Iterations	Server #	s/it	Iterations	Server #	
1	10.89	53500	4†	2.77	102560	3	240.77
2	10.89	53500	4†	3.15	103080	1	251.93
3	2.71	68110	1	3.24	113490	3	153.18
4	9.14	33550	4†	7.84	56215	4	207.57
5	9.14	33550	4†	8.03	58215	4	215.01
6	2.79	34205	1	8.46	59855	4	167.17
7	10.49	48875	4†	3.98	65770	3	215.21
8	19.49	48875	4†	3.11	79440	1	210.98
9	6.49	65845	4	3.14	88090	1	195.51
10	2.07	31925	3	4.10	51095	2	76.52
11	2.07	31925	3	3.13	54615	1	65.88
12	2.09	32070	3	4.29	54635	2	83.79

†Only 30 cores were employed out of the 32 available

3.2.2 Particle distribution

Table 3.2 tabulates the particle distribution over the liver segments for Study I simulations. The non-exiting particle percentage is indicated in the last column. Moreover, the flow split for Sc1 and Sc2 is shown in the last two rows.

Table 3.2: Exiting and non-exiting particle distribution for simulations and flow split for cancer scenarios in Study I.

Sim. or scenario	S2 (%)	S3 (%)	S1-S4 (%)	S5 (%)	S6 (%)	S7 (%)	S8 (%)	Non-exiting (%)
1	15.58	9.60	36.41	4.49	4.13	2.42	27.37	12.77
2	23.98	13.23	30.79	2.93	3.60	2.06	23.42	22.17
3	18.22	7.68	24.34	4.00	16.43	4.77	24.56	39.97
4	8.45	7.16	17.82	15.87	14.16	11.86	24.68	10.88
5	11.67	7.48	14.13	14.50	13.47	12.73	26.01	11.49
6	4.35	3.15	6.10	18.55	22.13	13.87	31.86	12.57
7	0	0	0	13.37	27.92	8.42	50.29	16.49
8	0	0	0	12.09	30.30	5.73	51.88	15.46
9	16.87	11.64	39.47	4.12	4.07	1.70	22.13	19.70
10	0	0	0	18.43	25.12	16.62	39.83	8.93
11	0	0	0	17.86	20.81	15.63	45.69	4.58
12	11.82	5.08	10.98	18.27	10.30	10.47	33.10	12.42
Sc1	7.15	7.13	14.02	6.87	19.28	7.04	38.52	–
Sc2	3.76	3.75	7.38	13.51	19.15	13.59	38.86	–

Figure 3.1 summarizes the segment-to-segment particle distribution. For each chart the information represented denotes a particular position of the microcatheter tip (i.e., near the inlet or near the bifurcation) and a particular cancer scenario (i.e., scenario 1 or scenario 2). The percentage of exiting particles deposited in the segments is depicted along with the blood flow split and the cancer volume at each segment (S1 to S8).

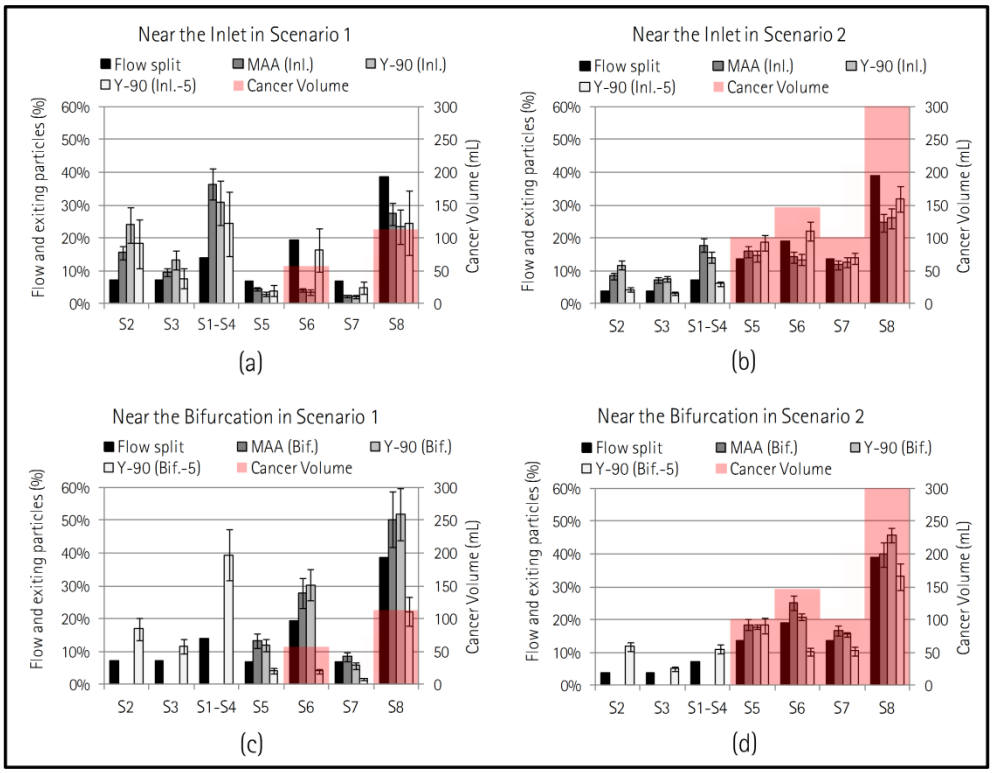

Figure 3.1: Flow split and particle distribution over segments in Study I: liver segments on *x*-axes, flow split and particle distribution on primary *y*-axes, and cancer volume on secondary *y*-axes. (a) Results for simulations 1–3, (b) results for simulations 4–6, (c) results for simulations 7–9, and (d) results for simulations 10–12.

3.2.3 Particle characteristics and quantity

Unlike particle density, the size (i.e., diameter and shape) and number of particles are proven to play an important role in terms of the final distribution of particles. Due to a skimming effect, particles that have a bigger diameter will tend to travel more centripetally than those that have a smaller diameter, which will tend to travel more peripherally. Thus, the biggest particles will tend to travel through the main branches, while the smallest particles will tend to travel through side branches [74].

However, results suggest that in terms of segment-to-segment distribution, although the abovementioned phenomenon is important, the number of bifurcations that the particles must pass through to be directed to a specific segment might be more important, as the skimming effect might not occur if the length of the branches is not sufficiently large. In fact, there could be cases in

which, after crossing the first bifurcation, the particles have already reached the target zone. For instance, if the microcatheter is placed in the PHA (as in this study) and the entire right lobe is to be treated (as in the case of cancer scenario 2), the particles may behave the same way regardless of the particle size and shape and be carried by the flow surrounding the particles.

In fact, if Figure 3.1(a), (b), (c), and (d) are analyzed and the second and third bars are observed (each pair share the same microcatheter tip position), there are subtle differences (compared with other influential parameters) between injecting ^{99m}Tc-MAA microparticles and ^{90}Y resin microspheres. Even though the differences are small, on some occasions the differences might be larger (see Figure 3.1(a)).

Thus, particle quantity and diameter are not critical parameters. The possible mismatches between the paired pre- and actual RE treatments reported in the literature may be due to intrasegmental events (which is beyond the scope of this thesis).

3.2.4 Microcatheter tip position

The importance of matching the microcatheter tip position in pretreatment and actual RE treatment is widely recognized. Many works have analyzed this point both clinically [25,26,29] and numerically [45–50,62], and explicit recommendations have been made [1,23] (e.g., "Irrespective of the location of MAA injection, it is imperative that the MAA be delivered with flow rates and catheter position that mimic the anticipated Y90 infusion rate." [1]). If the third and fourth bars in Figure 3.1(a), (b), (c), and (d) are observed, it can be seen that the exiting-particle segment-to-segment distribution greatly depends on microcatheter tip position.

The exiting-particle segment-to-segment distribution depends on microcatheter tip position due to the fact that the injection is made at a certain point in the lumen and not through the entire cross section of the lumen. Therefore, local issues (pressure and velocity fields in the vicinity of the microcatheter tip) matter; indeed they are what matter most. If the flow-split bar (global blood flow split) and exiting-particle-percentage bars are compared in Figure 3.1(a), (b), (c), and (d), it can be seen that the flow-split percentage and exiting-particle percentages do not coincide, and therefore particle distribution depends on local hemodynamics.

Therefore, the matching of exiting-particle distribution in cases where the microcatheter tip is 5-mm shifted may be a matter of pure coincidence. If the flow

is straight to some extent because the artery is straight, the hemodynamic pattern near a microcatheter tip position could be similar to that of a 5-mm shifted point. And it is easier for this similarity to occur in straight vessels rather than in bifurcations, where the flow is disturbed and redirected. That is why some authors might explicitly suggest avoiding drug injections near a bifurcation [25,26].

If the results of Study I are analyzed, it can be seen that a 5-mm shift in the microcatheter tip position during the injection of particles leads to vast differences of exiting-particle segment-to-segment distribution; and the differences are markedly higher when the microcatheter tip is close to the bifurcation (see the third and fourth bars in Figure 3.1(c) and (d)). While injecting in the 'Bif.' position leads to right-lobe-targeted particle distribution, injecting at 'Bif.–5 mm' leads to microsphere deposition in the left lobe as well. It is important to consider that resin microspheres are believed to be transported by blood flow [21]. Figure 3.2 shows, for the entrance of the domain of interest (a) and for six different temporal points (b), the streamlines from the flow exiting the microcatheter for simulation 8 (microcatheter tip placed at the 'Bif.' position in cancer scenario 1) (c) and simulation 9 (microcatheter tip placed at the 'Bif.–5 mm' position in cancer scenario 1) (d). These streamlines are not strictly particle pathlines, but are supposedly similar to the pathlines to be followed by the particles.

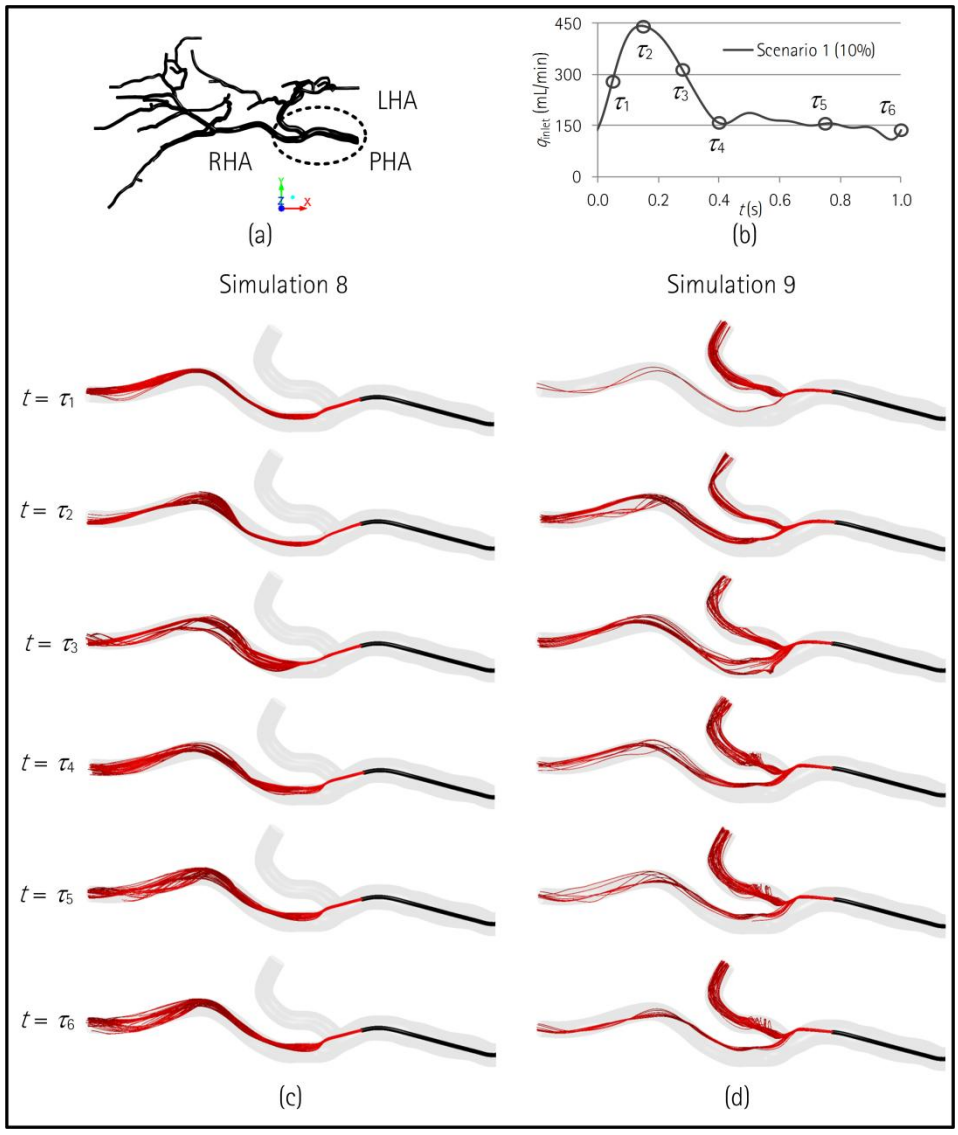

Figure 3.2: Streamlines at (a) the entrance of the domain of interest for (c) cancer scenario 1 with the microcatheter tip near the bifurcation and (d) cancer scenario 1 with the microcatheter tip near the bifurcation with a 5-mm shift. (b) Six temporal points are depicted: τ_1=0.05 s (systolic acceleration), τ_2=0.15 s (systolic peak), τ_3=0.28 s (systolic deceleration), τ_4=0.40 s (early diastole), τ_5=0.75 s (late diastole), and τ_6=1.00 s (cycle end).

There is only a 5-mm shift between microcatheter tip positions, but the exiting-particle segment-to-segment distribution is radically different. These differences come from the fact that bifurcations are sites where the local flow is very position-dependent.

3.2.5 Cancer burden

When the cancer burden is higher (cancer scenario 2 in this case), i.e., more blood is flowing to those cancer-bearing segments, the differences in microcatheter tip position seem to play a less important role because blood flow to tumor-bearing segments is clearly greater as the cancer volume increases, which may result in a greater power to transport particles through those tumor-bearing segments. Consider the third and fourth bars in Figure 3.1: the differences in exiting-particle segment-to-segment distribution are significantly higher for the cases of cancer scenario 1, i.e., a cancer burden that involves 10% of the liver.

Similarly, in this case, the issue of cancer burden, which is directly related to systemic flow rate, can be analyzed from the particle-injection standpoint. Indeed, in this study the volumetric flow rate of the infused particle suspension was the same for both scenario 1 and 2. Therefore, altering the cancer burden (i.e., systemic flow rate) means altering the ratio between the microcatheter-exiting particles' average speed and the artery-lumen average velocity. This issue has been reported as being critical in the literature.

For example, a numerical study by Kleinstreuer et al. [47] reported that when microspheres are injected at velocities higher than the velocity of the surrounding bloodstream, particle inertia takes over and microspheres will have an increased tendency to cross blood flow streamlines. However, drag force tends to minimize that velocity difference, as noted by Jernigan et al. [75] in an experimental study, leading them to remark that fluid drag force (eqn. (2.10)) is one of the most important forces in microsphere transport.

Thus, the same conclusion reached by Kleinstreuer et al. [47] can be drawn here: the higher the ratio between microsphere speed and blood velocity, the more unpredictable the particle distribution (i.e., greater differences between exiting-particle and blood flow segment-to-segment distributions for cancer scenario 1).

3.3 Study II: The role of the catheter type and location

3.3.1 Computational times

Table 3.3 tabulates the information regarding the computational cost of Study II simulations. Specifically, the time per iteration, the number of iterations, and the server utilized are specified for presimulations (t=−2 s to t=0) and simulations (t=0 to t=4 s). The total wall-clock hours that took each complete simulation is indicated.

Table 3.3: Computational cost of Study II simulations in terms of seconds per iteration (s/it), number of iterations (Iterations), and server number (Server #) for presimulation (t=−2 s to t=0) and simulation (t=0 to t=4 s). The total wall-clock hours that took each complete simulation is also indicated (Time (h)).

Sim.	t=−2 s to t=0			t=0 to t=4 s			Time (h)
	s/it	Iterations	Server #	s/it	Iterations	Server #	
1	9.14	33550	4[†]	8.03	58215	4	215.01
2	12.29	61400	4	3.70	147255	3	360.95
3	2.07	31925	3	3.13	54615	1	65.88
4	5.80	55600	1	6.79	126375	1	327.79
5	7.44	30775	4	4.91	62200	4	148.33
6	3.54	68835	3	3.81	166000	3	243.43

[†]Only 30 cores were employed out of the 32 available

3.3.2 Particle distribution

Table 3.4 tabulates the particle distribution over the liver segments for Study II simulations. The non-exiting particle percentage is indicated in the last column. Moreover, the flow split for Sc2 and Sc3 is shown in the last two rows.

Table 3.4: Exiting and non-exiting particle distribution for simulations and flow split for cancer scenarios in Study II.

Sim. or scenario	S2 (%)	S3 (%)	S1-S4 (%)	S5 (%)	S6 (%)	S7 (%)	S8 (%)	Non-exiting (%)
1	11.67	7.48	14.13	14.50	13.47	12.73	26.01	11.49
2	0.50	0.39	0.68	15.93	22.71	14.16	45.63	6.80
3	0	0	0	17.86	20.81	15.63	45.69	4.58
4	0	0	0	18.55	23.87	15.43	42.15	7.68
5	25.37	21.34	18.79	9.55	6.27	9.19	9.50	7.64
6	7.07	4.97	11.99	17.82	23.35	21.32	13.48	9.75
Sc2	3.76	3.75	7.38	13.51	19.15	13.59	38.86	–
Sc3	14.29	14.29	14.29	14.29	14.29	14.29	14.29	–

Figure 3.3 summarizes the segment-to-segment particle distribution. For each chart the information represented denotes a particular position of the catheter tip (i.e., near the bifurcation or far from the bifurcation) and a particular cancer scenario (i.e., scenario 2 or scenario 3). The percentage of exiting particles deposited in the segments is depicted along with the blood flow split and the cancer volume at each segment (S1 to S8).

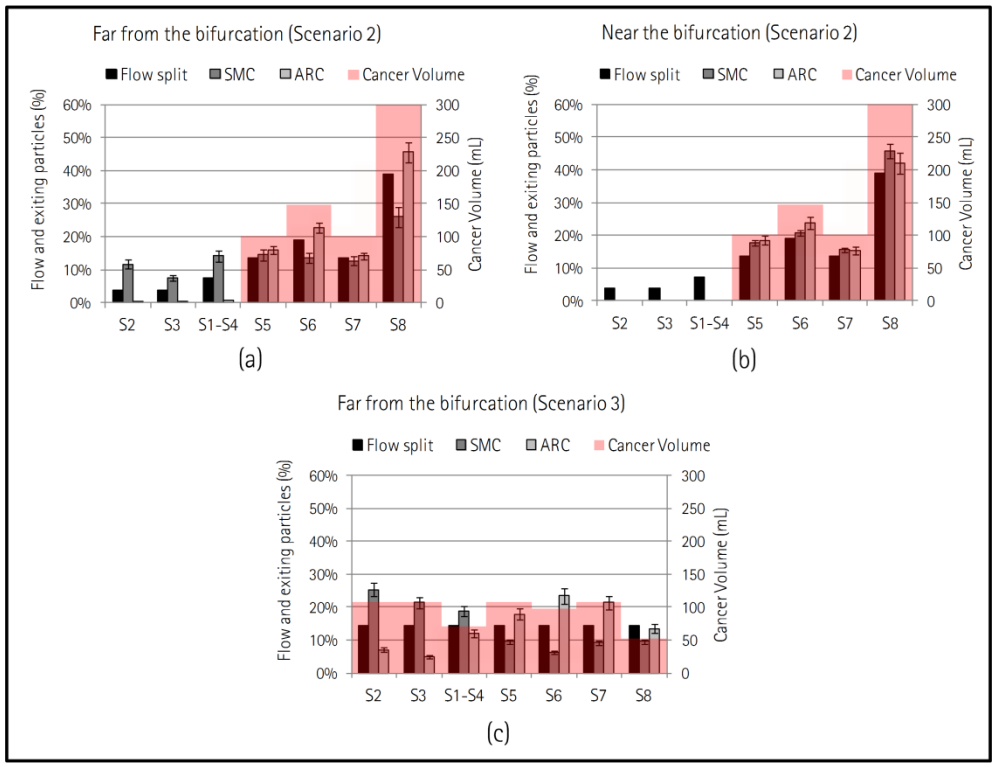

Figure 3.3: Flow split and particle distribution over segments in Study II: liver segments on *x*-axes, flow split and particle distribution on primary *y*-axes, and cancer volume on secondary *y*-axes. (a) Results for simulations 1 and 2, (b) results for simulations 3 and 4, and (c) results for simulations 5 and 6.

3.3.3 Near-tip hemodynamics

Figure 3.4 shows, for (a) the catheter tip vicinities (b) during systolic peak, (c) various velocity contours at different sections and the velocity vectors at a cross-sectional plane for blood in simulations 1 and 2.

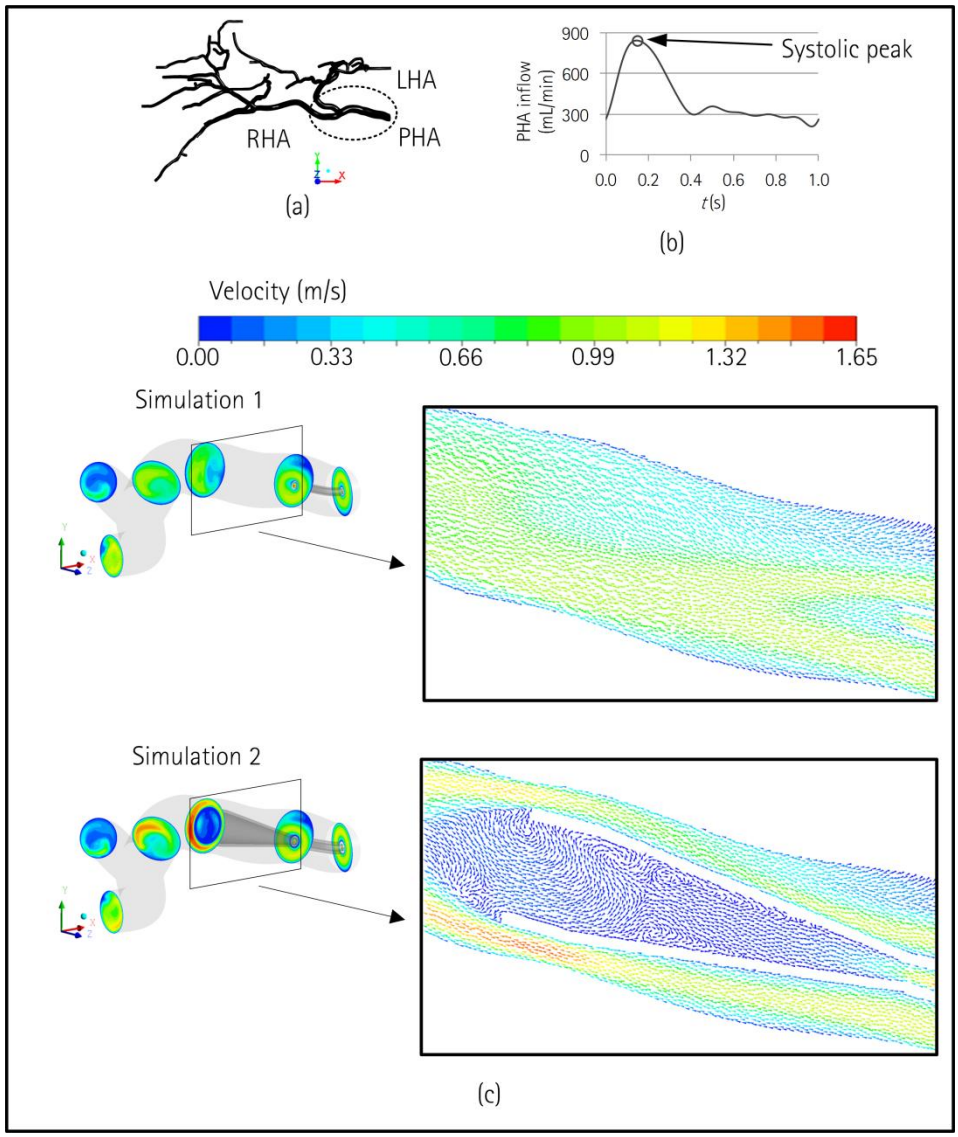

Figure 3.4: For (a) catheter tip vicinities and at (b) systolic peak, (c) the blood velocity contours at different sections and velocity vectors on a plane parallel to flow direction in the catheter tip vicinities for simulation 1 and simulation 2.

Figure 3.4(c) clearly depicts the influence of the expandable tip. Even though the velocity contours on the left present the same pattern but at a different magnitude, the vectors in the box show marked differences. The presence of the funnel-shaped expandable tip in simulation 2 reduced the velocity of the flow coming from the ARC and accelerated the bloodstream. The combination of the flow coming from the

ARC and the bloodstream created recirculations near the expandable tip inner wall (see Figure 3.4(c)).

The first direct consequence of injecting via an SMC or an ARC is the blood flow alteration in the vicinities of the catheter tip, as seen in Figure 3.4. This results in different particle injection patterns, and thus different particle distributions over the liver segments would be expected. Kleinstreuer et al. [47] and Childress et al. [46] also reported on the alteration of the near-tip hemodynamics and the resulting particle distribution. Figure 3.5 shows the streamlines colored by velocity magnitude for simulations 1–4. These streamlines confirmed the point made by van den Hoven et al. [41], who observed that injecting via SMC results in particles entering the bloodstream in a laminar-like smooth fashion in contrast to injecting via ARC, which results in the particles entering the bloodstream in a turbulent-like manner. (Note that strictly speaking blood flow streamlines are not particle pathlines, but it can be observed that the streamlines follow the same pattern throughout the cardiac cycle (see Figure 3.5(c)–(f)), so the particle pathlines are going to be of similar structure. Furthermore, turbulent-like in this case does not mean turbulent flow, but laminar flow with big vortices).

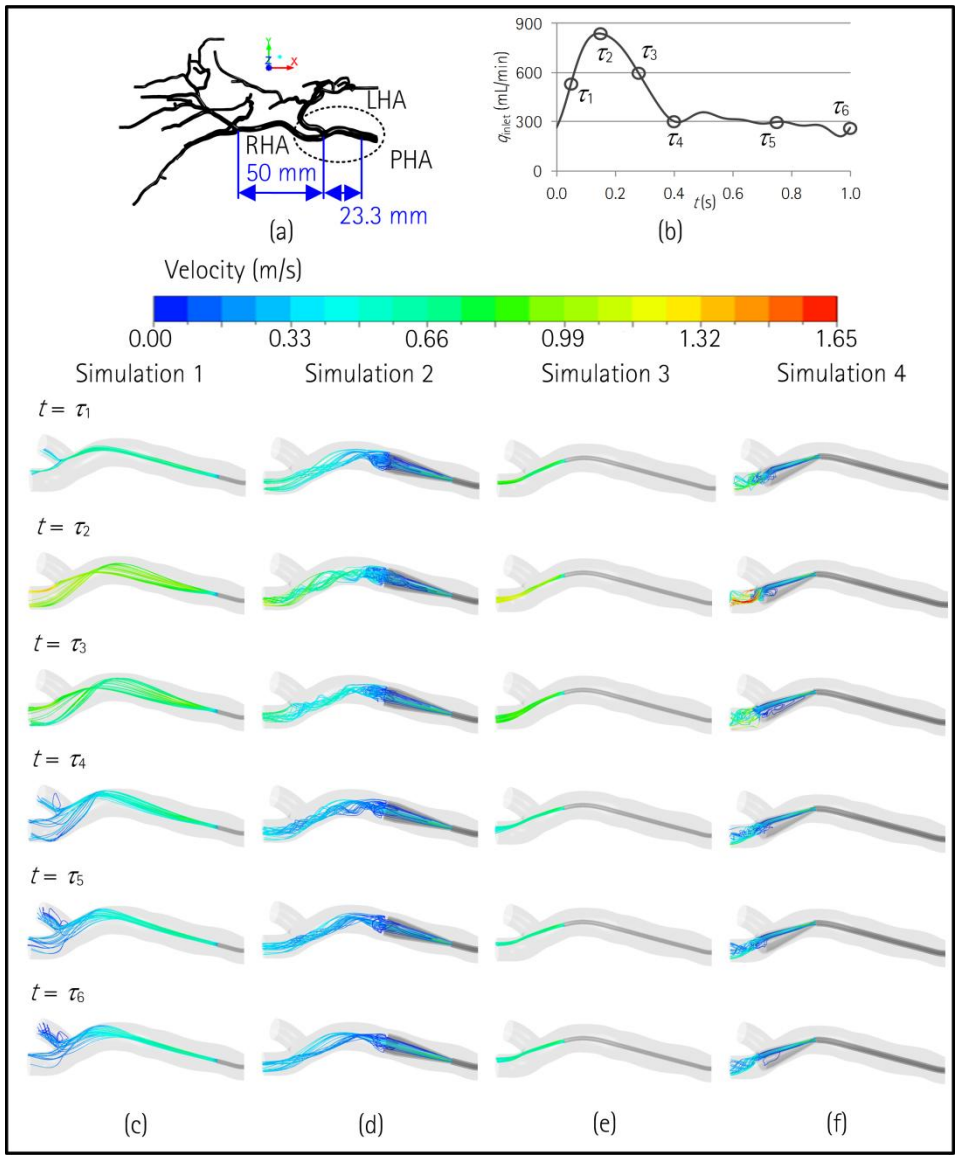

Figure 3.5: (a) Part of the computational domain where the streamlines are analyzed. (b) Temporal points (τ_1 to τ_6) where streamlines are shown. (c)–(f) Streamlines for simulations 1–4. The color of the streamlines corresponds to velocity magnitude.

This near-tip hemodynamics alteration led to differences in particle distribution when the tip was at the 'inlet' position (see Figure 3.3(a) and (c)), i.e., particle segment-to-segment distribution was very much dependent on the near-tip hemodynamics alteration due to the catheter used. Nonetheless, when the tip was at the 'bifurcation' position, the catheter type seemed to be of little importance and,

in addition, particle distribution seemed to be closer to the flow split (see Figure 3.3(b)).

It can be concluded that injecting near a bifurcation was of little importance in terms of segment-to-segment particle distribution when injecting via different devices. However, the presence of the bifurcation is very important when it comes to analyzing the segment-to-segment particle distribution, because the first bifurcation that the particles encounter defines their final fate [67]. In the present case, results indicated that injecting near the bifurcation (from the 'bifurcation' position) with different devices resulted in very similar particle distribution (see Figure 3.3(b)). The bottom line here is that the injections are not performed strictly near a bifurcation. Regarding the ARC, particles are already delivered into the RHA (see Figure 2.12(b)). As for the SMC, even though the microcatheter was close to the RHA (see Figure 2.12(b)) the injection was made at a speed such that particle inertia made them cross blood streamlines and the particles were directly inserted into the RHA, meaning it was like injecting directly from the RHA. Kleinstreuer et al. [47] studied the relative velocity between catheter flow and artery flow, and they concluded that for catheter flow velocities higher than twice the artery flow velocity, particles were able to cross blood streamlines due to the high particle inertia. Indeed, for simulation 3 in the present study, the SMC flow velocity is, on average, 3 times the artery flow velocity, which is higher than the value of 2 reported by Kleinstreuer et al. [47].

3.3.4 Particle distribution in the right lobe

A further analysis was carried out for the right lobe particle distribution due to the surprising results of there being no influence of catheter type over particle distribution when injecting near the bifurcation, which led to exclusively right lobe-directed treatment (see Figure 3.3(b)). To that end, the blood flow and number of microspheres that ended up in right lobe segments (S5 to S8) were quantified and the percentages were studied.

Only qualitative representation of results is given here, by means of Figure 3.6; for quantitative analysis refer to Paper IV in 'C: Papers'. Figure 3.6 illustrates particle distribution for the particles that exited right lobe segments.

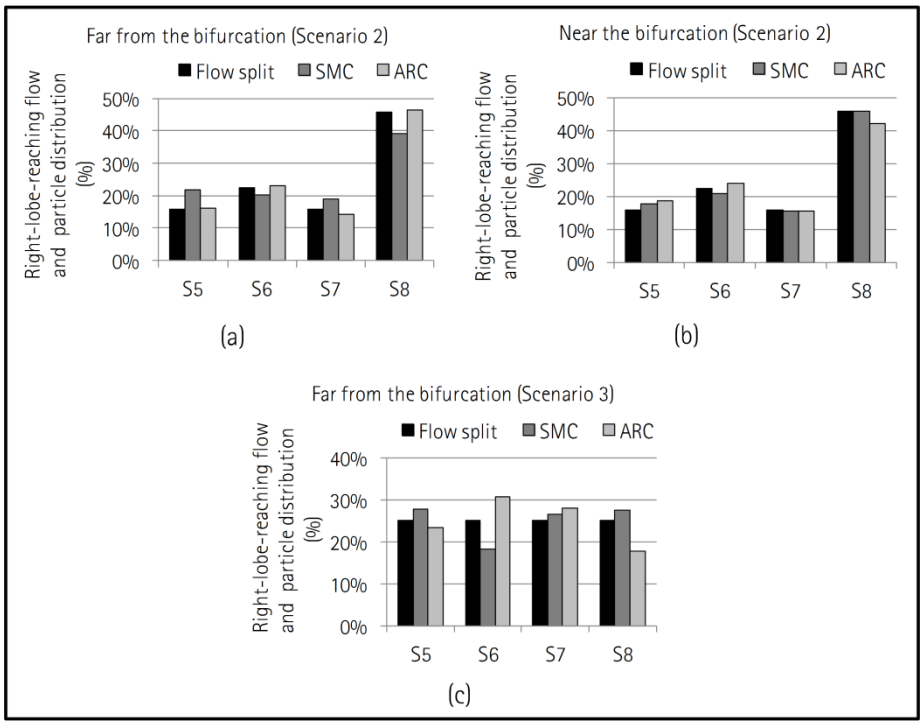

Figure 3.6: Particle distribution over right lobe segments in Study II: liver segments on *x*-axes and particle distribution on *y*-axes. (a) Results for simulations 1 and 2, (b) results for simulations 3 and 4, and (c) results for simulations 5 and 6.

Furthermore, based on this lobe-to-lobe analysis, it was observed for the right lobe that not only was the influence of near-tip hemodynamics reduced, but also the particle distribution tended to match the right lobe-directed blood flow split.

For this patient-specific hepatic artery, once the particles entered the RHA, the artery branch that the particles traveled through was quite long and tortuous, enabling conditions that were favorable for the proper redistribution of microspheres in the bloodstream, so that particle distribution matched the flow split through the downstream branches. It is hypothesized that under the aforementioned favorable conditions, the final particle distribution did not rely on the near-tip hemodynamics alteration. In addition, it was observed that the final particle distribution follows the flow split.

It is noteworthy that in this patient-specific hepatic artery the distance between the injection 'inlet' point and the first bifurcation was about 23.3 mm, while between the proximal and distal points of the RHA it was about 50 mm (see Figure 3.5(a)). The appropriate combination of length and tortuosity may be essential in terms of

particle distribution. This point might be useful in everyday practice, either in order to avoid it or to take advantage of it, depending on the specific case. For example, if infusion must occur from the PHA (e.g., due to high tortuosities of the LHA and RHA) and tumors are over the whole liver, it would be interesting to inject far from a bifurcation so that the particles distribute according to the flow split and cover the eight segments where the tumors are located. On the contrary, if tumors are located in one lobe, it could be more effective to inject closer to the bifurcation and at a sufficient speed so that particles are more clearly directed to that tumor-bearing lobe. Directing particles to tumor-bearing segments is the purpose of the direct drug-targeting strategy, whereby the goal is to target the tumor and spare healthy tissue [43].

3.4 Study III: The role of the microcatheter distal direction and injection point and velocity

3.4.1 Computational times

Table 3.5 tabulates the information regarding the computational cost of Study III simulations. Specifically, the time per iteration, the number of iterations, and the server utilized are specified for presimulations (t=−2 s to t=0) and simulations (t=0 to t=4 s). The total wall-clock hours that took each complete simulation is indicated.

Table 3.5: Computational cost of Study III simulations in terms of seconds per iteration (s/it), number of iterations (Iterations), and server number (Server #) for presimulation (t=−2 s to t=0) and simulation (t=0 to t=4 s). The total wall-clock hours that took each complete simulation is also indicated (Time (h)).

Sim.	t=−2 s to t=0			t=0 to t=4 s			Time (h)
	s/it	Iterations	Server #	s/it	Iterations	Server #	
1	5.83	27970	4	3.44	56575	3	99.43
2	3.03	34898	1	9.82	72245	1	226.47
3	5.54	34410	3	5.74	71925	3	167.67
4	5.06	32270	4	2.64	66345	3	94.07
5	2.60	33080	1	3.03	68130	1	81.20
6	8.44	31135	4	2.71	63795	3	121.11
7	2.94	26790	1	5.48	66705	1	123.38
8	3.04	32160	1	3.44	78105	1	101.69
9	1.95	31990	3	2.88	77780	3	79.61
10	1.87	29405	3	2.42	75490	3	66.02
11	2.60	31345	1	2.96	76515	1	85.49
12	1.94	28755	3	3.68	73100	3	90.22

3.4.2 Particle distribution

Table 3.6 tabulates the particle distribution over the liver segments for Study III simulations. The non-exiting particle percentage is indicated in the last column. Moreover, the flow split for Sc2 is shown in the last row.

Table 3.6: Exiting and non-exiting particle distribution for simulations and flow split for the cancer scenario in Study III.

Sim.	S2 (%)	S3 (%)	S1-S4 (%)	S5 (%)	S6 (%)	S7 (%)	S8 (%)	Non-exiting (%)
1	0	0	0	17.82	31.72	16.59	33.87	3.59
2	0	0	0	21.31	12.57	12.37	53.76	4.32
3	0	0	0	19.46	17.50	14.46	48.58	5.15
4	0	0	0	19.03	19.58	14.09	47.30	4.76
5	31.71	20.77	36.34	2.95	1.63	2.72	3.88	20.26
6	36.79	22.10	36.37	1.13	0.85	0.94	1.82	22.35
7	0	0	0	15.49	41.08	12.80	30.63	9.51
8	0	0	0	18.81	42.06	11.11	28.02	10.65
9	0	0	0	20.43	24.01	15.91	39.64	9.25
10	0	0	0	15.75	38.90	19.82	25.53	8.97
11	17.51	8.56	20.17	13.22	11.45	8.77	20.34	23.87
12	27.39	18.52	27.14	6.26	6.44	4.16	10.11	24.24
Flow	3.76	3.75	7.38	13.51	19.15	13.59	38.86	–

Figure 3.7 summarizes the segment-to-segment particle distribution. For each chart the information represented denotes a particular injection point (i.e., points S, W or E). The percentage of exiting particles deposited in the segments is depicted along with the blood flow split and the cancer volume at each segment (S1 to S8).

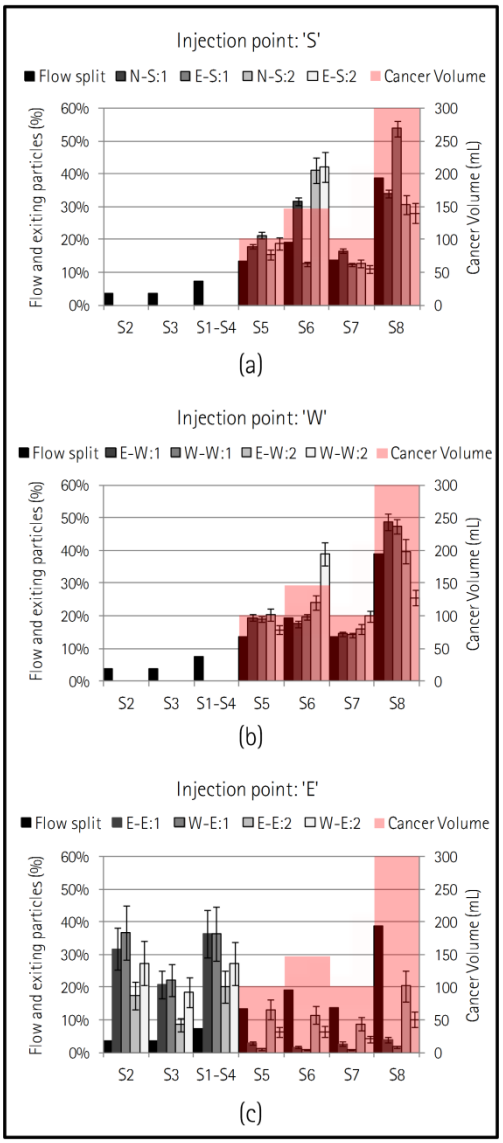

Figure 3.7: Flow split and particle distribution over segments in Study III: liver segments on *x*-axes, flow split and particle distribution on primary *y*-axes, and cancer volume on secondary *y*-axes. (a) Injection point S and directions N-S and E-S (simulations 1, 2, 7, and 8), (b) injection point W and directions E-W and W-W (simulations 3, 4, 9, and 10), and (c) injection point E and directions E-E and W-E (simulations 5, 6, 11, and 12) (See simulation codes in Table 2.11).

Overall, the influence of the injection point was clear. When the injection was performed at points S and W only the right lobe was targeted (see Figure 3.7(a) and Figure 3.7(b)). Yet when injection was at point E, while both lobes were targeted, the tumor-lacking lobe received more particles than the right lobe (see Figure 3.7(c)).

More specifically, if injection point S is analyzed in Figure 3.7(a), it can be seen that for all the cases depicted the particle distribution was similar except E-S:1 for S6 and S8. While the average amount of particles exiting S6 and S8 were 38.28% and 30.83% for N-S:1, N-S:2 and E-S:1, these values were 12.57% and 53.76% for E-S:1 (see Table 3.6). The same thing happened for injection point W, where simulation W-W:2 differs from the others (E-W:1, W-W:1, E-W:2) in terms of the particles exiting S6 and S8 (see Figure 3.7(b)). While the average amount of particles exiting S6 and S8 were 20.36% and 45.17% for E-W:1, W-W:1 and E-W:1, these values were 38.90% and 25.53% for W-W:2 (see Table 3.6). For injection point E, the differences in particle distribution for different microcatheter directions and injection velocities were more marked than for injection points S and W (see Figure 3.7(c)). Therefore, microcatheter direction and injection velocity also played a role in particle distribution. Regarding microcatheter direction, for the same injection point and injection velocity, differences in particle distribution were observed between N-S:1 and E-S:1, E-W:2 and W-W:2, and E-E:2 and W-E:2. As for injection velocity, for the same injection point and microcatheter direction, differences in particle distribution were observed between E-S:1 and E-S:2, W-W:1 and W-W:2, and E-E:1 and E-E:2.

In order to illustrate the influence of the parameters studied, i.e. particle injection point, microcatheter distal direction, and injection velocity, Figure 3.8 depicts the streamlines of the flow that was incorporated into the bloodstream via the microcatheter. It is worth noting that the streamlines are not the exact particle pathlines, but they are similar because the particles are mainly transported by the bloodstream. Figure 3.8(a) shows the anterior view of the hepatic artery; the two areas where the streamlines were analyzed are enclosed within the dashed lines. Figure 3.8(b) depicts the systolic peak (t=0.15 s) and early diastole (t=0.40 s) points, and Figure 3.8(c)–(e) illustrate the influence of the aforementioned parameters.

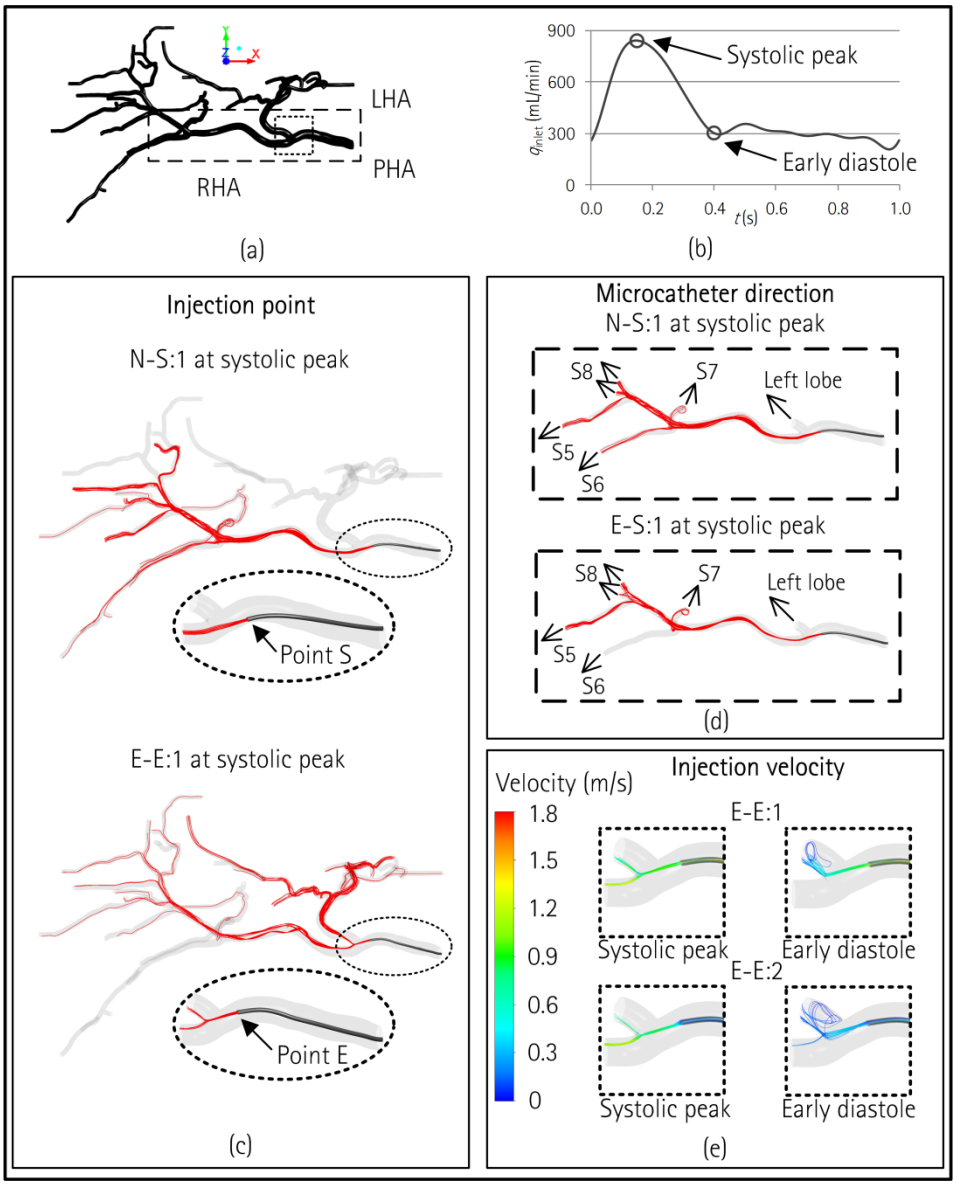

Figure 3.8: (a) Hepatic artery geometry where the injection point, the microcatheter direction (large dashed line box), and injection velocity (small dashed line box) are analyzed. (b) Temporal points for systolic peak (t = 0.15 s) and early diastole (t = 0.40 s) depicted over the inflow flow rate waveform. (c) Injection point analysis via the streamlines of microcatheter exiting flow in N-S:1 vs. E-E:1 at systolic peak, i.e., injection point S vs. E. (d) Microcatheter direction analysis via the streamlines of microcatheter exiting flow in N-S:1 vs. E-S:1 at systolic peak, i.e., direction N-S vs. direction E-S. (e) Injection velocity analysis via the streamlines (colors indicating velocity magnitude) of microcatheter exiting flow in E-E:1 vs. E-E:2 at systolic peak and early diastole.

Figure 3.8(c) compares injection points S and E by showing the streamlines for N-S:1 (injection point at S) and E-E:1 (injection point at E) at the systolic peak. Injection at point S results in a right lobe-directed treatment, while injection at point E treats both liver lobes. Figure 3.8(d) compares the directions N-S and E-S by illustrating the streamlines at the systolic peak for the cases N-S:1 and E-S:1 and indicating the liver zone that fed each branch. The lack of particle deposition in S6 can be observed for the direction E-S. Figure 3.8(e) compares the injection velocities for the direction E-E (i.e., E-E:1 vs. E-E:2) by showing the streamlines (colors indicating velocity magnitude) of the flow incorporated into the bloodstream at systolic peak and early diastole. The streamline pattern shows higher differences during early diastole than during systolic peak.

3.4.3 Discussion

In this study a patient-specific geometry under a literature-based cancer scenario was used in order to study a set of delivery parameters in a RE procedure with resin microspheres loaded with ^{90}Y. In particular, the injection point within a cross-section, the microcatheter distal direction, and the injection velocity were analyzed. The injection distance from a bifurcation was previously analyzed in Aramburu et al. [67].

The study showed that the presence of a microcatheter in the artery alters the hemodynamic parameters (i.e., blood velocity and pressure fields) in the nearby artery lumen. Moreover, if an additional injection fluid flow is incorporated into the bloodstream from the microcatheter tip, then the blood flow pattern near the tip greatly depends on that incoming flow. This blood flow alteration is dispersed after some distance from the microcatheter tip, because it is mainly the downstream vasculature that sets the flow split due to the resistive behavior of arterioles and sinusoids (i.e., the liver-specific capillaries) [66]. However, as far as the injected particles are concerned, this flow alteration may be essential in terms of the final particle deposition. As soon as the microparticles are incorporated into the bloodstream, the near-tip hemodynamics is essential in defining their final destination. The combination of a specific location and velocity for a particle and a specific blood flow velocity and pressure fields results in a specific particle path. Therefore, the particle might end up deposited either in a target or a nontarget zone.

The following subsections analyze the parameters that alter the near-tip hemodynamics—the injection point, the microcatheter distal direction, and the injection velocity—that in turn influence the segment-to-segment particle distribution.

It is important to note that the reported results and the discussion are specific for this patient-specific hepatic artery, the cancer scenario posited, and the injection characteristics defined for simulations 1 to 12 (see Table 2.11). Therefore, the conclusions reached in this Study III should be carefully tested for each patient being treated with RE.

3.4.3.1 Injection point

Basciano et al. [45] showed that the injection point within a given cross-section is of paramount importance for the downstream particle distribution. In the present study, the geometry used was a more complex geometry (a patient-specific one) under a (literature-based) cancer scenario, but the same conclusion was reached here. In fact, it was observed that particles went mainly to the left lobe (where there were no tumors) when injected at point E and they went to the right lobe (target zone) when injected from points S and W (see Figure 3.7).

3.4.3.2 Microcatheter distal direction

Depending on the path described by the microcatheter distally and the microcatheter's rigidity, the microcatheter direction may change for a given injection point (see Figure 2.13) (either from pretreatment to actual treatment or during the treatment as well). This is the first time that this parameter has been studied and it seems that it may also be very important in the segment-to-segment particle distribution; differences were observed between N-S:1 and E-S:1, E-W:2 and W-W:2, and E-E:2 and W-E:2 (see Figure 3.7).

3.4.3.3 Injection velocity

For a given injection point and microcatheter direction, the injection velocity may also be an important parameter in the particle distribution. This can be observed when comparing the particle distribution in segments S6 and S8 in cases E-S:1 vs. E-S:2 and W-W:1 vs. W-W:2. Moreover, large differences due to the injection velocity can be also observed in any segment in the case of E-E:1 vs. E-E:2 (see Figure 3.7(c)).

Kleinstreuer et al. [47] studied the influence of injection velocity for a representative hepatic artery. It was shown that for values of the ratio between the average

microcatheter lumen velocity and average artery lumen velocity (i.e., the velocity ratio) below 2, particles are propelled by the bloodstream; however, for velocity ratios above 5, particles are able to cross the blood flow streamlines due to high inertia, making the particle pathlines unpredictable. In analyzing the case of E-E:1 vs. E-E:2, Figure 3.8(e) illustrates the streamlines of the flow incorporated into the bloodstream at systolic peak and early diastole. During the systolic peak, injecting at 18.5 mL/min or at 5 mL/min led to a velocity ratio of 1.26 and 0.34, respectively. This resulted in a similar streamline pattern during the systolic peak regardless of the injection velocity because the incoming flow adopted the bloodstream flow characteristics rapidly. However, during the early diastole that ratio took the values of 3.5 and 0.94. Therefore, for the injection at 18.5 mL/min the velocity at which particles were released was sufficiently high so that they were capable of crossing the bloodstream streamlines due to the high inertial force. It is important to note that the diastole lasts for 60% of the cardiac cycle and with almost the same blood flow rate (between 210 and 350 mL/min) compared with the systolic peak flow rate (840 mL/min) (see Figure 3.8(b)). Therefore, given that the differences due to injection velocity occur more markedly during the longest time interval with similar characteristics (i.e., diastole) it is clear that this may lead to differences in segment-to-segment particle distribution.

3.5 Study IV: The role of the orientation of an angled-tip microcatheter and injection velocity

3.5.1 Computational times

Table 3.7 tabulates the information regarding the computational cost of Study VI simulations. Specifically, the time per iteration, the number of iterations, and the server utilized are specified for presimulations (t=−2 s to t=0) and simulations (t=0 to t=4 s). The total wall-clock hours that took each complete simulation is indicated.

Table 3.7: Computational cost of Study IV simulations in terms of seconds per iteration (s/it), number of iterations (Iterations), and server number (Server #) for presimulation (t=−2 s to t=0) and simulation (t=0 to t=4 s). The total wall-clock hours that took each complete simulation is also indicated (Time (h)).

Sim.	t=−2 s to t=0			t=0 to t=4 s			Time (h)
	s/it	Iterations	Server #	s/it	Iterations	Server #	
1	8.80	30145	3	3.50	62555	3	134.45
2	7.56	27570	3	4.88	70385	3	153.28
3	3.40	31210	5	2.32	63905	5	70.61
4	9.93	28530	3	5.06	73925	3	182.59
5	1.89	31105	5	8.24	64030	1	162.82
6	1.88	27095	5	6.38	71485	1	140.79
7	1.87	28300	5	5.27	60050	5	102.61
8	6.10	27685	3	2.39	71690	3	94.47

3.5.2 Particle distribution

Table 3.8 tabulates the particle distribution over the liver segments for Study VI simulations. The non-exiting particle percentage is indicated in the last column. Moreover, the flow split for Sc2 is shown in the last row.

Figure 3.9 illustrates the exiting particle distribution for (a) the U and R microcatheter tip orientations and (b) the D and L orientations. The liver segments are along the x-axis, flow split and particle distribution are along the primary y-axis, and cancer volume is along the secondary y-axis.

Table 3.8: Exiting and non-exiting particle distribution for simulations and flow split for Study IV.

Sim.	S2 (%)	S3 (%)	S1-S4 (%)	S5 (%)	S6 (%)	S7 (%)	S8 (%)	Non-exiting (%)
1	0.07	0.03	0.17	17.69	24.29	15.18	42.57	5.19
2	0	0	0	20.01	27.52	16.99	35.48	5.93
3	3.37	2.53	3.70	17.27	25.76	14.98	32.38	13.33
4	5.65	4.07	13.38	13.99	23.22	11.36	28.33	9.84
5	3.01	2.51	7.08	16.81	21.97	14.58	34.04	12.50
6	6.91	5.49	8.29	14.82	21.36	12.25	30.88	10.17
7	1.62	0.49	1.26	17.00	30.42	14.50	34.72	5.54
8	0.11	0.07	0.14	20.11	21.37	15.47	42.72	5.81
Flow	3.76	3.75	7.38	13.51	19.15	13.59	38.86	–

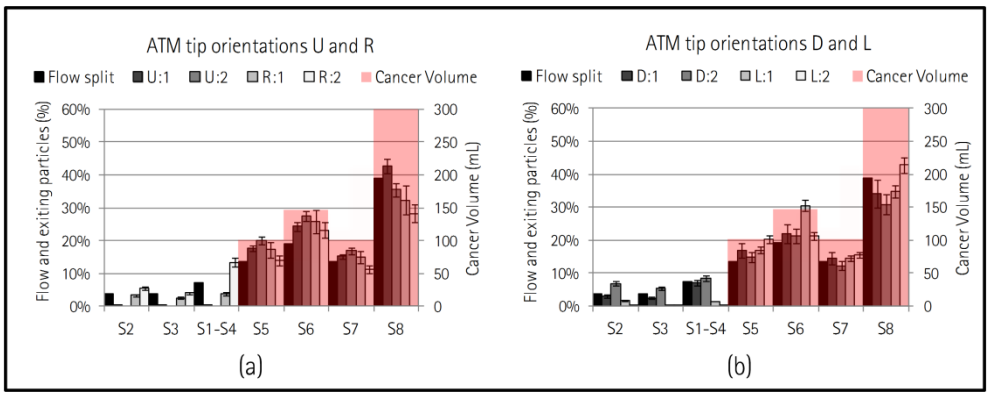

Figure 3.9: Flow split and particle distribution over segments in Study IV: liver segments on *x*-axes, flow split and particle distribution on primary *y*-axes, and cancer volume on secondary *y*-axes. (a) ATM tip at U and R orientations (simulations 1–4) and (b) ATM tip at D and L orientations (simulations 5–8).

Results indicate qualitatively that particle distribution tries to follow the flow split (see Figure 3.9(a)–(b)) almost without regard to injection velocity and tip orientation. Nevertheless, if Table 3.8 is analyzed, it is apparent that both injection velocity and tip orientation play a role in terms of particle transport. Specifically, if the exiting particle percentage and flow split are compared for each segment (columns 2–8 in Table 3.8), defining s:{'min', 'max', 'flow'}, where 'min' and 'max' are

the minimum and maximum value for exiting particle percentage and where 'flow' is the flow split for each segment *s*, then the results are the following: S2:{0%, 6.91%, 3.76%}, S3:{0%, 5.49%, 3.75%}, S1-S4:{0%, 13.38%, 7.38%}, S5:{13.99%, 20.11%, 13.51%}, S6:{21.36%, 30.42%, 19.15%}, S7:{12.25%, 16.99%, 13.59%}, S8:{30.88%, 42.72%, 38.86%}. The maximum difference between maximum or minimum particle percentage and flow split takes place for S6 in simulation 7, where the maximum particle distribution minus flow split is 11.27%. Therefore, in general particle distribution tends to follow flow split, although differences can be expected simply due to injection velocity and the ATM tip orientation, as occurs in this study.

3.5.3 Injection velocity

The presence of a microcatheter with an incoming flow alters the near-tip hemodynamics in the hepatic artery. Indeed, if the ratio of ATM lumen and PHA lumen average velocities is computed, for 18.5 mL/min the maximum ratio is 8 and the average ratio is 4.7, meaning that the velocity of the flow incorporated into the bloodstream is on average 4.7 times the bloodstream velocity with a maximum value of 8. For a 5 mL/min incoming flow, the average ratio is 1.3 with a maximum ratio of 2.2. Given that it is the downstream vasculature which sets the flow split via the BCs [66], the incoming flow only affects the near-tip hemodynamics, although it might be essential in terms of particle distribution [67].

In this study, the near-tip particle–hemodynamics is more closely studied. Figure 3.10 shows (a) for the near-tip geometric domain and (b) at five temporal points (t_2 to t_6), (c) the position of the injected particles for simulation 1 (18.5 mL/min ATM inflow) and simulation 2 (5 mL/min ATM inflow). Therefore, the influence of injection velocity is analyzed for the microcatheter tip in the U orientation. Results show how particles take longer to exit the microcatheter for simulation 2 (see Figure 3.10(c) at $t=t_2$). Furthermore, if Figure 3.10(c) at $t=t_2$ to $t=t_4$ are analyzed, in simulation 1 the particles exit the microcatheter by approaching the wall and in a more spread out fashion (i.e., occupying larger portion of the cross-sectional area of the lumen) than in simulation 2, where they follow the bloodstream.

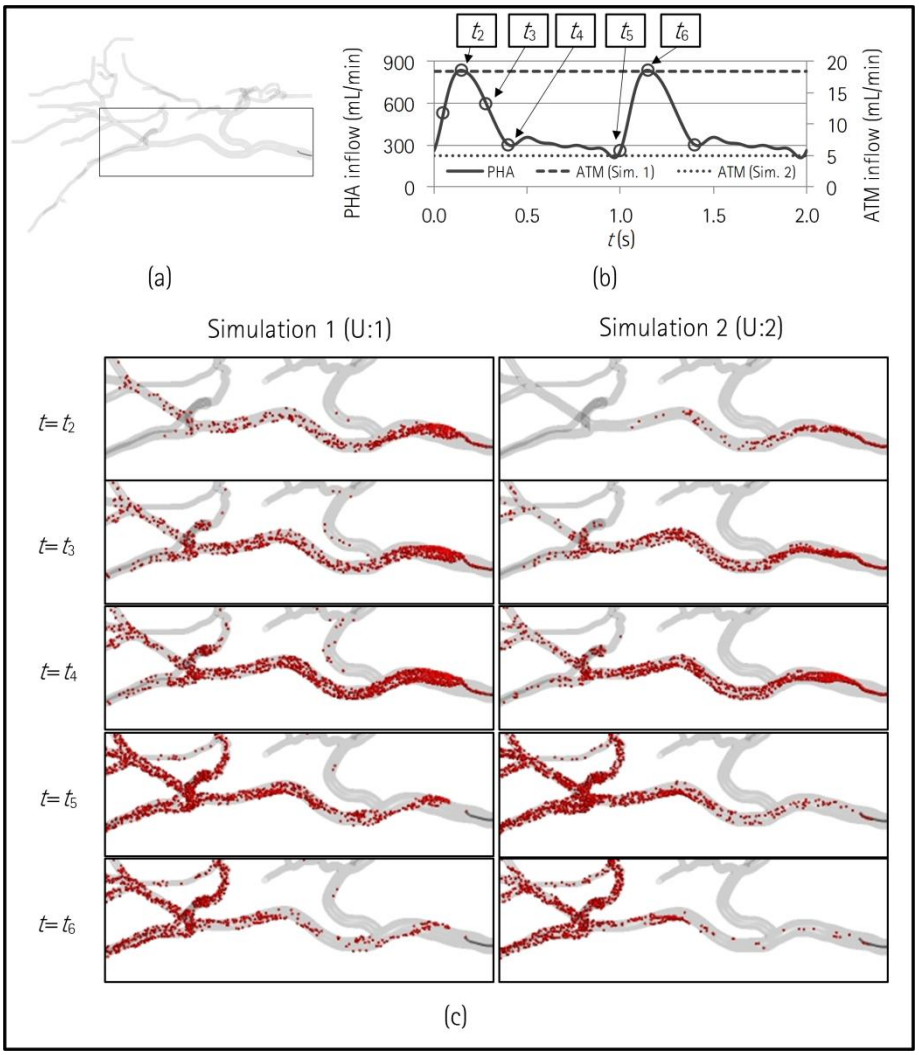

Figure 3.10: (a) For the PHA, RHA, and LHA, (b) at t_2–t_6, (c) the location of microspheres for simulations 1 and 2. t_2=0.15 s (systolic peak); t_3=0.28 s (systolic deceleration); t_4=0.40 s (early diastole); t_5=1.00 s (cycle end); t_6=1.15 s (systolic peak).

In order to analyze how the particles are spread and distributed along the artery, Figure 3.11 shows (a) for cross-sections A and C and (b) for t_2 to t_6 (c) the velocity magnitude contours and particle position and number of particles for simulation 1 and simulation 2. The number in the bottom left corner of each panel indicates what percentage of the area contains particles. The color of the grayscale spheres depicted in Figure 3.11 indicates the number of particles in that mesh element. Distances between the tip and section A (5 mm) and between sections A and C (15.5 mm) are specified in Figure 3.11(a).

Figure 3.11 indicates that in this specific case (i) particles always travel closer to the artery wall in simulation 1, (ii) particles describe clockwise helical paths, and (iii) particles are almost always (except at t_6) more spread out in simulation 1 than in simulation 2. These three facts come as a result of the complex hemodynamics pattern through complex hepatic artery branches.

The influence of injection velocity had been explored in terms of particle distribution [47,48,67]. Aramburu et al. [67] analyzed this point by observing how the artery to microcatheter velocity ratio affected the segment-to-segment particle distribution. For example, this ratio could vary due to an increase of blood flow for the same injection velocity [67]. Basciano et al. [48] and Kleinstreuer et al. [47] analyzed the artery to microcatheter velocity ratio in terms of the pathlines described by the particles. They studied ratios of 0.01, 1, 2, 5, and 10. As the ratio increased from 0.01 to 2, particles tended to travel through the artery lumen in a more spread out manner, but driven by the bloodstream. However, for ratios of 5 and 10, particle inertia was able to make particles cross blood flow streamlines rather than being driven by the bloodstream at least until the initial momentum was dissipated by the drag force actuating on the particles. However, these previous studies did not analyze the particle location in time, as shown here in Figure 3.10 and Figure 3.11.

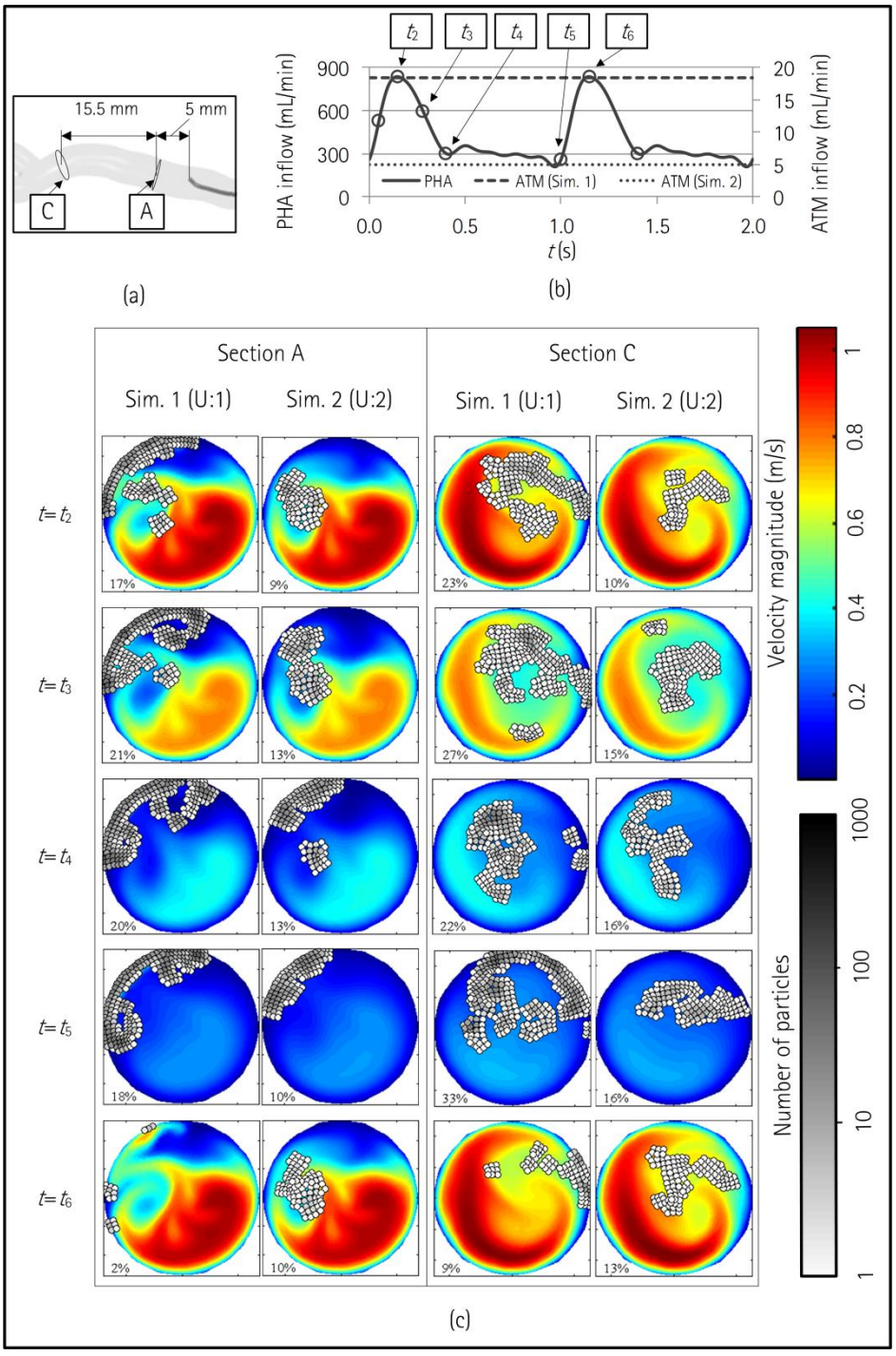

Figure 3.11: (a) For sections A and C in the PHA, (b) at t_2–t_6, (c) the location of microspheres for simulations 1 and 2. t_2=0.15 s (systolic peak); t_3=0.28 s (systolic deceleration); t_4=0.40 s (early diastole); t_5=1.00 s (cycle end); t_6=1.15 s (systolic peak).

3.5.4 Tip orientation

This is the first time that this ATM-related parameter is being analyzed.

In this case, the ATM is placed in the PHA and the target branch after the bifurcation is the RHA, where tumors are located (see Figure 2.14). The blood flow through complex arterial trees describes helical and chaotic bloodstreams—even though in laminar regime. Therefore, the particle travel not only depends on the relative position of the ATM tip and the target artery branch of a bifurcation but also on the blood flow resulting from the complex hepatic artery geometry. In other words, particles, which are driven by the bloodstream, do not necessarily travel towards the artery branch the ATM tip is pointing at, because the helical blood flow might make the particles describe pathlines that end up crossing the nontargeted branch.

Figure 3.12 shows the particle location (Figure 3.12(c)) along the hepatic artery (Figure 3.12(a)) for five temporal points t_2 to t_6 (Figure 3.12(b)) for simulations 1 (U:1) and 5 (D:1). As seen in Figure 2.14, the RHA and the LHA are pointing leftward and rightward, respectively. Even though the ATM tips are pointed upward and downward, the helical flow makes the particles travel through both RHA and LHA. The flow split is 85.11% to RHA and 14.89% to LHA, so it is logical that the majority of particles go through RHA. However, Figure 3.12(c) illustrates for simulation 5 at t_5 and t_6 that particles are located in the LHA as a result of the helical flow; a helical flow can be noticed in the temporal evolution of particle location illustrated by Figure 3.12(c). Specifically, the particle distribution is 99.63% to RHA and 0.37% to LHA for simulation 1; and 87.4% to RHA and 12.6% to LHA for simulation 5 (see Table 3.8). That is, in simulation 1 the targeted lobe is the right lobe, while in simulation 5 both right and left lobes are bombarded.

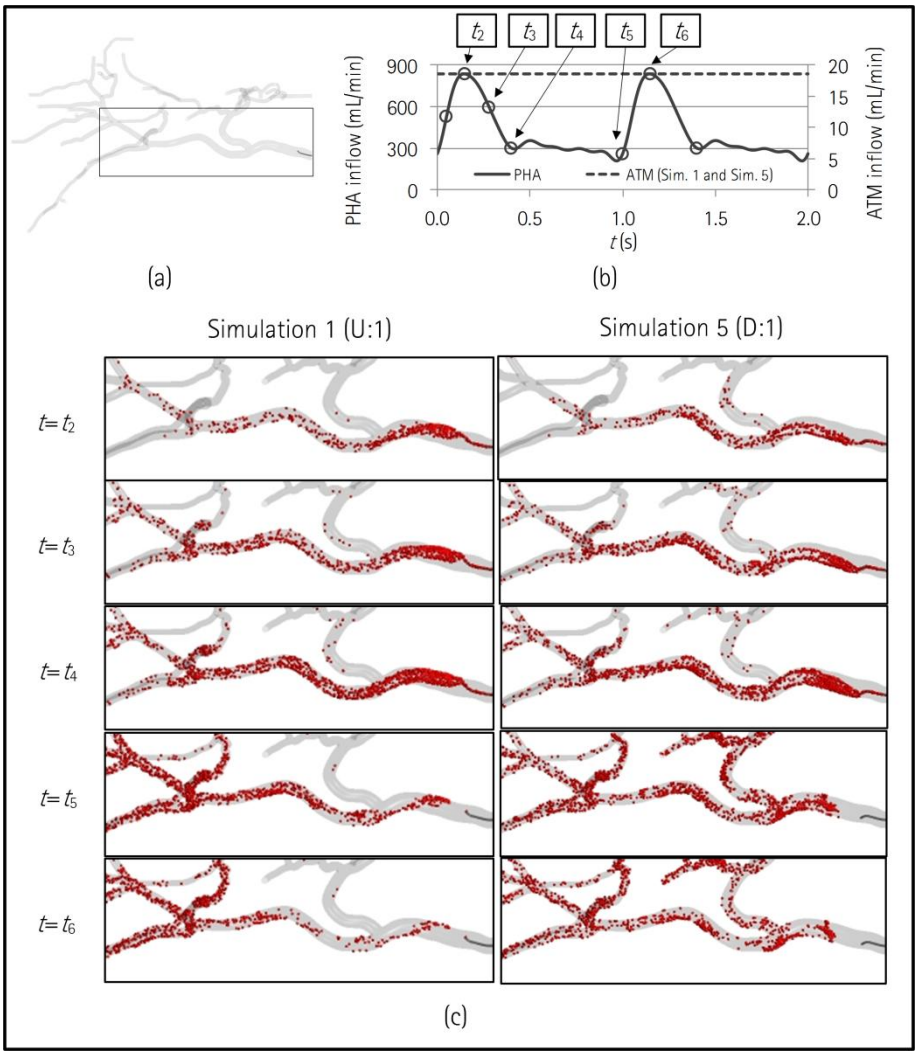

Figure 3.12: (a) For the PHA, RHA, and LHA, (b) at t_2–t_6, (c) the location of microspheres for simulations 1 and 5. t_2=0.15 s (systolic peak); t_3=0.28 s (systolic deceleration); t_4=0.40 s (early diastole); t_5=1.00 s (cycle end); t_6=1.15 s (systolic peak).

Figure 3.13 shows for sections A and C, which are located at 5 mm and 20.5 mm from the ATM tip (see Figure 3.13(a)), for t_2 to t_6 (see Figure 3.13(b)), how the near-tip hemodynamics influences particle travel for simulation 1 (U:1) and simulation 5 (D:1) (see Figure 3.13(c)). As in Figure 3.11(c), there is a clockwise rotation in the particle location as they move forward.

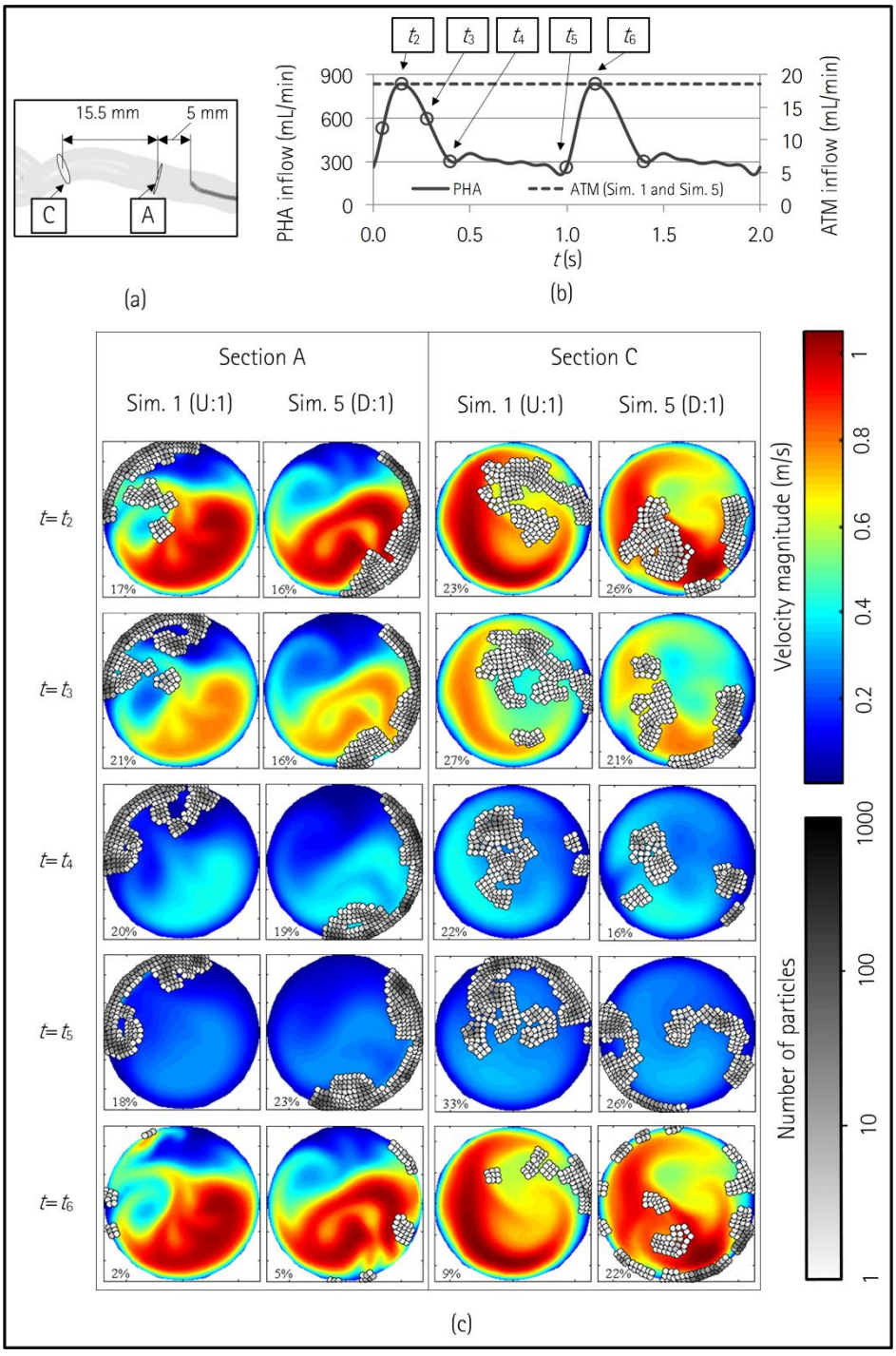

Figure 3.13: (a) For sections A and C in the PHA, (b) at t_2–t_6, (c) the location of microspheres for simulations 1 and 5. t_2=0.15 s (systolic peak); t_3=0.28 s (systolic deceleration); t_4=0.40 s (early diastole); t_5=1.00 s (cycle end); t_6=1.15 s (systolic peak).

Chapter 4

Concluding Remarks

"*A conclusion is simply the place where you got tired of thinking.*" Dan Chaon

---

This final chapter sums up the contributions made by this thesis, the conclusions of the four studies carried out, the study limitations, and the closing thoughts.

4.1 Summary of contributions

Two types of contributions can be distinguished. First, those related to the development of methodologies to derive BCs for numerical simulations. In this regard, methodologies for deriving outflow BCs small arteries with multiple outlets (see Paper I in 'C Papers') [65] and for deriving BCs in hepatic arteries (see Paper II in 'C Papers') [66] have been developed.

Second, it has been possible to provide numerical simulation-based insights into matters that concern physicians and these insights will hopefully help in the decision making process of everyday practice. The conclusions reached via the four main studies this thesis is based on are summarized in the following section.

4.2 Conclusions

4.2.1 Study I: The pretreatment as an actual treatment surrogate

Results suggest that microcatheter placement is of paramount importance in particle distribution, both in terms of the location in the artery (near a bifurcation or not) and in the shifting between the pretreatment and RE treatment microcatheter tip locations. Moreover, the higher the cancer burden, the better the tumor targeting due to the enhanced particle transport power.

4.2.2 Study II: The role of the catheter type and location

The main conclusion that can be drawn from this study is that injecting from a sufficiently long and tortuous artery branch may ensure a downstream particle distribution that matches flow split, almost regardless of the catheter type (even if the catheter influences the local near-tip hemodynamic patterns, and in turn the particle injection pattern) because of the likely adequate conditions for microsphere redistribution in the bloodstream.

4.2.3 Study III: The role of the microcatheter distal direction and injection point and velocity

It can be concluded that even though the injection point seems to be a very important parameter in RE treatment, microcatheter direction and injection velocity may also play an important role in terms of particle distribution. Therefore, the interventional radiologist should be aware that even if the microcatheter placement and an injection rate are planned during pretreatment work-up, unintentional modifications to microcatheter tip position, microcatheter direction, and injection rate may lead to differences in particle distribution during tumor targeting, possibly influencing the procedure outcome.

4.2.4 Study IV: The role of the orientation of an angled-tip microcatheter and injection velocity

Although particle distribution seems to follow the flow split, particle injection velocity and microcatheter tip orientation have been proved to be of some importance in terms of segment-to-segment particle distribution because they are influencing the near-tip hemodynamics. Furthermore, it has been observed that the

higher the injection velocity the more spread out the particle distribution across cross-sectional areas of the artery lumen. Moreover, it is not possible to accurately predict which branch of the bifurcation will take the particles beforehand when only focusing on tip orientation because the complex geometry of hepatic arteries makes the bloodstream take the form of helical and chaotic streamlines, so the particle pathlines are not initially intuitive, even though the particle distribution will be similar to the flow split.

4.3 Study limitations

Despite the encouraging results, the modeling approach is open to several improvements, which are listed below:

- The travel of particles only from the PHA to the subsegmentals was modeled; what occurs intrasegmentally was beyond the scope of this study.
- The first stage of the treatment was modeled. Therefore, the dynamic blood flow redistribution due to the embolic effect of particles was not considered.
- Only one hepatic artery was analyzed. More hepatic artery geometries would help generalize the conclusions reached.
- The injection fluid was assumed to be of the same characteristics of blood in terms of density and viscosity, although it is an aqueous solution in reality.
- The injected microparticles were modeled with constant diameter and density.
- Rigid artery walls were assumed, so no real-life events that cause arterial response were modeled.
- The devices employed for the particle injection (SMC, ARC, and ATM) were rigidly placed in the computational domain, therefore the movement resulting from the interaction between the blood flow and those devices was not taken into consideration.

4.4 Closing thoughts and future perspectives

The great number of scientific publications suggesting the incorporation of biomedical engineering tools to everyday medical practice makes me think that we could be on track to confirm numerical simulations as an invaluable tool for medical standard practice in the not-too-distant future [76].

For example, our unlucky Matthew might have been cured from his metastatic liver disease in 2010 if some of the conclusions reached from the studies reported in this dissertation were known at that time.

In addition, as for the research lines related to this work, the aforementioned study limitations regarding the modeling approach should be overcome. Some of the modeling approaches that would bring us closer to reality include:

- The numerical modeling of intrasegmental events.
- The numerical modeling of embolization-caused blood flow redistribution.
- The numerical simulation of the interaction between two different fluids, i.e., blood and the aqueous solution in which particles are carried through the injection device.
- The inclusion of the variability in diameter for the injected microagent.
- The modeling of the interaction between the patient and their hepatic arterial response and between the injection device and the blood flow via FSI simulations.

However, it is not clear whether the inclusion of these complexities significantly improves the accuracy of the results and the consequent conclusions.

Finally, some experimental research should be conducted in order to validate the numerical modeling approach. As stated by Ballyk [77], "this—referring to numerical studies—is an excellent first step. However, before these results can be taken to the bedside, it is important to determine whether they can be verified or supported by experiments…".

Chapter 5

Bibliography

"*There is no friend as loyal as a book.*" Ernest Hemingway

[1] Kennedy, A., Nag, S., Salem, R., Murthy, R., McEwan, A. J., Nutting, C., Benson, A., Espat, J., Bilbao, J. I., Sharma, R. A., Thomas, J. P., and Coldwell, D., 2007, "Recommendations for radioembolization of hepatic malignancies using yttrium-90 microsphere brachytherapy: A consensus panel report from the Radioembolization Brachytherapy Oncology Consortium," Int. J. Radiat. Oncol. Biol. Phys, **68**(1), pp. 13–23.

[2] Sun, Q., and Wu, G. X., 2013, "Coupled finite difference and boundary element methods for fluid flow through a vessel with multibranches in tumours.," Int. J. Numer. Method. Biomed. Eng., **29**(3), pp. 309–31.

[3] Cattaneo, L., and Zunino, P., 2014, "A computational model of drug delivery through microcirculation to compare different tumor treatments.," Int. J. Numer. Method. Biomed. Eng., **30**(11), pp. 1347–71.

[4] Dooley, J. S., Lok, A. S. F., Burroughs, A. K., and Heathcote, E. J., eds., 2011, Sherlock's Diseases of the Liver and Biliary System, Wiley-Blackwell, Oxford,

UK.

[5] Rutkauskas, S., Gedrimas, V., Pundzius, J., Barauskas, G., and Basevicius, A., 2006, "Clinical and anatomical basis for the classification of the structural parts of liver.," Medicina (Kaunas)., **42**(2), pp. 98–106.

[6] Couinaud, C., 1992, "The anatomy of the liver," Ann. Ital. Chir., **63**(6), pp. 693–697.

[7] Lautt, W. W., 1981, "Role and control of the hepatic artery," Hepatic circulation in health and disease, W.W. Lautt, ed., Raven Press, New York, pp. 203–226.

[8] Eipel, C., Abshagen, K., and Vollmar, B., 2010, "Regulation of hepatic blood flow: The hepatic arterial buffer response revisited," World J. Gastroenterol., **16**(48), pp. 6046–6057.

[9] Torre, L. A., Bray, F., Siegel, R. L., Ferlay, J., Lortet-Tieulent, J., and Jemal, A., 2015, "Global cancer statistics, 2012," CA. Cancer J. Clin., **65**(2), pp. 87–108.

[10] Llovet, J. M., Zucman-Rossi, J., Pikarsky, E., Sangro, B., Schwartz, M., Sherman, M., and Gores, G., 2016, "Hepatocellular carcinoma," Nat. Rev. Dis. Prim., **2**(3), p. 16018.

[11] Salem, R., and Thurston, K. G., 2006, "Radioembolization with 90Yttrium microspheres: a state-of-the-art brachytherapy treatment for primary and secondary liver malignancies. Part 1: Technical and methodologic considerations.," J. Vasc. Interv. Radiol., **17**(8), pp. 1251–78.

[12] El-Serag, H. B., 2011, "Hepatocellular carcinoma," N. Engl. J. Med., **365**(12), pp. 1118–1127.

[13] Sangro, B., Iñarrairaegui, M., and Bilbao, J. I., 2012, "Radioembolization for hepatocellular carcinoma," J. Hepatol., **56**(2), pp. 464–473.

[14] Saxena, A., Bester, L., Shan, L., Perera, M., Gibbs, P., Meteling, B., and Morris, D. L., 2014, "A systematic review on the safety and efficacy of yttrium-90 radioembolization for unresectable, chemorefractory colorectal cancer liver metastases," J. Cancer Res. Clin. Oncol., **140**(4), pp. 537–547.

[15] Bester, L., Meteling, B., Boshell, D., Chua, T. C., and Morris, D. L., 2014, "Transarterial chemoembolisation and radioembolisation for the treatment of primary liver cancer and secondary liver cancer: A review of the literature," J. Med. Imaging Radiat. Oncol., **58**(3), pp. 341–352.

[16] Ariel, I. M., 1965, "Treatment of inoperable primary pancreatic and liver

cancer by the intra-arterial administration of radioactive isotopes (Y90 radiating microspheres)," Ann. Surg., **162**(2), pp. 267–278.

[17] Gaba, R. C., Lewandowski, R. J., Hickey, R., Baerlocher, M. O., Cohen, E. I., Dariushnia, S. R., D'Othée, B. J., Padia, S. A., Salem, R., Wang, D. S., Nikolic, B., and Brown, D. B., 2016, "Transcatheter therapy for hepatic malignancy: standardization of terminology and reporting criteria," J. Vasc. Interv. Radiol., **27**(4), pp. 457–473.

[18] Bilbao, J. I., and Reiser, M. F., 2014, Liver Radioembolization with 90Y Microspheres, Springer Berlin Heidelberg, Berlin, Heidelberg.

[19] Breedis, C., and Young, G., 1954, "The blood supply of neoplasms in the liver," Am. J. Pathol., **30**(5), pp. 969–985.

[20] Ahmadzadehfar, H., Biersack, H.-J., and Ezziddin, S., 2010, "Radioembolization of liver tumors with yttrium-90 microspheres," Semin. Nucl. Med., **40**(2), pp. 105–121.

[21] Murthy, R., Kamat, P., Nuñez, R., and Salem, R., 2008, "Radioembolization of yttrium-90 microspheres for hepatic malignancy.," Semin. Intervent. Radiol., **25**(1), pp. 48–57.

[22] Vesselle, G., Petit, I., Boucebci, S., Rocher, T., Velasco, S., and Tasu, J.-P., 2015, "Radioembolization with yttrium-90 microspheres work up: Practical approach and literature review," Diagn. Interv. Imaging, **96**(6), pp. 547–562.

[23] Denys, A., Pracht, M., Duran, R., Guiu, B., Adib, S., Boubaker, A., and Bize, P., 2015, "How to prepare a patient for transarterial radioembolization? A practical guide," Cardiovasc. Intervent. Radiol., **38**(4), pp. 794–805.

[24] Riaz, A., Lewandowski, R. J., Kulik, L. M., Mulcahy, M. F., Sato, K. T., Ryu, R. K., Omary, R. A., and Salem, R., 2009, "Complications following radioembolization with yttrium-90 microspheres: A comprehensive literature review," J. Vasc. Interv. Radiol., **20**(9), pp. 1121–1130.

[25] Jiang, M., Fischman, A., Nowakowski, F. S., Heiba, S., Zhang, Z., Knesaurek, K., Weintraub, J., and Machac, J., 2012, "Segmental perfusion differences on paired Tc-99m macroaggregated albumin (MAA) hepatic perfusion imaging and yttrium-90 (Y-90) bremsstrahlung imaging studies in SIR-sphere radioembolization: Associations with angiography," J. Nucl. Med. Radiat. Ther., **3**(122).

[26] Wondergem, M., Smits, M. L. J., Elschot, M., de Jong, H. W. A. M., Verkooijen, H. M., van den Bosch, M. A. A. J., Nijsen, J. F. W., and Lam, M. G. E. H., 2013, "99mTc-Macroaggregated albumin poorly predicts the intrahepatic

distribution of 90Y resin microspheres in hepatic radioembolization," J. Nucl. Med., **54**(8), pp. 1294–1301.

[27] Kao, Y. H., 2013, "A clinical dosimetric perspective uncovers new evidence and offers new insight in favor of 99mTc-macroaggregated albumin for predictive dosimetry in 90Y resin microsphere radioembolization," J. Nucl. Med., **54**(12), pp. 2191–2192.

[28] Lam, M. G. E. H., Wondergem, M., Elschot, M., and Smits, M. L. J., 2013, "Reply: A clinical dosimetric perspective uncovers new evidence and offers new insight in favor of 99mTc-macroaggregated albumin for predictive dosimetry in 90Y resin microsphere radioembolization," J. Nucl. Med., **54**(12), pp. 2192–2193.

[29] Ulrich, G., Dudeck, O., Furth, C., Ruf, J., Grosser, O. S., Adolf, D., Stiebler, M., Ricke, J., and Amthauer, H., 2013, "Predictive value of intratumoral 99mTc-macroaggregated albumin uptake in patients with colorectal liver metastases scheduled for radioembolization with 90Y-microspheres.," J. Nucl. Med., **54**(4), pp. 516–522.

[30] Eisenhauer, E. A., Therasse, P., Bogaerts, J., Schwartz, L. H., Sargent, D., Ford, R., Dancey, J., Arbuck, S., Gwyther, S., Mooney, M., Rubinstein, L., Shankar, L., Dodd, L., Kaplan, R., Lacombe, D., and Verweij, J., 2009, "New response evaluation criteria in solid tumours: Revised RECIST guideline (version 1.1)," Eur. J. Cancer, **45**(2), pp. 228–247.

[31] Dhabuwala, A., Lamerton, P., and Stubbs, R. S., 2005, "Relationship of 99mtechnetium labelled macroaggregated albumin (99mTc-MAA) uptake by colorectal liver metastases to response following Selective Internal Radiation Therapy (SIRT)," BMC Nucl. Med., **5**(1), p. 7.

[32] Lam, M. G. E. H., and Smits, M. L. J., 2013, "Value of 99mTc-macroaggregated albumin SPECT for radioembolization treatment planning," J. Nucl. Med., **54**(9), pp. 1681–1682.

[33] Ulrich, G., Dudeck, O., Grosser, O. S., and Amthauer, H., 2013, "Reply: Value of 99mTc-macroaggregated albumin SPECT for radioembolization treatment planning," J. Nucl. Med., **54**(9), pp. 1682–1682.

[34] Chiesa, C., Lambert, B., Maccauro, M., Ezziddin, S., Ahmadzadehfar, H., Dieudonne, A., Cremonesi, M., Konijnenberg, M., Lassmann, M., Pettinato, C., Strigari, L., Vanderlinden, B., Crippa, F., Flamen, P., and Garin, E., 2014, "Pretreatment dosimetry in HCC radioembolization with 90Y glass microspheres cannot Be invalidated with a bare visual evaluation of 99mTc-MAA uptake of colorectal metastases treated with resin microspheres," J.

Nucl. Med., **55**(7), pp. 1215–1216.

[35] Amthauer, H., Ulrich, G., Grosser, O. S., and Ricke, J., 2014, "Reply: pretreatment dosimetry in HCC radioembolization with 90Y glass microspheres cannot be invalidated with a bare visual evaluation of 99mTc-MAA uptake of colorectal metastases treated with resin microspheres," J. Nucl. Med., **55**(7), pp. 1216–1218.

[36] Morshedi, M. M., Bauman, M., Rose, S. C., and Kikolski, S. G., 2015, "Yttrium-90 resin microsphere radioembolization using an antireflux catheter: An alternative to traditional coil embolization for nontarget protection," Cardiovasc. Intervent. Radiol., **38**(2), pp. 381–388.

[37] Rose, S. C., Kikolski, S. G., and Chomas, J. E., 2013, "Downstream hepatic arterial blood pressure changes caused by deployment of the Surefire antireflux expandable tip," Cardiovasc. Intervent. Radiol., **36**(5), pp. 1262–1269.

[38] Arepally, A., Chomas, J., Kraitchman, D., and Hong, K., 2013, "Quantification and reduction of reflux during embolotherapy using an antireflux catheter and tantalum microspheres: ex vivo analysis," J. Vasc. Interv. Radiol., **24**(4), pp. 575–580.

[39] van den Hoven, A. F., Prince, J. F., Samim, M., Arepally, A., Zonneberg, B. A., Lam, M. G. E. H., and van den Bosch, M. A. A. J., 2014, "Posttreatment PET-CT-confirmed intrahepatic radioembolization performed without coil embolization, by using the antireflux Surefire Infusion System," Cardiovasc. Intervent. Radiol., **37**(2), pp. 523–528.

[40] Pasciak, A. S., McElmurray, J. H., Bourgeois, A. C., Heidel, R. E., and Bradley, Y. C., 2015, "The impact of an antireflux catheter on target volume particulate distribution in liver-directed embolotherapy: A pilot study," J. Vasc. Interv. Radiol., **26**(5), pp. 660–669.

[41] van den Hoven, A. F., Lam, M. G. E. H., Jernigan, S., van den Bosch, M. A. A. J., and Buckner, G. D., 2015, "Innovation in catheter design for intra-arterial liver cancer treatments results in favorable particle-fluid dynamics," J. Exp. Clin. Cancer Res., **34**(1), p. 74.

[42] Xu, Z., Jernigan, S., Kleinstreuer, C., and Buckner, G. D., 2016, "Solid tumor embolotherapy in hepatic arteries with an anti-reflux catheter system," Ann. Biomed. Eng., **44**(4), pp. 1036–1046.

[43] Kleinstreuer, C., Feng, Y., and Childress, E., 2014, "Drug-targeting methodologies with applications: A review," World J. Clin. Cases, **2**(12), pp.

742–756.

[44] Kennedy, A. S., Kleinstreuer, C., Basciano, C. A., and Dezarn, W. A., 2010, "Computer modeling of yttrium-90–microsphere transport in the hepatic arterial tree to improve clinical outcomes," Int. J. Radiat. Oncol. Biol. Phys., **76**(2), pp. 631–637.

[45] Basciano, C. A., Kleinstreuer, C., Kennedy, A. S., Dezarn, W. A., and Childress, E., 2010, "Computer modeling of controlled microsphere release and targeting in a representative hepatic artery system," Ann. Biomed. Eng., **38**(5), pp. 1862–1879.

[46] Childress, E. M., Kleinstreuer, C., and Kennedy, A. S., 2012, "A new catheter for tumor-targeting with radioactive microspheres in representative hepatic artery aystems—Part II: Solid tumor-targeting in a patient-inspired hepatic artery system," J. Biomech. Eng., **134**(5), p. 51005.

[47] Kleinstreuer, C., Basciano, C. A., Childress, E. M., and Kennedy, A. S., 2012, "A new catheter for tumor targeting with radioactive microspheres in representative hepatic artery systems. Part I: Impact of catheter presence on local blood flow and microsphere delivery," J. Biomech. Eng., **134**(5), p. 51004.

[48] Basciano, C. A., Kleinstreuer, C., and Kennedy, A. S., 2011, "Computational fluid dynamics modeling of 90Y microspheres in human hepatic tumors," J. Nucl. Med. Radiat. Ther., **1**(1).

[49] Childress, E. M., and Kleinstreuer, C., 2013, "Computationally efficient particle release map determination for direct tumor-targeting in a representative hepatic artery system," J. Biomech. Eng., **136**(1), p. 11012.

[50] Childress, E. M., and Kleinstreuer, C., 2014, "Impact of fluid–structure interaction on direct tumor-targeting in a representative hepatic artery system," Ann. Biomed. Eng., **42**(3), pp. 461–474.

[51] Richards, A. L., Kleinstreuer, C., Kennedy, A. S., Childress, E., and Buckner, G. D., 2012, "Experimental microsphere targeting in a representative hepatic artery system," IEEE Trans. Biomed. Eng., **59**(1), pp. 198–204.

[52] Kleinstreuer, C., "Methods and devices for targeted injection of microspheres." United States patent US 20120190976 A1. 2010 Jul 26

[53] Oktar, S. Ö., Yücel, C., Demirogullari, T., Üner, A., Benekli, M., Erbas, G., and Özdemir, H., 2006, "Doppler sonographic evaluation of hemodynamic changes in colorectal liver metastases relative to liver size.," J. Ultrasound Med., **25**(5), pp. 575–82.

[54] Mise, Y., Satou, S., Shindoh, J., Conrad, C., Aoki, T., Hasegawa, K., Sugawara, Y., and Kokudo, N., 2014, "Three-dimensional volumetry in 107 normal livers reveals clinically relevant inter-segment variation in size," HPB, **16**(5), pp. 439–447.

[55] Michels, N. A., 1966, "Newer anatomy of the liver and its variant blood supply and collateral circulation," Am. J. Surg., **112**(3), pp. 337–347.

[56] Hiatt, J. R., Gabbay, J., and Busuttil, R. W., 1994, "Surgical anatomy of the hepatic arteries in 1000 cases," Ann. Surg., **220**(1), pp. 50–52.

[57] Hung, J. C., Redfern, M. G., Mahoney, D. W., Thorson, L. M., and Wiseman, G. A., 2000, "Evaluation of macroaggregated albumin particle sizes for use in pulmonary shunt patient studies.," J. Am. Pharm. Assoc. (Wash)., **40**(1), pp. 46–51.

[58] Batchelor, G. K., 2000, An Introduction to Fluid Dynamics, Cambridge University Press, Cambridge.

[59] Kenner, T., 1989, "The measurement of blood density and its meaning," Basic Res. Cardiol., **84**(2), pp. 111–124.

[60] Buchanan, J. R., Kleinstreuer, C., and Comer, J. K., 2000, "Rheological effects on pulsatile hemodynamics in a stenosed tube," Comput. Fluids, **29**(6), pp. 695–724.

[61] Chandran, K., Rittgers, S., and Yoganathan, A., 2012, Biofluid Mechanics: The Human Circulation, Second Edition, CRC Press, Taylor & Francis Group, Boca Raton , FL.

[62] Basciano, C. A., 2010, "PhD Thesis: Computational particle-hemodynamics analysis applied to an abdominal aortic aneurysm with thrombus and microsphere-targeting of liver tumors," North Carolina State University, North Carolina, USA.

[63] Morsi, S. A., and Alexander, A. J., 1972, "An investigation of particle trajectories in two-phase flow systems," J. Fluid Mech., **55**(2), pp. 193–208.

[64] Haider, A., and Levenspiel, O., 1989, "Drag coefficient and terminal velocity of spherical and nonspherical particles," Powder Technol., **58**(1), pp. 63–70.

[65] Aramburu, J., Antón, R., Bernal, N., Rivas, A., Ramos, J. C., Sangro, B., and Bilbao, J. I., 2015, "Physiological outflow boundary conditions methodology for small arteries with multiple outlets: A patient-specific hepatic artery haemodynamics case study," Proc. Inst. Mech. Eng. H, **229**(4), pp. 291–306.

[66] Aramburu, J., Antón, R., Rivas, A., Ramos, J. C., Sangro, B., and Bilbao, J. I., 2016, "Liver cancer arterial perfusion modelling and CFD boundary conditions methodology: a case study of the haemodynamics of a patient-specific hepatic artery in literature-based healthy and tumour-bearing liver scenarios," Int. J. Numer. Method. Biomed. Eng., **32**(11), p. e02764.

[67] Aramburu, J., Antón, R., Rivas, A., Ramos, J. C., Sangro, B., and Bilbao, J. I., 2016, "Computational particle–haemodynamics analysis of liver radioembolization pretreatment as an actual treatment surrogate," Int. J. Numer. Method. Biomed. Eng., p. e02791.

[68] Aramburu, J., Antón, R., Rivas, A., Ramos, J. C., Sangro, B., and Bilbao, J. I., 2016, "Computational assessment of the effects of the catheter type on particle–hemodynamics during liver radioembolization," J. Biomech., **49**(15), pp. 3705–3713.

[69] Aramburu, J., Antón, R., Rivas, A., Ramos, J. C., Sangro, B., and Bilbao, J. I., 2016, "Numerical investigation of liver radioembolization via computational particle–hemodynamics: The role of the microcatheter distal direction and microsphere injection point and velocity," J. Biomech., **49**(15), pp. 3714–3721.

[70] Aramburu, J., Antón, R., Rivas, A., Ramos, J. C., Sangro, B., and Bilbao, J. I., 2016, "The role of angled-tip microcatheter and microsphere injection velocity in liver radioembolization: a computational particle–hemodynamics study," SUBMITTED TO J. Biomech. Eng.

[71] Roache, P. J., 1997, "Quantification of uncertainty in computational fluid dynamics," Annu. Rev. Fluid Mech., **29**(1), pp. 123–160.

[72] Tsushima, Y., Funabasama, S., Aoki, J., Sanada, S., and Endo, K., 2004, "Quantitative perfusion map of malignant liver tumors, created from dynamic computed tomography data.," Acad. Radiol., **11**(2), pp. 215–223.

[73] Kim, D. H., Kim, S. H., Im, S.-A., Han, S.-W., Goo, J. M., Willmann, J. K., Lee, E. S., Eo, J. S., Paeng, J. C., Han, J. K., and Choi, B. I., 2012, "Intermodality comparison between 3D perfusion CT and 18F-FDG PET/CT imaging for predicting early tumor response in patients with liver metastasis after chemotherapy: Preliminary results of a prospective study," Eur. J. Radiol., **81**(11), pp. 3542–3550.

[74] Van de Wiele, C., Maes, A., Brugman, E., D'Asseler, Y., De Spiegeleer, B., Mees, G., and Stellamans, K., 2012, "SIRT of liver metastases: physiological and pathophysiological considerations," Eur. J. Nucl. Med. Mol. Imaging, **39**(10), pp. 1646–1655.

[75] Jernigan, S. R., Osborne, J. A., Mirek, C. J., and Buckner, G., 2015, "Selective internal radiation therapy: quantifying distal penetration and distribution of resin and glass microspheres in a surrogate arterial model," J. Vasc. Interv. Radiol., **26**(6), p. 897–904.

[76] Sznitman, J., and Steinman, D. A., 2016, "Relevance and challenges of computational fluid dynamics in the biomedical sciences," J. Biomech., **49**(11), p. 2101.

[77] Ballyk, P. D., 2015, "Numerical/experimental synergy: more than just a reality check," J. Vasc. Interv. Radiol., **26**(2), pp. 259–261.

[78] Westerhof, N., Stergiopulos, N., and Noble, M. I. M., 2005, Snapshots of Hemodynamics, Kluwer Academic Publishers, Boston.

[79] Grinberg, L., and Karniadakis, G. E., 2008, "Outflow boundary conditions for arterial networks with multiple outlets," Ann. Biomed. Eng., **36**(9), pp. 1496–1514.

[80] Avolio, A. P., 1980, "Multi-branched model of the human arterial system," Med. Biol. Eng. Comput., **18**(6), pp. 709–718.

[81] Torii, R., Oshima, M., Kobayashi, T., Takagi, K., and Tezduyar, T. E., 2010, "Role of 0D peripheral vasculature model in fluid–structure interaction modeling of aneurysms," Comput. Mech., **46**(1), pp. 43–52.

[82] Olufsen, M. S., 1998, "PhD Thesis: Modeling the arterial system with reference to anesthesia simulator.," Roskilde University.

[83] Day, M. A., 1990, "The no-slip condition of fluid dynamics," Erkenntnis, **33**(3), pp. 285–296.

Appendix A

Approach Justification

Six topics are discussed in this appendix:

- The expanding state of the ARC tip.
- The physical phenomena taken into account when modeling the fluid–particle dynamics.
- The use of rigid models for computational domain and downstream vasculature.
- The use of the no-slip condition.
- The simulation strategy in terms of injecting during the first cardiac cycle and simulating three additional pulses so that the majority of injected particles exit the computational domain.
- The time-step value chosen.

A.1 Expanding state of the ARC expandable tip

The expandable tip of the ARC is defined via the distal outer diameter (4 mm), the thickness (0.21 mm), the funnel-shaped length (10.5 mm) and the cylinder-shaped length (2.2 mm) (see Figure 2.3(b)).

In justifying the 4 mm diameter of the tip end, Rose at al. [37] wrote: "The tip is partially collapsed during forward blood flow of cardiac systole (Fig. 1A) with a minor degree of expansion during cardiac diastole that is subocclusive (Fig. 1B), thus allowing antegrade delivery of the agent. During this phase, the spring-like, self-expanding properties of the tip cover a relatively large portion of the vessel cross-sectional area, somewhat analogous to a high-grade stenosis. The tip fully expands if the blood pressure at the tip of the microcatheter plus the self-expandable forces of the funnel-shaped tip is greater than the blood vessel, usually during the course of embolization with occlusion of the downstream arterial branches, thus preventing reversal of blood flow and retrograde reflux of the agent into upstream arterial branches (Fig. 1C)."

In this thesis, the beginning of the treatment was simulated, meaning that the occlusion of the downstream branches that creates the retrograde reflux and the complete expansion of the tip was not taking place (see '4.3 Study limitations'). Therefore, the diameter is below 5 mm and a 4-mm diameter was opted to define the 'partially collapsed' and 'subocclusive' states.

A.2 Particle tracking model

The previous articles that simulated the blood flow through hepatic arteries with particle transport used the one-way coupling approach and the forces that considered were the drag force (eqn. (2.10)), the gravity force (eqn. (2.9)), and the pressure gradient force (eqn. (2.8)) [44–50]. In this investigation, in addition to the virtual mass force (eqn. (2.7)), the two-way coupling approach has been considered.

Regarding the virtual mass force, virtual mass force was included in the model following the recommendation given in the Theory Guide for Fluent® 15.0 (ANSYS Fluent® 15.0. ANSYS Fluent Theory Guide, November 2013), which states: "The virtual mass and pressure gradient forces are not important when the density of the fluid (ρ) is much lower that the density of the particles (ρ_p) as is the case for liquid/solid particles in gaseous flows ($\rho/\rho_p<<1$). For values of ρ/ρ_p approaching unity, the Virtual Mass and Pressure Gradient forces become significant and it is

recommended that they be included when the density ratio is greater than 0.1." In this study, the density ratio equals 0.656 (ρ/ρ_p=1050/1600=0.656) for resin microspheres and 0.954 (ρ/ρ_p=1050/1100=0.954) for MAA microparticles, which are greater than 0.1 and therefore the virtual mass force was included.

Regarding the two-way coupling between phases, we included it in the model in order to add more reality, given that the previous works studying the particle–hemodynamics in the hepatic artery employed the one-way coupling approach [44–50].

In addressing the importance of considering virtual mass force and the two-way coupling, an analysis of the influence of virtual mass force and one- or two-way coupling between phases on particle distribution over liver segments was carried out. This issue was addressed with the study about the effect of microcatheter distal direction and injection velocity (i.e., Study III) [69], with the case of simulation number one (N-S:1) (see Table 2.11). Table A.1 tabulates the characteristics (use or non-use of virtual mass force, and coupling between phases) of the three simulations (N-S:1_1, N-S:1_2, and N-S:1_3) that have been run.

Table A.1: Simulation characteristics regarding the use of virtual mass force and the coupling between phases.

Simulation	Virtual mass force: Yes or No	One-way or two-way coupling
N-S:1_1	Yes	Two way
N-S:1_2	No	Two way
N-S:1_3	Yes	One way

Figure A.1 illustrates the simulation results in terms of particle distribution. The liver segments from S1–S8 are on the *x*-axis and the particle distribution on the *y*-axis. In order to make it easier to compare results, data labels are included. Results indicate that the influence of virtual mass force is minimal (N-S:1_1 vs. N-S:1_2), as minor differences were observed in terms of particle distribution: 17.73% vs. 18.00% in S5, 31.72% vs. 31.40% in S6, 16.46% vs. 16.39% in S7, and 34.09% vs. 34.21% in S8. However, in this case the use of one- or two-way coupling seems to be more influential (N-S:1_1 vs. N-S:1_3): 17.73% vs. 19.47% in S5, 31.72% vs. 37.33% in S6, 16.46% vs. 11.29% in S7, and 34.09% vs. 31.91% in S8.

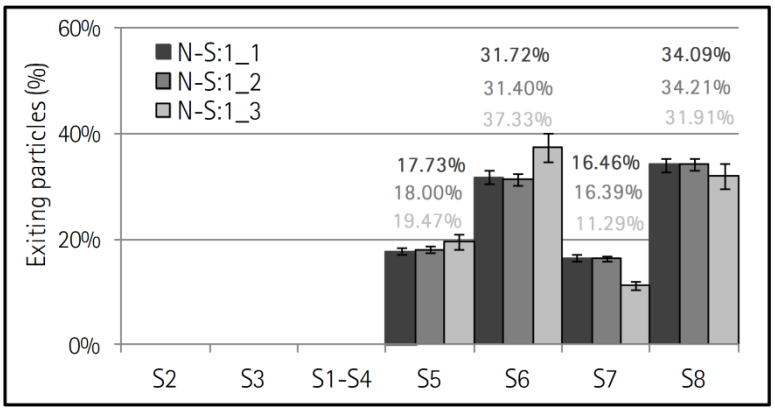

Figure A.1: Segment-to-segment exiting-particle distribution for N-S:1_1, N-S:1_2, and N-S:1_3; liver segments are on the *x*-axis and particle distribution on the *y*-axis.

As mentioned before, previous works in the literature that simulated blood flow and particle transport in hepatic arteries employed one-way coupling between phases [44–50]. The number of particles injected may play a role in the influence of particles on blood flow. In fact, 2500 particles are being injected per millisecond in N-S:1, while for the case of Kleinstreuer et al. [47] 163 particles per millisecond were injected: "Ten thousand SIR-Spheres® (average diameter 32 µm and density 1600 kg/m^3 from Sirtex Medical, Sydney, Australia) were released via a randomized distribution across the upstream injection plane over 0.0615 s…" [47]. This means that the particle number injected is about 15.3 times greater in our work, which suggests that the influence of particles over the blood flow may become considerable.

Regarding the use of virtual mass force (N-S:1_1 vs. N-S:1_2), the major inconvenience of using it would be that the number of equations to be solved per iteration would increase, therefore increasing the computational time per iteration. However, in the three-simulation study carried out, the number of iterations and time per iteration (N-S:1_1 and N-S:1_2 were both simulated at the same server) for N-S:1_1 and N-S:1_2 were: 56715 vs. 57335 in terms of number of iterations, and 2.4 seconds per iteration for both simulations, which means that N-S:1_2, which did not take virtual mass force into account, lasted longer than N-S:1_1.

To sum up, it can be stated that employing the two-way coupling was important in this case. Furthermore, including virtual mass force adds more reality to the model, and the computational resources (e.g., in terms of number of iterations) do not

increase significantly. In fact, in this particular study the computational time was reduced when employing the virtual mass force in the model.

A.3 Rigid geometry and 'outflow'-type BC

In this model, only the resistive effect of both the three-dimensional geometric domain (i.e., computational domain) and the downstream vasculature was considered. The computational domain was rigid and the downstream vasculature was modeled via 'outflow'-type BCs. These 'outflow'-type BCs are similar to having a high hydraulic resistance at each outlet such that these resistances define the flow split through the outlets of the computational domain. Therefore, both the computational domain and the downstream vasculature were pure resistive models, so no inertance nor capacitance was considered. What follows attempts to justify the validity of this approach.

There is a parameter defined in the Oscillatory Flow Theory which is known as the Womersley number, α (see Chapter 8 in Westerhof et al.[78]):

$$\alpha = \frac{d}{2}\sqrt{\frac{2\pi f \rho}{\mu}} \tag{A.1}$$

where d is the internal diameter of the vessel, f is the cardiac cycle frequency, ρ is the blood density, and μ is the dynamic viscosity of blood.

When this parameter is low (α<3) viscosity dominates and the pressure–flow relation can be described with resistive effects only. However, when the Womersley number is high (α>10), then the inertia dominates and it is necessary to consider the inertance. In this case, the Womersley number ath the PHA is 3.65 (d=5×10^{-3} m, f=1 Hz, ρ=1050 kg/m^3, and μ=0.00309 Pa·s in eqn. (A.1)), so it is sufficient to consider only resistive effects.

Therefore, the rigid model may be assumed. However, this may be a hurdle to overcome in future research, which would result in simulating via fluid–structure interaction (FSI) instead of via computational fluid dynamics (CFD) because the artery wall's physical characteristics would need to be modeled.

Regarding the downstream vasculature modeling, different approaches can be taken: constant pressure BCs, resistance BCs, Windkessel model BCs, and impedance or structured tree BCs [79]. The choice of which type of BC is set depends on the

arterial site where the BCs are imposed. When dealing with big arteries, it is necessary to take the effects of compliance and inertance into account. Nevertheless, for small arteries such as the one studied in this work, the literature suggests that it could be sufficient to use a pure resistive BC.

For example, Avolio [80] defined the peripheral resistance at the hepatic artery (one of the most distally located arteries in his model) as a pure resistance, even though the rest of the arteries (the ones that were not most distally located) were defined as impedances.

Additionally, a work from Torii et al. [81] showed that for arteries that have diameter values similar to ours, there was a very small difference between using the peripheral vasculature model (developed by Olufsen [82]) and a pure resistive model with a constant pressure source in series.

Furthermore, Basciano's PhD thesis [62] measured the flow rate and pressure waveforms in the right hepatic artery, and the time delay between both waveforms was only 0.02 s, so a BC which is equivalent to a pure resistive model seems a valid approach.

A.4 The no-slip condition

In general, the no-slip condition means that the artery wall is modeled as an impermeable wall, and that the there is no relative motion between the wall and the blood immediately in contact with the wall. The absence of motion perpendicularly to the wall is called the impermeability condition, while the absence in tangential motion is called the no-slip condition.

A discussion on the no-slip condition for fluid dynamics in general is found in Day [83], which justifies the no-slip condition via a literature review on experiments that involve the variation of a physical surface; comparisons between experiments and analytical solutions for simple fluid flow problems; observations of fluids near solid surfaces; and arguments that appeal to the interactions between fluids and solids.

This conclusion has been assumed to also apply to arterial hemodynamics. In fact, all the cited works that employ CFD and FSI techniques for particle–hemodynamics simulations employ the no-slip condition at the arterial walls [42–50,62,65–70].

A.5 Simulation strategy

In addressing the importance of considering more than four cardiac pulses for each simulation, an analysis of the influence of the number of simulated cardiac pulses on particle distribution over liver segments was carried out. This issue was addressed with the study about the effect of microcatheter distal direction and injection velocity (i.e., Study III) [69], with the case of simulations number one and seven (i.e., N-S:1 and N-S:2) (see Table 2.11). The exiting-particle distribution and the non-exiting particle percentage were analyzed to justify that simulating more than four cardiac pulses did not alter the exiting-particle distribution or did not reduce the non-exiting particle percentage considerably. To that end, both simulations N-S:1 and N-S:2 have been simulated until t=8 s, recording the exiting-particle distribution and non-exiting particle percentage at t=4 s, t=5 s, t=6 s, t=7 s, and t=8 s. (Recall that the exiting particles are the particles that were injected during the first cardiac cycle of the simulation and had exited the computational domain through any outlet by the end of the simulation. The non-exiting particles, in contrast, are the particles that were injected during the first cardiac cycle of the simulation and remained inside the computational domain at the end of the simulation.)

Figure A.2 depicts the exiting-particle distribution over the liver segments at t=4 s, t=5 s, t=6 s, t=7 s and t=8 s for N-S:1 (Figure A.2(a)) and for N-S:2 (Figure A.2(b)) and the non-exiting particle percentage for N-S:1 and N-S:2 at t=4 s, t=5 s, t=6 s, t=7 s and t=8 s (Figure A.2(c)).

Results indicate that the particle distribution does not vary considerably. For N-S:1, 17–18% exited S5, 31–32% exited S6, 16–17% exited S7, and 33–34% exited S8 (see Figure A.2(a)). For N-S:2, 15–16% exited S5, 40–41% exited S6, 12–13% exited S7, and 30–31% exited S8. In terms of non-exiting particle percentage, in N-S:1 that value decreased from 3.59% to 0.70%, while for N-S:2 that value decreased from 9.51% to 2.13%.

Simulating from t=0 s to t=8 would double the computational time (i.e., from approximately 100 wall-clock hours to 200 wall-clock hours on a 32-core server), and the segment-to-segment particle distribution would not be altered considerably (see Figure A.2(a) and (b)). Therefore, it was considered that simulating four pulses is sufficient for a proper analysis of particle distribution.

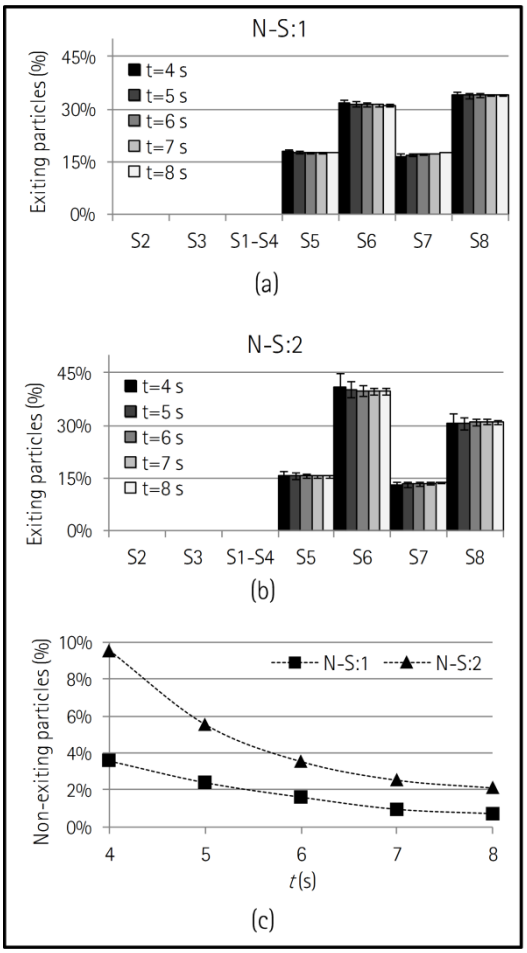

Figure A.2: (a) Exiting-particle distribution over the liver segments for N-S:1 at t=4 s, t=5 s, t=6 s, t=7 s and t=8 s. (b) Exiting-particle distribution over the liver segments for N-S:2 at t=4 s, t=5 s, t=6 s, t=7 s and t=8 s. (c) Non-exiting particle distribution over time for N-S:1 and N-S:2.

A.6 Time-step value

Other works modeling the same physical reality (blood flow through hepatic arteries) used a time step of 2.5 ms [45] and 2 ms [46,47]. A 2-ms time step was chosen because the time step is small enough (and therefore the simulation is more accurate than a simulation using a 2.5-ms time step) and because the convergence of the simulation might be even less time-consuming. Even though more time steps are computed, fewer iterations per time step could be required, which results in a faster simulation.

Appendix B

Copyright Permissions

This appendix includes the permissions for reuse of Papers I–V. No permission is still needed for Paper VI.

Paper I: SAGE Publications

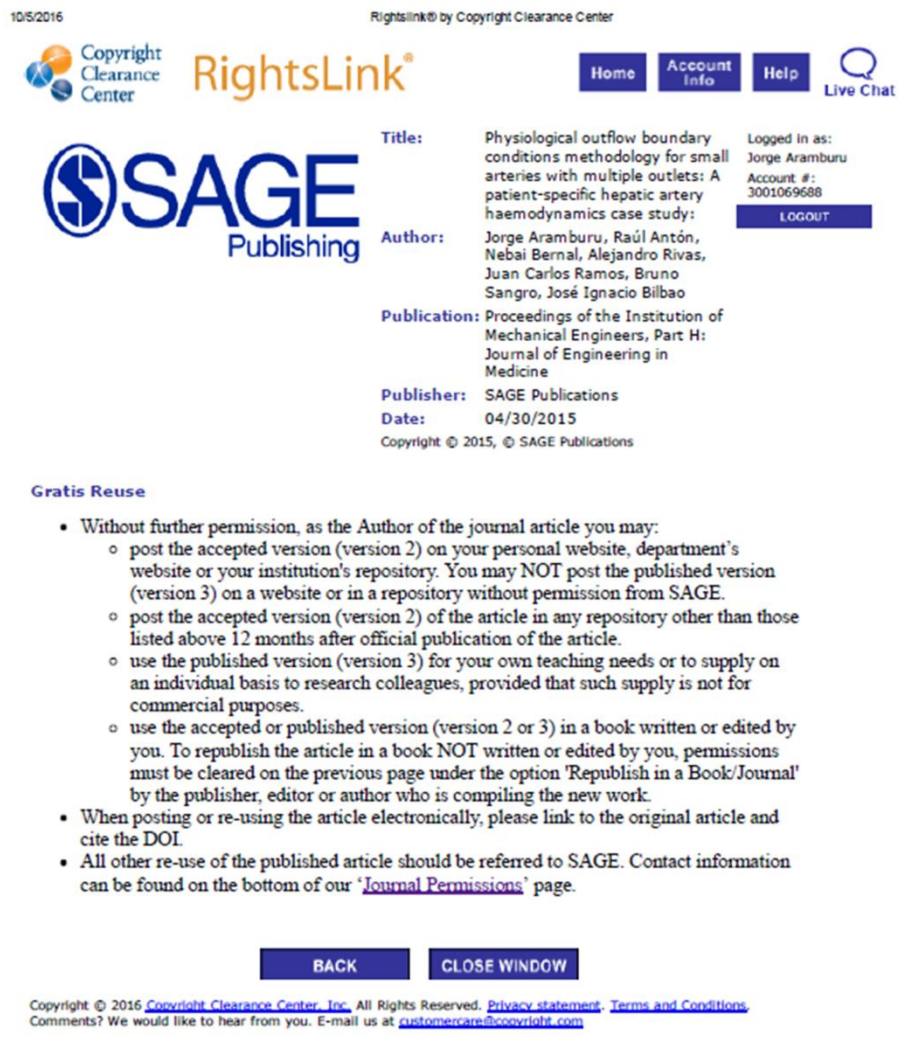

10/5/2016 Rightslink® by Copyright Clearance Center

Copyright Clearance Center RightsLink®

Home | Account Info | Help | Live Chat

SAGE Publishing

Title: Physiological outflow boundary conditions methodology for small arteries with multiple outlets: A patient-specific hepatic artery haemodynamics case study:

Author: Jorge Aramburu, Raúl Antón, Nebai Bernal, Alejandro Rivas, Juan Carlos Ramos, Bruno Sangro, José Ignacio Bilbao

Publication: Proceedings of the Institution of Mechanical Engineers, Part H: Journal of Engineering in Medicine

Publisher: SAGE Publications

Date: 04/30/2015

Copyright © 2015, © SAGE Publications

Logged in as: Jorge Aramburu
Account #: 3001069688
LOGOUT

Gratis Reuse

- Without further permission, as the Author of the journal article you may:
  - post the accepted version (version 2) on your personal website, department's website or your institution's repository. You may NOT post the published version (version 3) on a website or in a repository without permission from SAGE.
  - post the accepted version (version 2) of the article in any repository other than those listed above 12 months after official publication of the article.
  - use the published version (version 3) for your own teaching needs or to supply on an individual basis to research colleagues, provided that such supply is not for commercial purposes.
  - use the accepted or published version (version 2 or 3) in a book written or edited by you. To republish the article in a book NOT written or edited by you, permissions must be cleared on the previous page under the option 'Republish in a Book/Journal' by the publisher, editor or author who is compiling the new work.
- When posting or re-using the article electronically, please link to the original article and cite the DOI.
- All other re-use of the published article should be referred to SAGE. Contact information can be found on the bottom of our 'Journal Permissions' page.

BACK CLOSE WINDOW

Copyright © 2016 Copyright Clearance Center, Inc. All Rights Reserved. Privacy statement. Terms and Conditions.
Comments? We would like to hear from you. E-mail us at customercare@copyright.com

Paper II: John Wiley and Sons

JOHN WILEY AND SONS LICENSE TERMS AND CONDITIONS

Oct 25, 2016

This Agreement between Jorge Aramburu ("You") and John Wiley and Sons ("John Wiley and Sons") consists of your license details and the terms and conditions provided by John Wiley and Sons and Copyright Clearance Center.

License Number	3962411126745
License date	Oct 05, 2016
Licensed Content Publisher	John Wiley and Sons
Licensed Content Publication	International Journal of Numerical Methods in Biomedical Engineering
Licensed Content Title	Liver cancer arterial perfusion modelling and CFD boundary conditions methodology: a case study of the haemodynamics of a patient-specific hepatic artery in literature-based healthy and tumour-bearing liver scenarios
Licensed Content Author	Jorge Aramburu,Raúl Antón,Alejandro Rivas,Juan Carlos Ramos,Bruno Sangro,José Ignacio Bilbao
Licensed Content Date	Mar 2, 2016
Licensed Content Pages	1
Type of use	Dissertation/Thesis
Requestor type	Author of this Wiley article
Format	Print and electronic
Portion	Full article
Will you be translating?	Yes, including English rights
Number of languages	2
Languages	Basque and Spanish
Title of your thesis / dissertation	Liver Radioembolization: Computational Particle–Hemodynamics Studies in a Patient-Specific Hepatic Artery under Literature-Based Cancer Scenarios
Expected completion date	Dec 2016
Expected size (number of pages)	80
Requestor Location	Jorge Aramburu po Manuel Lardizabal, 13 Donostia-San Sebastián, Gipuzkoa 20018 Spain Attn: Jorge Aramburu
Publisher Tax ID	EU826007151
Billing Type	Invoice
Billing Address	Jorge Aramburu Mandabide Kalea 1H 4.D Zarautz, Spain 20800 Attn: Jorge Aramburu
Total	0.00 EUR
Terms and Conditions	

Paper III: John Wiley and Sons

JOHN WILEY AND SONS LICENSE TERMS AND CONDITIONS

Oct 25, 2016

This Agreement between Jorge Aramburu ("You") and John Wiley and Sons ("John Wiley and Sons") consists of your license details and the terms and conditions provided by John Wiley and Sons and Copyright Clearance Center.

License Number	3962420292048
License date	Oct 05, 2016
Licensed Content Publisher	John Wiley and Sons
Licensed Content Publication	International Journal of Numerical Methods in Biomedical Engineering
Licensed Content Title	Computational particle–haemodynamics analysis of liver radioembolization pretreatment as an actual treatment surrogate
Licensed Content Author	Jorge Aramburu,Raúl Antón,Alejandro Rivas,Juan Carlos Ramos,Bruno Sangro,José Ignacio Bilbao
Licensed Content Date	May 25, 2016
Licensed Content Pages	1
Type of use	Dissertation/Thesis
Requestor type	Author of this Wiley article
Format	Print and electronic
Portion	Full article
Will you be translating?	Yes, including English rights
Number of languages	2
Languages	Basque and Spanish
Title of your thesis / dissertation	Liver Radioembolization: Computational Particle–Hemodynamics Studies in a Patient-Specific Hepatic Artery under Literature-Based Cancer Scenarios
Expected completion date	Dec 2016
Expected size (number of pages)	80
Requestor Location	Jorge Aramburu Pº Manuel Lardizabal, 13 Donostia-San Sebastián, Gipuzkoa 20018 Spain Attn: Jorge Aramburu
Publisher Tax ID	EU826007151
Billing Type	Invoice
Billing Address	Jorge Aramburu Mandabide Kalea 1H 4.D Zarautz, Spain 20800 Attn: Jorge Aramburu
Total	0.00 EUR
Terms and Conditions	

TERMS AND CONDITIONS

Paper IV: Elsevier

Paper V: Elsevier

Appendix C

Papers

Paper I:

Aramburu, J., Antón, R., Bernal, N., Rivas, A., Ramos, J. C., Sangro, B., and Bilbao, J. I., 2015, "Physiological outflow boundary conditions methodology for small arteries with multiple outlets: a patient-specific hepatic artery haemodynamics case study," Proc. Inst. Mech. Eng. H, **229**(4), pp. 291–306. (doi:10.1177/0954411915578549)

Paper II:

Aramburu, J., Antón, R., Rivas, A., Ramos, J. C., Sangro, B., and Bilbao, J. I., 2016, "Liver cancer arterial perfusion modelling and CFD boundary conditions methodology: A case study of the haemodynamics of a patient-specific hepatic artery in literature-based healthy and tumour-bearing liver scenarios," Int. J. Numer. Method. Biomed. Eng., **32**(11), p. e02764. (doi:10.1002/cnm.2764)

Paper III:

Aramburu, J., Antón, R., Rivas, A., Ramos, J. C., Sangro, B., and Bilbao, J. I., 2016, "Computational particle-haemodynamics analysis of liver radioembolization pretreatment as an actual treatment surrogate," Int. J. Numer. Method. Biomed. Eng., p. e02791. (doi: 10.1002/cnm.2791)

Paper IV:

Aramburu, J., Antón, R., Rivas, A., Ramos, J. C., Sangro, B., and Bilbao, J. I., 2016, "Computational assessment of the effects of the catheter type on particle-hemodynamics during liver radioembolization," J. Biomech., **49**(15), pp. 3705–3713 (doi: 10.1016/j.jbiomech.2016.09.035)

Paper V:

Aramburu, J., Antón R., Rivas, A., Ramos, J. C., Sangro, B., and Bilbao, J. I., 2016, "Numerical investigation of liver radioembolization via computational particle-hemodynamics: The role of the microcatheter distal direction and microsphere injection point and velocity," J. Biomech., **49**(15), pp. 3714–3721 (doi: 10.1016/j.jbiomech.2016.09.034)

Paper VI:

Aramburu, J., Antón, R., Rivas, A., Ramos, J. C., Sangro, B., and Bilbao, J. I., 2016, "The role of angled-tip microcatheter and microsphere injection velocity in liver radioembolization: A computational particle-hemodynamics study," *Submitted to* J. Biomech. Eng.

Paper I: Physiological outflow boundary conditions methodology for small arteries with multiple outlets: a patient-specific hepatic artery haemodynamics case study

ABSTRACT

Physiological outflow boundary conditions are necessary to carry out computational fluid dynamics simulations that reliably represent the blood flow through arteries. When dealing with complex tree-dimensional trees of small arteries, and therefore with multiple outlets, the robustness and speed of convergence are also important. This study derives physiological outflow boundary conditions for cases in which the physiological values at those outlets are not known (neither in vivo measurements nor literature-based values are available) and in which the tree exhibits symmetry to some extent. The inputs of the methodology are the three-dimensional domain and the flow rate waveform and the systolic and diastolic pressures at the inlet. The derived physiological outflow boundary conditions, which are a physiological pressure waveform for each outlet, are based on the results of zero-dimensional model simulation. The methodology assumes symmetrical branching and is able to tackle the flow distribution problem when the domain outlets are at branches with different number of upstream bifurcations. The methodology is applied to a group of patient-specific arteries in the liver. The methodology is considered to be valid because the pulsatile computational fluid dynamics simulation with the inflow flow rate waveform (input of the methodology) and the derived outflow boundary conditions lead to physiological results, that is, the resulting systolic and diastolic pressures at the inlet match the inputs of the methodology, and the flow split is also physiological.

LABURPENA

Beharrezkoa da irteeretako muga-baldintzak fisiologikoak izatea arteriatan zehar igarotzen den odol-fluxua CFD-aren bidez modu egokian simulatzeko. Arteria txikiz osatutako 3D zuhaitz konplexuak (beraz, irteera askokoak) aztertzerakoan garrantzitsua da emaitzak eskuratzera garamatzan metodo matematikoa azkarra eta tinkoa izatea. Lan honek azaltzen du irteeretako muga-baldintza fisiologikoak nola kalkulatu, irteera horietan datuak ezagutzen ez diren kasuetarako —ez daude ez *in vivo* neurtutako datuak, ezta literaturan publikatutakoak ere— eta arteriak itxura sasi-simetrikoa duen kasuetarako. Arteriaren eredu konputazionalaz gain, hauek dira

eredu konputazionalaren sarreran behar diren *input*-ak metodologiarako: ziklo kardiakoko fluxu bolumetrikoaren uhina eta presioaren balio sistolikoa eta diastolikoa. Metolologia aplikatuz lortzen diren muga-baldintza fisiologikoak, hots, presio-uhin bana irteera bakoitzean, eredu zero-dimentsionalen simulazioen emaitzetan daude oinarrituta. Metodologia honek arterien banaketa simetrikoa du hipotesi, eta gai da irteerak maila ezberdinean egoteagatik fluxu banaketaren definizioan eman daitezkeen arazoei aurre egiteko. Gibela odoleztatzen duen arteria hepatiko bati aplikatu zaio metologia hau. Helburua betetzen denez, metodogia hau egokitzat hartzen dute autoreek: metodologiaren bidez lortutako presio-uhinak irteeretan ezartzean CFD simulazio baterako, lortzen den emaitzak zera erakusten du, bat datozela eredu hiru dimentsionalaren sarreran lortutako presio-uhinaren balio sistolikoa eta diastolikoa, eta presio-*input*-ak ziren balio sistolikoa eta diastolikoa.

RESUMEN

Las condiciones de contorno fisiológicas son necesarias para representar el flujo sanguíneo a través de las arterias mediante simulaciones CFD. Cuando se estudian árboles vasculares complejos con muchas ramas, la robustez y la velocidad en la convergencia de la solución también son importantes. Este estudio deduce condiciones de contorno de salida para el caso en el que los valores fisiológicos en esas salidas no son conocidos (no se dispone ni de medidas experimentales ni de valores publicados en la literatura) y el árbol vascular presenta una estructura más o menos simétrica. Los *inputs* de la metodología son el dominio tridimensional y la onda de flujo y las presiones sistólica y diastólica en la entrada del dominio. Las condiciones de contorno deducidas, que son ondas pulsátiles de presión, están basadas en los resultados de simulaciones cero-dimensionales. La metodología asume una división simétrica en la ramificación de las arterias y es capaz de solventar el problema de distribución del flujo cuando las salidas pertenecen a diferentes generaciones. La metodología ha sido aplicada a un grupo de arterias hepáticas. Esta metodología se considera válida porque las simulaciones CFD empleando las condiciones de contorno deducidas dan como resultado un flujo fisiológico; es decir, las presiones sistólica y diastólica resultado de la simulación coinciden con las que se habían empleado como *inputs* de la metodología.

Paper II: Liver cancer arterial perfusion modelling and CFD boundary conditions methodology: a case study of the haemodynamics of a patient-specific hepatic artery in literature-based healthy and tumor-bearing liver scenarios

ABSTRACT

Some of the latest treatments for unresectable liver malignancies (primary or metastatic tumors), which include bland embolization, chemoembolization, and radioembolization, among others, take advantage of the increased arterial blood supply to the tumors to locally attack them. A better understanding of the factors that influence this transport may help improve the therapeutic procedures by taking advantage of flow patterns or by designing catheters and infusion systems that result in the injected beads having increased access to the tumor vasculature. Computational analyses may help understand the hemodynamic patterns and embolic-microsphere transport through the hepatic arteries. In addition, physiological inflow and outflow boundary conditions are essential in order to reliably represent the blood flow through arteries. This study presents a liver cancer arterial perfusion model based on a literature review and derives boundary conditions for tumor-bearing liver-feeding hepatic arteries based on the arterial perfusion characteristics of normal and tumorous liver segment tissue masses and the hepatic artery branching configuration. Literature-based healthy and tumor-bearing realistic scenarios are created and hemodynamically analysed for the same patient-specific hepatic artery. As a result, this study provides boundary conditions for computational fluid dynamics simulations that will allow researchers to numerically study, for example, various intravascular devices used for liver disease intra-arterial treatments with different cancer scenarios.

LABURPENA

Gibeleko tumore primario eta metastasi hepatiko erauztezinen tratamendu berrienak (enbolizazioa, kimioenbolizazioa eta erradioenbolizazioa, esaterako) tumoreen arteria bidezko odoleztapenaz baliatzen dira tumoreak zuzenean erasotzeko. Arteriatan gertatzen dena hobeto ulertzeak tratamenduen hobekuntza ekar dezake. Ordenagailu bidezko analisiak arteria hepatikoaren hemodinamika eta mikroesfera enbolikoen garraioa hobeto ezagutzen lagun dezake. Gainera, sarrerako eta

irteeretako muga-baldintzak ezinbestekoak dira arterietako odol-fluxua modelizatzeko. Lan honek literaturan oinarritutako gibeleko minbiziaren perfusio arterialaren eredua aurkezten du eta muga-baldintzak nola kalkulatu azaltzen. Arteria hepatiko berarentzat literaturan oinarritutako gibel osasuntsu baten eta minbizia duen gibel baten hemodinamika aztertu da. Lan honek arteria bidezko tratamenduen simulazio numerikoak ahalbidetzen ditu hainbat minbizi-egoeratarako.

RESUMEN

Algunos de los tratamientos más recientes para el tratamiento de tumores hepáticos primarios y secundarios que no permiten la resección (embolización, quimioembolización y radioembolización, entre otros) se aprovechan del casi exclusivo aporte de sangre arterial por parte de los tumores. Comprender mejor el transporte de sangre arterial permitiría mejorar estos procedimientos terapéuticos. Los análisis computacionales podrían permitir conocer mejor los patrones hemodinámicos y el transporte de microesferas embolizantes. Además, las condiciones de contorno son esenciales para una correcta representación del flujo sanguíneo de manera computacional. Este estudio presenta un modelo de la perfusión arterial de tejidos del hígado basado en una revisión bibliográfica y deduce condiciones de contorno según los volúmenes hepáticos y su perfusión y la estructura de la arteria hepática. Para una misma arteria hepática específica de paciente, se ha analizado la hemodinámica para dos escenarios de hígado que se han creado basados en la literatura: un hígado sano y un hígado con cáncer. Este estudio proporciona las herramientas para crear escenarios de cáncer que puedan ser empleados en simulaciones numéricas para, por ejemplo, estudiar los dispositivos que se emplean en los procedimientos endovasculares.

Paper III: Computational particle–hemodynamics analysis of liver radioembolization pretreatment as an actual treatment surrogate

ABSTRACT

Liver radioembolization (RE) is a treatment option for patients with unresectable and chemorefractory primary and metastatic liver tumors. RE consists of intra-arterially administering via catheter radioactive microspheres that locally attack the tumors, sparing healthy tissue. Prior to RE, the standard practice is to conduct a treatment-mimicking pretreatment assessment via the infusion of 99mTc-labeled macroaggregated albumin microparticles. The usefulness of this pretreatment has been debated in the literature, and thus, the aim of the present study is to shed light on this issue by numerically simulating the liver RE pretreatment and actual treatment particle–hemodynamics in a patient-specific hepatic artery under two different literature-based cancer scenarios and two different placements of a realistic end-hole microcatheter in the proper hepatic artery. The parameters that are analyzed are the following: microagent quantity and size (accounting for RE pretreatment and treatment), catheter-tip position (near the proper hepatic artery bifurcation and away from it), and cancer burden (10% and 30% liver involvement). The conclusion that can be reached from the simulations is that when it comes to mimicking RE in terms of delivering particles to tumor-bearing segments, the catheter-tip position is much more important (because of the importance of local hemodynamic pattern alteration) than the infused microagents (i.e., quantity and size). Cancer burden is another important feature because the increase in blood flow rate to tumor-bearing segments increases the power to drag particles. These numerical simulation-based conclusions are in agreement with clinically observed events reported in the literature.

LABURPENA

Gibeleko erradioenbolizazioa (RE) aukera ona da erauztezinak eta kimioerresistenteak diren gibeleko minbiziak tratatzeko. Gibeleko zati osasuntsuak gehiegi kaltetu gabe, tumoreak zuzenean erasotzeko aukera ematen du RE-ak, arteria hepatikoan kokatutako kateter baten bidez mikroesfera erradioaktiboak injektatuz. RE-aren aurretik, albumina makroitsatsiak injektatzen dira aurretratamendu batean. Asko eztabaidatu izan da, literaturan, aurretratamendu

honen balioaren inguruan. Hori dela eta, lan honen helburua izan da aurretratamentu honen balioaz aritzea. Arteria hepatiko berarentzat, literaturan oinarritutako bi minbizi-egoera sortu dira eta bi posizio definitu mikrokateterrarentzat, simulazio numerikoen bidez hemodinamika eta partikulen garraioa ikertzeko. Ikertu diren parametroak hauek izan dira: injektatutako mikroagente kopurua eta horien tamaina, kateterraren muturraren kokapena eta tumoreen tamaina. Tratamenduaren eta aurretratamenduaren simulazioen emaitzak haintzat hartuz zera ondoriozta daiteke, garrantzitsuagoa dela kateterraren muturraren kokapena mikroagenteen ezaugarriak baino (ezaugarri hemodinamiko lokalak aldatzen direlako). Gainera, tumoreen tamainaren garrantzia agerian geratu da (tumoreetara partikulak garraiatzeko gaitasuna handiagoa da odol jarioa handiagoa denean). Simulazio numerikoetan oinarritutako ondorio hauek bat datoz literaturan argitaratutako ikerketa klinikoetan ikusitakoarekin.

RESUMEN

La radioembolización (RE) hepática es una opción terapéutica para pacientes con tumores hepáticos que no admiten la resección y que son quimioresistentes. La RE consiste en atacar directamente los tumores por medio de microesferas radioactivas insertadas mediante un microcatéter situado en la arteria hepática. Antes de la RE, se realiza una valoración mediante la inyección de micropartículas de macroagregados de albúmina. La validez de este pretratamiento se ha debatido en la literatura. Así, el objetivo de este estudio es estudiar computacionalmente la validez del pretratamiento analizando la hemodinámica y el transporte de partículas en una misma arteria hepática para la que se han creado dos escenarios de cáncer basados en la literatura y para dos posiciones de la punta del microcatéter en la arteria hepática propia. Los parámetros analizados son: la cantidad y el tamaño de los microagentes, la posición del microcatéter y el tamaño de los tumores. Se puede concluir que la punta del microcatéter desempeña un papel más importante que las características de los microagentes. Además, se ha visto la importancia del tamaño de los tumores, por su capacidad de arrastrar las partículas hacia ellos. Estas conclusiones basadas en los resultados de simulaciones numéricas concuerdan con resultados de estudios clínicos publicados en la literatura.

Paper IV: Computational assessment of the effects of the catheter type on particle–hemodynamics during liver radioembolization

ABSTRACT

Radioembolization, which consist of the implantation of radioactive microspheres via intra-arterially placed microcatheter, is a safe and effective treatment for liver cancer. Nevertheless, radioembolization-related complications and side effects may arise, which are an active area of ongoing research. The catheter design has been claimed as an option in reducing these complications. In this paper, the influence of catheter type and location are investigated. The study was undertaken by numerically simulating the particle–hemodynamics in a patient-specific hepatic artery during liver radioembolization. The parameters modified were cancer scenario (30% liver involvement in the right lobe, 'scenario A', and in both lobes, 'scenario B'), catheter type (standard end-hole microcatheter, SMC, and antireflux catheter, ARC), and the location of the tip in the proper hepatic artery (in the straight part, 'inlet', and near the bifurcation, 'bifurcation'). Comparing ARC with SMC, the average and maximum (over segments) absolute difference in the percentage of particles that reached each segment were 9.06% and 19.62% when injecting near the inlet for scenario A; 1.07% and 3.54% injecting near the bifurcation for scenario A; and 11.85% and 18.31% injecting near the inlet for scenario B. It seems, therefore, that the location of the catheter tip in the artery is crucial in terms of particle distribution. Moreover, even though the near-tip blood flow was altered due to the presence of a catheter, the particle distribution matched the flow split if the distance between the injection point and the first bifurcation encountered enabled the alignment of particles with blood flow.

LABURPENA

Erradioenbolizazioa, arteria hepatikoan kokatutako mikrokateter baten bidez mikroesfera radioaktiboak injektatzean datzana, gibeleko minbiziari aurre egiteko tratamendu segurua eta eraginkorra da. Hala ere, konplikazioak eta albo ondorioak eragin ditzake. Kateterra egoki diseinatzeak eta kokatzeak aukera sor dezake konplikazioak gutxitu eta, kasurik onenean, desagerrarazteko. Lan honetan, erradioenbolizazioaren azterketa numerikoa burutu da (arteria hepatikoan ematen den odol-fluxuaren eta partikulen garraioarena). Aztertutako parametroak hauek dira: minbizi-egoera (gibelaren %30eko minbizi masa eskuineko lobuluan, 'A egoera';

eta minbizi masa berdina bi lobuluetan banatuta, 'B egoera'), kateter mota (mikrokateter estandarra, SMC, eta errefluxua ekiditen duen kateterra, ARC), eta kateterraren muturraren kokapena (arteria hepatiko propioaren zati zuzenean, 'sarrera'; eta arteria hepatikoko bifurkaziotik gertu, 'bifurkazioa'). SMC eta ARC kateterrekin eskuratutako datuak alderatu dira, eta batezbesteko diferentzia absolutuak eta diferentzia maximoak neurtu (hurrenez hurren), gibeleko segmentuetara iristen diren partikulen ehunekotan: %9,06 eta %19,62 'sarrera'-tik injektatzean 'A egoera'-n, %1,07 eta %3,54 'bifurkazioa'-tik injektatzean 'A egoera'-n, eta %11,85 eta %18,31 'sarrera'-tik injektatzean 'B egoera'-n. Badirudi kateterraren muturraren kokapenak berebiziko garrantzia duela. Gainera, partikulen distribuzioak odol-fluxuaren distribuzioaren itxura hartzen du, baldin eta injekzio-puntutik partikulen ibilbideko lehen bifurkaziora dagoen distantziak ahalbidetzen badu partikulak odol-fluxuarekin lerrokatzea.

RESUMEN

La radioembolización, que consiste en la implantación de microesferas radiactivas mediante un microcatéter ubicado en la arteria hepática, es un tratamiento seguro y efectivo contra el cáncer hepático. Sin embargo, pueden surgir complicaciones y efectos secundarios. En este artículo se estudian el tipo de catéter empleado y su localización en la arteria hepática. El estudio se ha llevado a cabo mediante simulaciones numéricas del flujo sanguíneo con transporte de partículas en una arteria hepática específica de paciente durante la radioembolización. Los parámetros que se han modificado son el escenario de cáncer (30% de invasión hepática sólo en el lóbulo derecho, 'escenario A' y la misma cantidad expandida en toda la masa hepática, 'escenario B'), el tipo de catéter empleado (microcatéter estándar, SMC, y catéter antirreflujo, ARC) y la posición de la punta del microcatéter (en la parte recta de la arteria hepática propia, 'entrada', y cerca de la bifurcación de la arteria hepática propia, 'bifurcación'). Si se comparan los resultados de SMC versus ARC, se han observado las siguientes diferencias absolutas medias y máximas sobre el porcentaje de partículas radiactivas que llegaban a los segmentos del hígado: 9,06% y 19,62% inyectando desde 'entrada' en el 'escenario A', 1,07% y 3,54% inyectando desde 'bifurcación' en el 'escenario A', y 11,85% y 18,31% inyectando desde 'entrada' en el 'escenario B'. Por tanto, parece que el punto de inyección es muy importante en cuanto a la distribución de partículas segmento a segmento. Además, la distribución de partículas tiende a asemejarse a la distribución del flujo sanguíneo cuando la distancia entre el punto de inyección y la distancia a la primera bifurcación que se encuentran las partículas permite el alineamiento de las partículas con el flujo.

Paper V: Numerical investigation of liver radioembolization via computational particle–hemodynamics: The role of the microcatheter distal direction and microsphere injection point and velocity

ABSTRACT

Liver radioembolization is a treatment option for patients with primary and secondary liver cancer. The procedure consists of injecting radiation-emitting microspheres via an intra-arterially placed microcatheter, enabling the deposition of the microspheres in the tumoral bed. The microcatheter location and the particle injection rate are determined during a pretreatment work-up. The purpose of this study was to numerically study the effects of the injection characteristics during the first stage of microsphere travel through the bloodstream in a patient-specific hepatic artery (i.e., the near-tip particle–hemodynamics and the segment-to-segment particle distribution). Specifically, the influence of the distal direction of an end-hole microcatheter and particle injection point and velocity were analyzed. Results showed that the procedure targeted the right lobe when injecting from two of the three injection points under study and the remaining injection point primarily targeted the left lobe. Changes in microcatheter direction and injection velocity resulted in an absolute difference in exiting particle percentage for a given liver segment of up to 20% and 30%, respectively. It can be concluded that even though microcatheter placement is presumably reproduced in the treatment session relative to the pretreatment angiography, the treatment may result in undesired segment-to-segment particle distribution and therefore undesired treatment outcomes due to modifications of any of the parameters studied, i.e., microcatheter direction and particle injection point and velocity.

LABURPENA

Gibeleko erradioenbolizazioa tumore hepatiko primarioei eta metastasi hepatikoei aurre egiteko erabiltzen den tratamenduetako bat da. Prozedura horretan, partikula erradioaktiboak injektatzen dira arterian kokatutako mikrokateter baten bitartez, aprobetxatuz odol-fluxuak tumoreen ehunera garraiatzen dituela partikula horiek. Mikrokateterraren posizioa eta partikulen injekzio-abiadura aurretratamenduan erabakitzen dira. Lan honen helburua da numerikoki injekzioaren ezaugarriak aztertzea. Horretarako, simulazio numerikoak egin dira arteria hepatiko batean eta

mikrokateterraren inguruko hemodinamika eta partikulen garraioa aztertu; mikrokateterraren direkzio distala, injekzio-puntua eta partikulen injekzio-abiadura, hain zuzen. Simulazioen emaitzek erakutsi dute injektatzeko erabiltzen diren ikertutako hiru puntuetatik bik eskuineko lobulua bonbardatzen duen tratamendua osatzen dutela, eta hirugarrenak osatzen duen tratamenduak ia bere osotasunean ezkerreko lobulua bonbardatzen duela. Mikrokateterraren direkzio distala eta injekzio-abiadura aldatu izanak %20 eta %30-erainoko diferentzia absolutuak sortu dituzte, gibeleko segmentu jakin batera iritsi diren partikulen ehunekotan. Zera ondoriozta daiteke: mikrokateterraren kokapena eta injekzio-abiadura aurretratamenduko berak izanda ere, ikertutako hiru parametro hauetakoren batean (mikrokateterraren direkzio distala, injekzio-puntua eta partikulen injekzio-abiadura aztertu dira) sortutako aldaketa txikiek eragin dezakete nahi ez diren tratamenduak eskuratzea.

RESUMEN

La radioembolización hepática es una alternativa para el tratamiento de tumores hepáticos primarios y metástasis hepáticas. El procedimiento consiste en inyectar microesferas radiactivas mediante un microcatéter emplazado en la arteria hepática, de modo que las microesferas se depositan en la malla tumoral. Tanto la localización como la velocidad de inyección de partículas se deciden durante el pretratamiento. El objetivo de este estudio ha sido analizar numéricamente la influencia de las características de la inyección durante la primera fase del transporte de las partículas en el torrente sanguíneo; es decir, la hemodinámica con transporte de partículas cerca de la punta del microcatéter y la distribución de partículas segmento a segmento. Los parámetros analizados han sido la dirección distal del microcatéter, y el punto y la velocidad de inyección de las partículas. Los resultados muestran que dos de los tres puntos de inyección dan como resultado el bombardeo del lóbulo derecho, mientras que el punto de inyección restante da como resultado un tratamiento que principalmente bombardea el lóbulo izquierdo. Cambios en la dirección distal del microcatéter y en la velocidad de inyección han originado diferencias absolutas en el porcentaje de partículas que llegan a un segmento dado de hasta 20% y 30%. Puede concluirse que aunque se procure colocar el microcatéter en la misma posición que en el pretratamiento e inyectar a la misma velocidad, pequeñas variaciones en los parámetros estudiados pueden llevar a tratamientos no deseados.

Paper VI: The role of angled-tip microcatheter and microsphere injection velocity in liver radioembolization: a computational particle–hemodynamics study

ABSTRACT

Liver radioembolization is a promising treatment option for combating liver tumors. It is performed by placing a microcatheter in the hepatic artery and administering radiation-emitting microspheres through the arterial bloodstream so that they get lodged in the tumoral bed. In avoiding nontarget radiation, the standard practice is to conduct a pretreatment, in which the microcatheter location and injection velocity are decided. However, between pretreatment and actual treatment some of the parameters that influence the particle distribution in the liver can vary, resulting in radiation-induced complications. The present study aims to analyze the influence of a commercially available microcatheter with an angled tip and particle injection velocity in terms of segment-to-segment particle distribution. Specifically, four tip orientations and two injection velocities were combined to yield a set of eight numerical simulations of the particle–hemodynamics in a patient-specific truncated hepatic artery. For each simulation, four cardiac pulses were simulated. Particles were injected during the first cycle, and the remaining pulses enabled the majority of the injected particles to exit the computational domain. Results indicate that particles seem to follow the blood flow split, although particle injection velocity and microcatheter tip orientation also play a role in particle travel. In terms of injection velocity, particles are more spread out in the cross-sectional lumen areas as the injection velocity increases. The tip's orientation plays a role because it influences the near-tip hemodynamics, which consists of helical and chaotic bloodstreams when the arterial tree exhibits complex branching, as in the case of hepatic arteries. Therefore, only focusing on the angled-tip orientation does not predetermine the particle distribution.

LABURPENA

Gibeleko erradioenbolizazioa gibeleko tumoreei aurre egiteko aukera bat bezala agertu da. Mikrokateter bat arteria hepatikoan kokatuz burutzen da tratamendua, erradiazioa emititzen duten mikroesferak odol-fluxuan injektatuz. Irradiatu nahi ez diren guneak babesten direla ziurtatzeko, aurretratamendu bat egin ohi da. Aurretratamendu hortan mikrokateterraren muturra non kokatu eta partikulak ze abiadurarekin sartu erabakitzen da. Hala ere, aurretratamendutik tratamendura bitarteko tartean, partikulen distribuzioan eragiten duten parametroek aldaketak jasan ditzakete, eta horrek konplikazioak sor ditzake; irradiazioak gune osasuntsuak kaltetu ditzake. Lan honetan, zera aztertu nahi izan da: muturra 45º-ko angeluan duen mikrokateter baten orientazioak eta partikulen injekzio-abiadurak nola eragiten duten partikulen distribuzioan. Muturrarentzako lau orientazio definitu dira, eta bi

injekzio-abiadura; hau da, zortzi simulazio burutu dira. Simulazio bakoitzean, lau ziklo kardiako simulatu dira: lehenengoan, partikulak injektatu dira, eta gainerako hiruretan, helburua izan da injektatutako partikula gehienak eredu konputazionaletik kanporatzea. Emaitzen arabera, partikulen distribuzioak odol-fluxuaren distribuzioaren antza izan ohi du; hala ere, muturraren orientazioak eta partikulen injekzio-abiadurak ere badute zeresanik partikulen distribuzioan. Injekzio-abiaduraren eragina garbia da: abiadurak gora egin ahala, partikulek modu barreiatuago batean egiten dure ibilbidea, sakabanatuago. Muturraren orientazioa ere garrantzitsua da, aldaketak sortzen baititu muturraren inguruko hemodinamikan, zeina, berez, kaotikoa den hepatikoa bezalako arteria konplexuetan. Beraz, ezin daiteke esan muturraren orientazioak, berak bakarrik, partikulen distribuzioa definitzen duenik.

RESUMEN

La radioembolización hepática es una técnica prometedora en el tratamiento de tumores hepáticos. Se lleva a cabo mediante un microcatéter colocado en la arteria hepática y administrando microesferas radiactivas por el torrente sanguíneo arterial, de modo que se quedan atrapadas en la malla tumoral. Para evitar la irradiación a zonas sanas, se realiza un pretratamiento mediante el cual se deciden tanto la posición del microcatéter como la velocidad de inyección de las partículas. Sin embargo, entre el pretratamiento y el tratamiento hay parámetros que influyen en la distribución de las partículas que pueden variar, dando lugar a complicaciones causadas por irradiación no deseada en zonas sanas. Este estudio tiene como objetivos analizar la influencia de la orientación de un microcatéter con la punta acabada en ángulo de 45º y la velocidad de inyección de las partículas en la distribución de partículas segmento a segmento. Se han combinado cuatro posibles orientaciones de la punta y dos velocidades de inyección, dando lugar a un estudio de ocho simulaciones numéricas del flujo sanguíneo con transporte de partículas en un modelo específico de paciente de la arteria hepática. Las partículas son inyectadas durante el primer pulso y se simulan tres pulsos más de modo que la mayoría de las partículas inyectadas abandonan el modelo computacional. Los resultados indican que la distribución de partículas tiende a parecerse a la distribución del flujo sanguíneo, aunque los parámetros estudiados también desempeñan una función importante en la trayectoria de las partículas. En cuanto a la velocidad de inyección, las partículas tienden a esparcirse más en la sección transversal del lumen a medida que la velocidad de inyección aumenta. La orientación de la punta del microcatéter influye porque altera la hemodinámica, que consiste en líneas de corriente helicoidales y caóticas cuando la estructura de la arteria es compleja, como en el caso de las arterias hepáticas. Por tanto, fijarse en la orientación de la punta del microcatéter no predetermina la distribución de las partículas.